The expression and function of the killer-specific secretory protein of 37 kDa (Ksp37) in natural killer (NK) cells

Gabriel A. Sanchez Maltese
Malmberg Lab - University of Oslo

Author Note

In collaboration with the Hybrid Technology Hub

i. Table of contents

ii. List of Abbreviations

Abbreviation	Definition
NK cells	Natural Killer cells
PRRs	Pattern recognition receptors
PAMPs	Pathogen-associated molecular patterns
RNA	Ribonucleic acid
DAMPs	Damage-associated molecular patterns
IFNs	Type I interferons
ILCs	Innate lymphoid cells
HLA	Human leukocyte antigen
HLA (-A/B/C/E)	Human leukocyte antigen, alpha chain A/B/C/E
KIR	Killer immunoglobulin-like receptors
DCs	Dendritic cells
TNF (-α)	Tumor necrosis factor (-α)
IFN-γ	Interferon gamma
MHC (I-II)	Major histocompatibility complex (Class I – II)
ITIM(s)	Immunoreceptor tyrosine-based inhibition motif(s)
CD	Cluster of differentiation
CLPS(s)	Common lymphoid progenitor(s)
NKPs	NK cell precursors
mNK cells	Mature NK cells
FGF	Fibroblast growth factor
FGFBP(2)	Fibroblast growth factor binding protein (2)
Ksp37	Killer cell secretory protein of 37kDa
IL	Interleukin
wt	Wild type
FGFR1	Fibroblast growth factor receptor 1
FBS	Fetal bovine serum
PBMCs	Peripheral blood mononuclear cells

HTH	Hybrid Technology Hub
PFA	Paraformaldehyde
DMSO	Dimethyl sulfoxide
RNP	Ribonucleoprotein (sgRNA/Cas9)
PCR	Polymerase chain reaction
rt-qPCR	Reverse transcription-quantitative PCR
TBS	Tris-Buffered Saline
FAM	Fluorescein amidite
Ct	Cycle threshold
FcεRI	High-affinity IgE receptor
B2M	Beta-2 microglobulin
Δ Ct	Delta cycle threshold
Bp	Base pairs
ET	Effector-target ratio
RCU x μm^2/Image	Total red object integrated intensity per image

iii. List of Tables

iv. List of Figures

v. Abstract

Natural killer (NK) cells in the human body play a critical role in immunosurveillance and the control of cancer metastasis, mainly due to their capacity to respond spontaneously to targets without the need for prior antigen exposure. The latter, in junction with reported manageable safety profiles and encouraging signs of efficacy, have posed natural killer cell-based immunotherapies as a promising area of clinical research. Nonetheless, there remain pressing hurdles that need to be addressed, including how to deal with immunosuppressive factors and how to overcome the scarcity of growth factors needed for NK cell proliferation and persistence in-vivo.

In this regard, the present project aimed at contributing to a more comprehensive understanding of NK cell biology by means of investigating the yet unknown role of the Killer cell secretory protein of 37kDa (Ksp37). In concrete, the thesis focused on the current data available hinting at a potential involvement of Ksp37 in cell-mediated cytolysis and its stipulated ability to bind FGF2. With this purpose in mind, genetically modified NK-92 cell lines overexpressing Ksp37 were employed as effector cells, whilst Panc-1 cells, both with and without fibroblast growth factor 2 (FGF2) gene knockout, were used as targets.

In summary, the cytotoxicity appeared to be intrinsically lower in NK92 cells overexpressing Ksp37. This finding is somewhat unexpected and needs confirmation in further experiments. Notwithstanding, the overexpression models used in the present project render a simple yet reliable fashion to secrete Ksp37 protein into the media. Tool that, in light of the new evidence for the binding of Ksp37 to FGF2 herein discussed, opens up a new path for a more targeted approach to decipher the biological relevance of Ksp37.

All in all, this project has provided preliminary evidence for (i) the capacity of Ksp37 to physically interact with FGF2, (ii) the lack of direct cytolytic involvement of Ksp37, and (iii) the suitability of pumpless microfluidic chip systems for studying NK cells in a dynamic 3D context. Insights that carry the potential for bringing forth a better understanding of FGF2 dysregulation in cancer development and perhaps even additional tools to address it.

vi. Acknowledgment

The present project was carried out mainly in Karl Johan Malmberg's group at the Department of Immunology at Oslo Radium Hospital. First and mostly I would like to give huge thanks to Kalle for opening the doors of his lab and giving me the opportunity to be part of his group. The advice and guidance Kalle shared throughout have been pivotal for the project to find north, intellectually challenging, and of great meaning professionally. Thank you very much Kalle, you are a true leader.

Especial thanks go also to Aleksandra Aizenshtadt, Mathias Busek, and Stefan Krauss from the Hybrid Technology Hub. The trust they placed in me to access their platform signified a huge learning experience for which I am deeply grateful. By the same token, I want to express my immense gratitude to Merete Thunberg. Her vast scientific knowledge and resilient patience with my many (and often unstructured) questions, were on countless occasions crucial to propel forward the project. Thank you so much Merete!

Thank you to all other members of the Malmberg group: Silje Zandstra, Julie Hoel, Lamberto Torralba-raga, Lise Kveberg, Edina Szabo, and Marianna Vincenti. I would also like to thank previous members, Dennis Clement, Rakesh Kumar, and Daniel Palacios, whom I had the pleasure to meet and were never shy when sharing their experiences and advice.

Oslo, July 2023

Alonso Sánchez

1 Introduction

1.1 The innate immune system

The mechanisms of the innate immune system do not require prior exposure to microbes to elicit an immune response. It is therefore the host's first line of defense against pathogens and damaged cells. Its cellular components comprise both the epithelial barrier of the body as well as its cellular components: neutrophils, macrophages, dendritic cells (DCs) natural killer (NK) cells, mast cells, and lymphocytes with fixed antigen receptors: Innate lymphoid cells (ILC) 1, ILC2, and ILC3 [2].

One of the key features of innate immune cells is the expression of germline-encoded pattern recognition receptors (PRRs) on their cell surface, or within specific intracellular compartments. PRRs can recognize molecular structures named pathogen-associated molecular patterns (PAMPs) [3]. The latter are not present in mammalian cells, but rather in microbes and viruses. Examples of these include lipopolysaccharides found in bacterial cell wall and double-stranded ribonucleic acid (RNA) produced during viral infection. PRRs can also recognize damage-associated molecular patterns (DAMPs), a set of molecules that are released from the host's cells in response to cell stress and death, leading to sterile inflammation [4]. The innate immune response's function can be categorized into two main processes. The first process involves the induction of inflammation and thus the recruiting of cytotoxic leukocytes and delivery of effector molecules from the blood to the affected tissue. The second process deals with antiviral defense, eliciting the killing of infected cells and preventing viral replication mainly through the action of type I interferons (IFNs) [5]. This second protective process does not require inflammation to induce an immune response, however, the latter can also be part of the reaction [2, 5].

Another important characteristic of the innate immune system is its capability to prime the adaptive response. On the one hand, the former serves as a regulatory switch to avoid uncontrolled response or self-antigen targeting. It is therefore the case that antigen-specific lymphocytes, such as B and T cells, for the most part only respond to foreign antigens if the innate system has been activated first [6]. On the other hand, molecules produced during the innate reaction act as signals for lymphocyte activation and proliferation, such as costimulatory molecules (effect over T cells) and cytokines (effect over T and B cells) [6].

1.2 Natural killer cells

As their name suggests, NK cells are a subset of the innate immune system's cellular components, distinguished by spontaneous response to targets without prior antigen exposure and their large granular morphology [7, 8]. In humans, NK cells represent a minor fraction of lymphocytes found in most tissues and only ~ 2 - 8% of the same subset in peripheral blood. They can be divided into two major groups based on the surface density of the CD56 marker: $CD56^{dim}$ and $CD56^{bright}$ NK cells. Whilst $CD56^{bright}$ NK cells are more prominent in secondary lymph tissue and display high proliferation potential, $CD56^{dim}$ NK cells in contrast are predominant in peripheral blood and have a lower proliferative capacity [9]. Differences in cytotoxic potential further distinguish these two groups, with $CD56^{dim}$ NK cells expressing a high amount of perforin and granzyme B, which their bright counterparts lack [10]. Additionally, the expression of other surface markers involved in the binding of effector cells to their targets such as CD2, CD11a/CD18, CD54, and CD58 [11], is also considerably lower in the $CD56^{bright}$ phenotype, providing another possible reason for the difference in cytotoxic potential [12].

Furthermore, NK cells lack specificity and antigen memory, thus the magnitude of their cytotoxic reaction does not differ between subsequent encounters with the same target [2]. They belong to the group of innate lymphoid cells (ILCs) composed of NK cells, ILC1s, ILC2s, and ILC3s, from which NK cells can be viewed as the innate counterpart of cytotoxic $CD8^+$ T cells from the adaptive immune system [13]. Meanwhile, ILC1s, ILC2s, and ILC3s display similar roles as $CD4^+$ T helper 1 (TH1), TH2, and TH17 cells respectively. Unlike their adaptive counterparts, however, ILCs do not express rearranged antigen-specific cell receptors [13].

Despite these differences, NK cells fulfill a complementary role to that of B and T cells. Whereas the latter respond to antigens presented by other cells on the surface of major histocompatibility complex (MHC) proteins, NK cells react to the lack of MHC class I proteins [14, 15]. A concept defined as "missing self" that grants NK cells recognition of infected or tumor-transformed cells that have suppressed MHC I expression to avoid detection by adaptive immune lymphocytes. Moreover, the lytic activity of NK cells over their targets releases antigens that can be internalized by dendritic cells and subsequently cross-presented to $CD8^+$ and $CD4^+$ T cells, inducing antigen-specific adaptive immune responses [16].

Lastly, this complementary role is further strengthened by the ability of NK cells to produce and secrete the IFN-gamma (IFN-γ) and tumor necrosis factor α (TNF- α), both cytokines that promote maturation and activation of DCs and T cells [17] [18].

1.2.1 NK cell-mediated cellular cytotoxicity

NK cell-mediated cytotoxicity is a result of signal integration from multiple activating and inhibitory receptors, with the outcome however pitched in favor of inhibition [19]. From the inhibition side, NK cells are in constant patrol for the absence of constitutively expressed MHC class I on the surface of cells [20]. The absence of MHC class I would tag the cell in question as foreign, causing loss of the inhibitory signal and prompting NK cell-mediated lysis [20]. Some of the key inhibitory receptors in NK cells are the members of the killer-cell immunoglobulin-like receptors (KIR) family[1].

The main cognate ligands of KIR proteins are the human leukocyte antigen (HLA) alpha chain A, B, and C molecules [22, 23], which are expressed on the surface of almost every healthy nucleated cell in the human body. These three antigens are part of the HLA class I molecules, holding the primary role of presenting on the self-surface peptide fragments from cleaved cytosolic proteins [24]. Their corresponding genes are considered the most polymorphic in humans, with several thousand alleles encoding functional proteins [25, 26]. Above all, HLA-A, B, and C, as members of the HLA class I family, play the crucial role of facilitating the immune system to recognize “self” versus “non-self” molecules. [23].

On the other hand, activating receptors gauge cells for the presence of stress induced self-ligands and non-self-ligands. One of the best-known activating receptors is NKG2D, member of the NKG2 family, a group of type II transmembrane proteins with C-type lectin-like extracellular domain, transmembrane segment, and cytoplasmic tail [27]. NKG2D can recognize eight different ligands: MICA\B and UL16-binding proteins 1–6 [28, 29]. Another well characterized activating receptor of the same family is NKG2C which interacts with the HLA -E [30, 31].

[1] It is worth noting that the KIR family possesses both inhibitory and activating receptors. 21. Pegram, H.J., et al., *Activating and inhibitory receptors of natural killer cells.* Immunology & Cell Biology, 2011. **89**(2): p. 216-224.

A third way in which NK cells identify potential targets is through the antibody dependent cell-mediated cytotoxicity (ADCC) [17]. Cytolytic event mediated primarily by the fragment crystallizable receptor (FcR) CD16A that binds to Immunoglobulin G (Ig G) [32]. Protein encoded by the FCRG3A gene in humans and expressed in ~90% of cell in the peripheral blood [33].

Both the degree of intensity and quality of the cytotoxic response resulting from the signal integration of the above-mentioned pathways will, however, be determined based on the cytokine environment where the stimulation is taking place as, well as interaction with other immune cells such as T cells, DCs, and macrophages [34]. Amon the most potent cytokine for inducing NK cells effector functions are IFNs, interleukin-2 (IL-2), IL-12, IL-18, and IL-15 [8, 35].

1.2.2 NK cell development

In contrast to T cells, NK cell development is not dependent on a master transcriptional factor, but rather a plethora of these including T-bet, Eomes, E4BP4, Id2, and BLIMP [36]. As for all other blood-cell lineages, however, this process starts from hematopoietic stem cells (HSCs) in the bone marrow that will further differentiate into common lymphoid progenitors (CLPs) [7]. The latter are known precursors of the lymphoid lineage that encompass all subsets of ILCs, B, and T cells [37]. CLPs are characterized by the expression of IL-7Rα (CD127), c-kit (CD117), Sca-1, and Flt-3 (CD135), as well as the lack of markers such as CD3, CD4, and CD19 [38].

CLPs in turn develop into NK cell precursors (NKPs), which can be recognized by expression of IL-15 receptor β chain (CD122), as well as lack of CLP common lineage markers such as NK1.1 and DX5 (CD49b) [39]. NKP phenotype acquisition marks the stage where cells can only continue developing into mature NK cells, and no longer into any other hematopoietic lineage [40]. Moreover, recent evidence has also demonstrated the presence of NK progenitors and immature NK cells in secondary lymph tissues such as the lymph node, tonsils, and spleen [41-43]. Thus, indicating NKPs capacity to egress from the bone marrow and continue their development in different tissues.

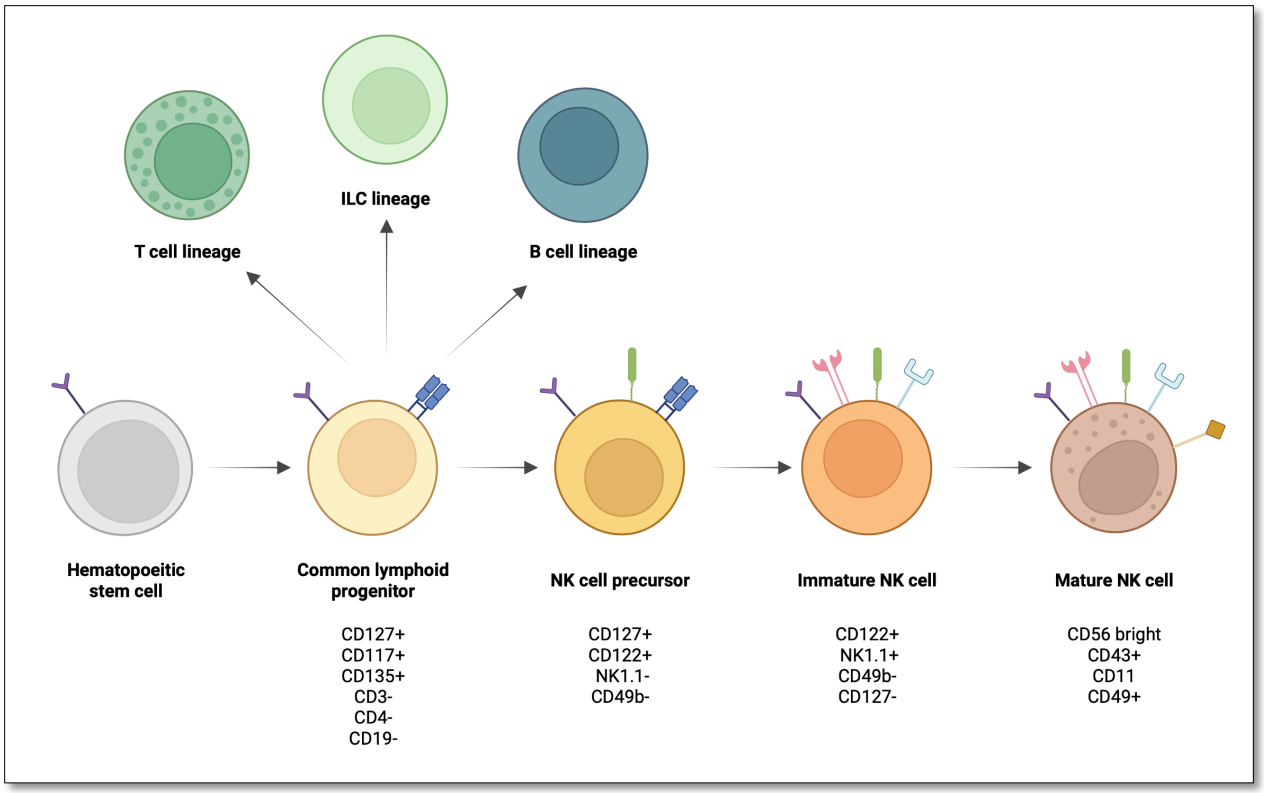

Figure 1 - NK cell development

Schematic graphs with the main stages of NK cell development. Note: receptors on the cell surface are just for illustration purposes of the gain and loss of markers throughout the developmental process.

$CD122^{+}$IL-$7R\alpha^{+}$ NKPs proceed to develop into immature NK cells, a process distinguished by loss of IL-7Rα expression and acquisition of NK1.1 [39]. As immature NK cells start to become mature NK (mNK) cells, they gain functional cytotoxicity and production of IFN-γ, as well as expression of CD11b, CD43, Ly49 receptors, and CD49b (DX5) [44]. The culmination of this transition is delineated by the appearance of CD56 (NCAM), more particularly the $CD56^{bright}$ NK cell subset, that for the most part (~90%) will become mature $CD56^{dim}$ [45]. A recapitulation of the NK cell development process is found in **Figure 1**.

1.2.1 NK cell differentiation

The process of NK cell differentiation takes place along a continuum that relies on genetic and environmental factors [1]. As previously stated, fully developed NK cells can be broadly divided between the two subsets of $CD56^{bright}$ and $CD56^{dim}$ cells.

In this context, the differentiation process starts with the naive CD56^{bright} phenotype, characterized by a strong proliferative capacity and IFN-γ production upon cytokine stimulation [46, 47]. CD56^{bright} cells progressively lose the expression of CD56 and shift towards a CD56^{dim} profile, losing the previously held proliferative capacity and IFN-γ production, acquiring instead high cytotoxic potential [46, 48]. CD56^{dim} NK cells continue to further differentiate, gradually losing expression of NKG2A and NKG2D [49, 50]. A process that is accompanied by the acquisition of CD57, CD16, and KIRs, where CD57 defines the final stage of NK cell maturation [49, 51, 52].

Additionally, under certain circumstances, NK cells can further differentiate into an adaptive phenotype capable of antigen-driven clonal expansion and generation of long-lived memory [52]. The most widely studied example of adaptive NK cells in humans is linked to cytomegalovirus (CMV) infection [53, 54]. The process leading to adaptive NK cells is marked by a decrease in the high-affinity IgE receptor (FcεRI) and increased expression of the activating receptor NKG2C [55]. These CD56^{dim} CD57^{+} NKG2C^{+} FcεRI^{-} NK cells display a decreased cytotoxicity and responsiveness to cytokines IL-2 and IL-8, but rather an increased CD16-mediated ADCC and IFN-γ production [56]. A summary of the main stages of NK cell differentiation can be found in Figure 2.

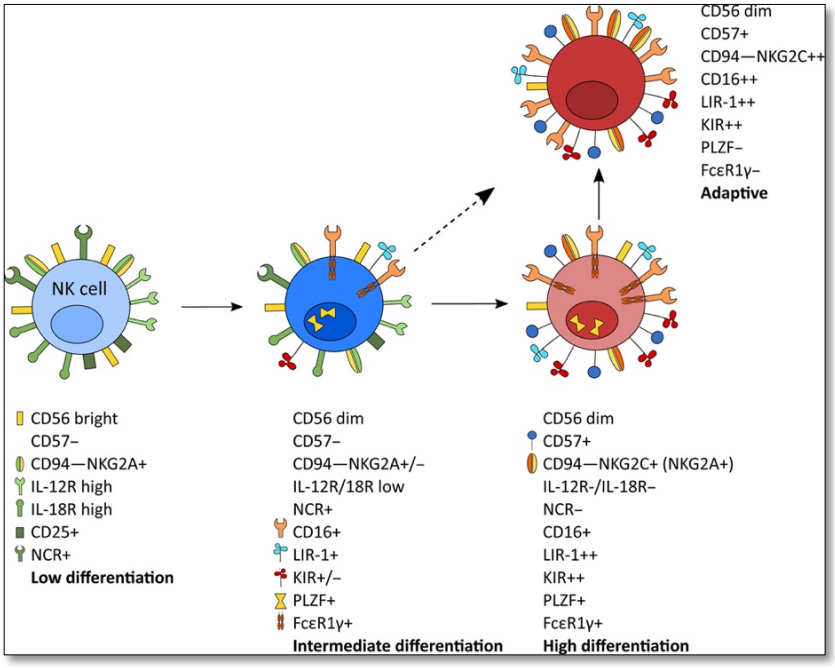

Figure 2 - Main stages of Human NK cell differentiation

Illustration showing several markers associated with the differentiation stages of NK cells. Naive CD56^{bright} NK cells (left) are at the start phase. Followed by decreased CD56 expression and KIR and CD16 acquisition, these cells move to an intermediate differentiated state. In turn, further expression of CD57 marks a stage of high NK cell differentiation. Adaptive NK cells are in turn at the last end of the process, marked by increased NKG2C+FcεRI- phenotype. Image adopted from [1]

1.2.2 NK cell education

The lack of knowledge regarding the molecular mechanism upstream of NK cell education renders the topic highly debated within the field of immunology [57]. Nonetheless, this process can be conceptualized as the fine-tuning of NK cells to their host environment and how they acquire a fully functional phenotype [58, 59].

Despite the unresolved underlying mechanism, it is well established that the main driver behind NK cell education lies in the inhibitory input resulting from the interaction between MHC class I molecules and their corresponding receptors belonging to the KIR superfamily [60-62]. Cell-to-cell interactions with the host's cell are therefore imperative for education to successfully take place, where mounting evidence portrays hematopoietic cells as being dominantly involved in the education process, with stromal cells also participating to a lesser extent [63, 64].

The ultimate objective of the education process is to generate an NK cell repertoire that is tolerant to "self" and capable of detecting "missing self". Hence, its outcome will determine the degree to which NK cells respond to activating signals (e.g., DAMPs), inflammatory cytokines, and FcR engagement (ADCC) [58]. Inversely, NK cells that lack self-reactive receptors will not be educated, becoming anergic and hyporesponsive to stimulation with MHC class I-deficient target cells. Notable evidence of the latter is found in both mice and humans afflicted by a deficiency in the transporter associated with antigen presentation (TAP) and thus a significantly reduced surface MHC expression compared to healthy individuals. These subjects have normal counts of phenotypically mature NK cells, but these are hyporesponsive to MHC-I-deficient targets (i.e. non-self) [65-67].

Here it is relevant to note that NK cell education is more appropriately viewed as a dynamic process rather than a one-way funnel. Accordingly, mature educated NK cells transplanted from MHC-sufficient to MHC-deficient mice, lose their responsiveness within 4 days. In contrast, the transfer of mature hyporesponsive NK cells from MHC I–deficient mice become responsive when introduced into wild-type mice, leading to a resetting in the functionality [64].

1.3 Immune surveillance of cancer

Immunosurveillance refers to the process whereby the immune system components identify and eliminate cancerous and precancerous cells expressing specific molecules that set them apart from healthy host cells. For the adaptive immune system, these take the form of antigens derived from mutated genes, while for the innate immune system, they are stress-induced ligands presented on the surface of the cancerous cells.

As of yet, several lines of evidence have been laid out to back this notion [68]. Notably, patients diagnosed with monoclonal gammopathy are reported to mount sharp T-cell responses targeting pre-malignant B-cells, whilst the same reaction is not detected from multiple myeloma patients [69]. Perhaps even more elucidating of the immune system's role in cancer suppression is found in immunosuppressed transplant recipients and immunodeficient patients, with both groups bearing an increased risk of developing certain types of cancers [70, 71].

Tumors, however, deploy a wide array of strategies to elude immunosurveillance, otherwise known as immune evasion or selection. A noteworthy example is the downregulation of HLA I molecules to escape T-cell-mediated responses [72]. Another common strategy comprises the overexpression of granzyme-B and perforin pathway inhibitors, such as serine-protease inhibitor PI9, blocking thus lysis of the target cell [73].

As tumors progress, a process termed immunosubversion starts to take hold. An event characterized by changes within the tumor microenvironment that begin to tilt the balance from effector immune cells toward a greater proportion of regulatory and suppressive cells. Although the exact mechanisms mediating immunosubversion at the molecular level are still under intense investigation [74], mouse models have provided clear evidence of this process as a step to an advanced cancer stage. For instance, tumor-specific $CD8^+$ and $CD4^+$ T cells show signs of activation at the initiation of tumor growth, yet they progressively lose their anti-tumor capabilities at later stages [75, 76]. All the while the T_{Reg} cell population increases substantially [77].

In sum, immunosurveillance of cancer can broadly lead to three scenarios (Figure 3) [78]. First lies the possibility that effector immune cells will detect premalignant lesions and proceed to eliminate them. Second, if the balance between immune effector cells and their regulatory and suppressive counterparts is even, premalignant lesions could remain in equilibrium without further progression. Lastly, the balance could be shifted towards a more immunosuppressive and regulatory immune cell makeup, allowing thus premalignant lesions to escape immunosurveillance and progress to metastatic cancer.

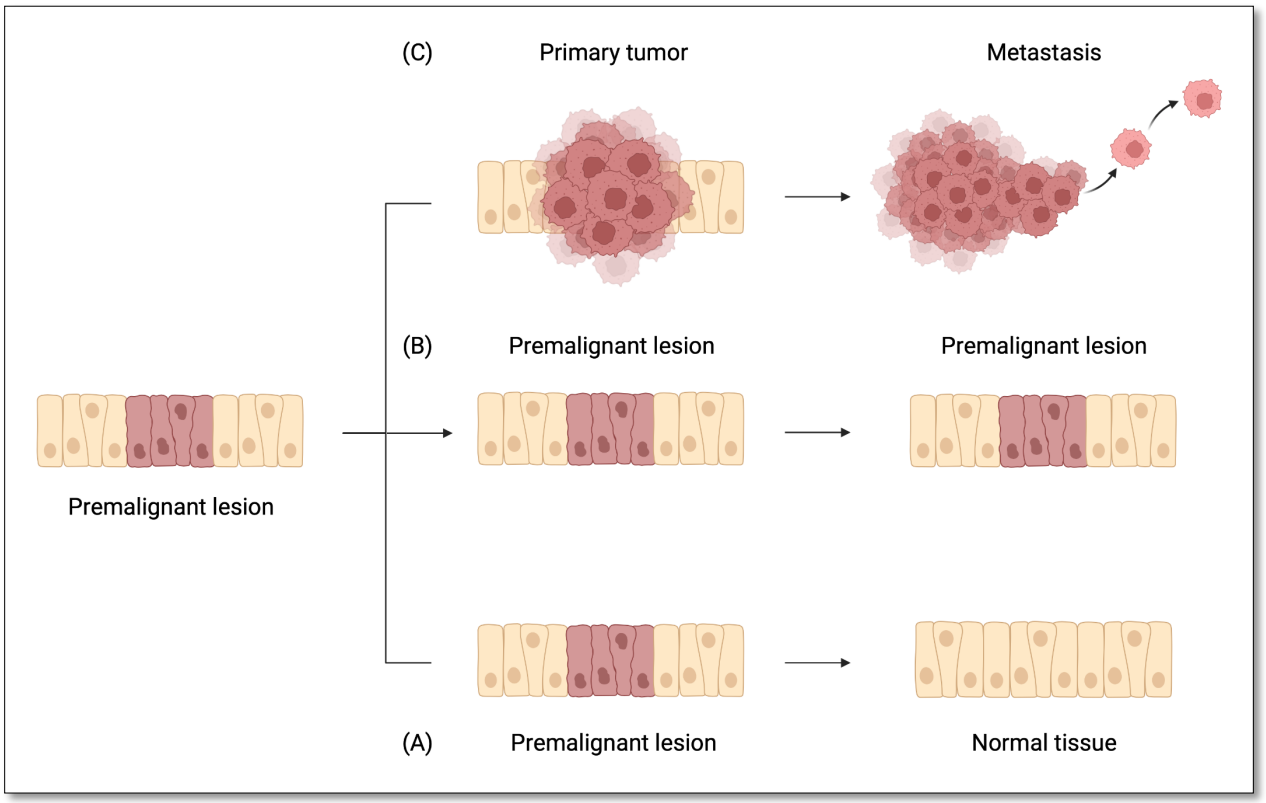

Figure 3 - Possible cancer development scenarios upon premalignant lesion formation

Schematic diagram displaying the three general pathways a premalignant lesion can follow: (A) If the lesion is recognized by cytotoxic immune cells the cancerous cells could be eliminated bringing the tissue back to a homeostatic state. (B) The premalignant lesion could also remain in equilibrium without further development. (C) Lastly, hyperplasia, dysplasia, and tissue invasion could take hold potentially leading to metastasis.

1.3.1 Natural killer cell-mediated immunosurveillance of cancer

Due to their innate ability to detect and kill transformed or infected cells, NK cells also participate in cancer immunosurveillance. However, NK cells appears best suited for controlling hematological cancers and tumor metastasis rather than solid tumors. For instance, clinical trials of adoptive transfer of allogeneic chimeric antigen receptor NK cells have provided positive responses in patients with chronic lymphocytic leukemia without meaningful toxicity [79]. In addition, the amount of circulating NK cells has been observed to negatively correlate with the metastatic burden of patients afflicted with carcinomas [80, 81], gastrointestinal sarcoma [82], melanoma [83], and breast cancer [84]. Conversely, the levels of NK cell infiltration found in solid tumors with epithelial barriers, such as colorectal cancer, have been significantly low [85].

As discussed above, the decision for NK cells to kill stems from the signal integration from a myriad of inhibitory and activating receptors on the cell surface. These signals can stimulate the killing of cancerous cells either directly or indirectly. On the one hand, direct cytotoxicity mediated by NK cells can come about from four different mechanisms: (1) Upon direct cell contact and receptor engagement, NK cells release cytotoxic granules containing granzyme and perforin to induce apoptotic cell death. A method that represents the predominant mode of action in the NK $CD56^{dim}$ population [86]. (2) Secondly, NK cells can also trigger apoptosis of tumor cells independent of cell-to-cell contact, by means of secreting TNF molecules that bind to tumor cell membrane ligands [87]. (3) Thirdly, engagement of the Fc receptor on NK cells with cancer cells opsonized by tumor reactive antibodies sets off ADCC [88]. (4) Lastly, NK cell secretion of IFN-γ can exert anti-tumor effects such as activation of adaptive immunity and inhibition of tumor angiogenesis [89].

NK cells can also stimulate anti-tumor responses by activating other immune cells, such as DCs, macrophages, B cells, and T cells. For instance, evidence suggests NK cells possess the potential to induce humoral immunity by stimulating B cell antibody production through IFN-y signaling [90, 91] and CD40 - CD40 ligand interactions [92].

Likewise, IFN-γ secretion from NK cells can also promote anti-tumor responses from the adaptive immune system through the induction of $CD8^+$ T cell expansion [93, 94] and T helper type 1 cell polarization [95]. Lastly, depending on the mode of cancer cell death induced by NK cells, the latter can stimulate DCs in different fashions [96, 97]. On the one hand, material derived from necrosis cell death may drive maturation of DCs. In comparison, the induction of apoptosis by NK cells on cancer cells provides DCs with antigen material that can later be processed and further presented to T cells, inducing an adaptive immune response [98]. Nonetheless, it is worth highlighting the bi-directionality of the NK-DC interaction, where DCs, for instance, provide cytokines such as IL-2, IL-15, CXCL8, and CCL3 at the injury site that promote further NK cell activation and recruitment [99].

1.4 Fibroblast growth factor binding protein 2 (FGFBP2)

Fibroblast growth factor (FGF) signaling plays a key role in several cellular processes such as regulation of cellular proliferation, differentiation, and cell migration. One of the mechanisms that modulate this pathway is the action of the fibroblast growth factor binding proteins (FGFBPs), which act as ligands to FGFs. Humans carry three different loci of the FGBP family: FGFBP1, FGFBP2, and FGFBP3 [100]. FGFBP2, or also known as killer cell secretory protein of 37kDa (Ksp37), is almost exclusively expressed in NK cells, $CD8^+$ T cells, γδ T cells, and $CD4^+$ T cells [101], and is the least characterized protein from the FGFBP family with an unknown function [102]. For clarity purposes and to avoid confusion with FGF2, the protein will be referred to as Ksp37 from this point onwards.

In humans, the Ksp37 gene resides in chromosome 4p16 and bears two exons that code for the Ksp37 protein (OMIM 607713). Composed of 223 amino acids, the calculated molecular mass of Ksp37 is 24,581 kDa, its transcription in-vitro, however, yields a protein of ~28 kDa [101]. Analysis of the Ksp37 primary structure has revealed nine potential O-glycosylation sites and a signal sequence for secretion in the N-terminus [100, 101] (Figure 4). By the same token, sequence homology based prediction has also identified a Heparin-binding domain for Ksp37 [103], as well as potential binding sites for FGF1 and FGF2 [103].

Additionally, immunoprecipitation and Western blot results of serum and cell lysate of Ksp37 expressing cells, has unveiled the presence of both 28 and 37 kDa variants within the cells, yet only the 37 kDa form was present in sera [101]. In perspective, these results suggest that Ksp37 is synthesized as a polypeptide of 28 kDa that is then posted transcriptionally modified and secreted into the extracellular space as a 37 kDa form.

Despite the lack of knowledge regarding the mechanism of action behind Ksp37, reports correlating its expression in humans with diverse conditions and prognoses have also been attempted. For instance, Ogawa et al. [101] have reported a transient increase of Ksp37 serum level in patients suffering from infectious mononucleosis during the early acute phase of Epstein–Barr virus (EBV) infection. Also, by means of weighted gene co-expression network analysis, Liu et al. [104] have found evidence for the potential use of Ksp37 as a biomarker for acute myocardial infarction diagnosis. In line with the latter, the lack of functional Ksp37 protein expression has been linked to congenital heart disease [105]. Lastly, Hayano et al. [106] noted Ksp37 serum levels rise during the last trimester of pregnancy, with the $CD16^{+}$ NK cells in the decidua of term placenta exhibiting the highest expression.

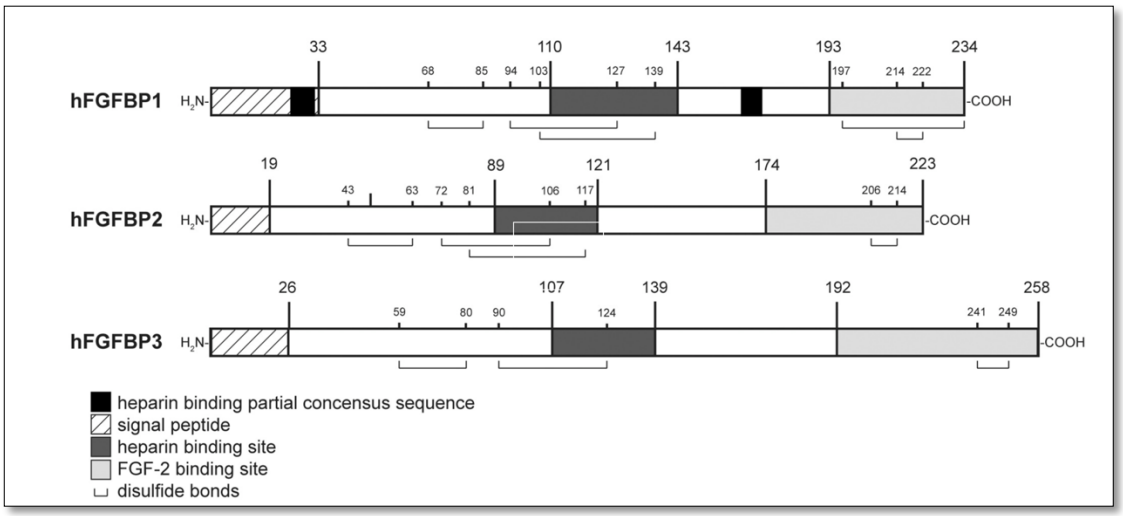

Figure 4 - Functional domains present in human FGFBP proteins.

The illustration depicts the heparin-binding sites for FGFBP2. FGF binding sites for FGFBP2 are predicted based on sequence homology. The signal peptide for secretion is also highlighted near the N-terminus. The aforementioned domains are aso conserved in FGFBP1 and FGFBP3. Numbers above domains indicate amino acids. Image adopted from [100].

1.4.1 Implications of fibroblast growth factors 2 in cancer development

There is mounting evidence of aberrant FGF signaling in the pathogenesis of several cancer types [107]. The latter, together in junction with the potential for FGFBPs to intervene during signaling events [100], and the almost exclusive expression of Ksp37 by cytotoxic lymphocytes [101], brings forward the question of whether Ksp37 takes part in some extent in the oncogenesis process, either as friends or foes.

Thus far, answers to the previous question have been limited. Notwithstanding, relevant interactions have been proposed. As is with the case of clear cell carcinomas of stage I, where Ksp37 mRNA levels were observed to be six to eight folds higher than in more advanced stages and strongly correlated with favorable prognosis [108]. Likewise, elevated Ksp37 expression has been observed to correlate positively with glioma patient survival [109]. Lastly, Ksp37 downregulation has also been found in colorectal cancer patients afflicted with postoperative intra-abdominal infection [110]. Thus, suggesting that the inflammatory environment created by postoperative infection could favor immune evasion of the tumor. All the above signs of Ksp37 involvement during immune response development.

1.5 Microfluidic-based tumor models

Conventional preclinical models in cancer research fall mainly within two categories: 2D in vitro cell and in vivo animal models [111]. Both approaches, however, bear substantial downsides. For instance, evidence has shown marked discrepancies between the average inhibitory effects (IC50) in monolayer cultures (2D) compared to the IC50 resulting from spheroids (3D) cultures [112]. Plausibly due to the difference in the uneven exposure to drugs and effector cells in the 3D setting, where inner cells have limited exposure to the treatments [111]. Concerning animal models, despite being highly valuable tools for capturing the complexity of in vivo interactions, they are labor-intensive, lack high throughput, and show only 8% concordance with clinical trial results [113, 114]. Not to mention the growing pressure the private sector, academia, and civil society have brought forward to phase out preclinical animal testing [115, 116].

In light of these challenges, the use of microfluidics in 3D models has emerged as an attractive alternative. The technology allows for the incorporation of variables such as interstitial fluid, cell-matrix interactions, and nutrient or drug gradients [117]. Thus, providing the possibility of mimicking the tumor microenvironment more closely than what is otherwise possible with 2D models.

One of the realms where microfluidics has shown the most success thus far has been organ-on-chip techniques. Recent advances in this regard have been able to recapitulate the micro-physiology and pathology of tissues and organs ranging from the lung [118] and kidney [119, 120] to more complex tissue such as the brain [121-123] and eye [124, 125]. These developments have also been deployed to strengthen the current understanding of oncogenesis and the metastatic cascade.

A notable example of the latter is found in the microfluidics system developed by Ni et al., capable of modeling the migration and intravasation through the endothelial barrier of cancer cells under flow conditions [126]. Potentially, if similar platforms are further developed, the entire metastatic process could be laid out. Beginning at the initial invasion/intravasation phase, passing through migration, extravasation, and angiogenesis, and concluding with the metastatic niche establishment [127]. Notwithstanding, there are some challenges ahead the technology needs to overcome before widespread integration within the clinical setting pharmaceutical industry takes place. Perhaps the incorporation of complex signal responses from nonadjacent organs constitutes the hardest challenge [111], although advances in chip manufacturing standardization and exploration of new biocompatible materials would signify meaningful steps forward [111].

1.6 Aim of the study

The central hypothesis is that Ksp37 levels in proximity to the tumor microenvironment have a cytotoxic effect on cancer cells. Previous studies on gene expression have found positive correlations between Ksp37 and overall survival rates in glioma and ovarian carcinoma patients [108] [109]. However, evidence of the function at the protein level remains unsolved.

Therefore, the overarching theme of the project is to shed light on the direct implication Ksp37 levels bear over cancer cell migration and invasion. Thus, the specific aims are as follow:

I. Establishing cellular and molecular tools to study Ksp37 biology
II. Generate a reliable microfluidics setup to assess migration behavior changes of PANC-1 cells in response to different concentrations of extracellular Ksp37.
III. To harness collected information in junction with data from previous experiments in Malmberg's lab to produce a cohesive proposal of Ksp37 mode of action.

2 Methods

2.1 Cell lines

2.1.1 NK-92 cell lines

IL-2-dependent NK cell line (ATCC, #CRL-2407) derived from peripheral blood mononuclear cells of a 50-year-old male patient with progressive non-Hodgkin's lymphoma. A $CD56^{bright}$ phenotype and the lack of most known KIR inhibitory receptors distinguish this cell line [128]. The latter in junction with the expression of adhesion molecules and activating receptors (NKp30, NKp46, 2B4, NKG2D/E, CD28), account for the broad cytotoxicity displayed by NK-92 cells [128]. Three different NK92 cell lines were employed along the thesis as detailed in Table 1.

Table 1 - NK92 cell lines

Cell line	***Description***
NK-92 Wild type (wt)	Wild type NK 92 cell lines as received from the manufacturer.
NK-92 V51	Green fluorescent protein (GFP) - KSP37 insert transduced into NK-92 wt cells.
NK-92 V84	Six histidine (His) - KSP37 insert transduced into NK-92 wt cells.
NK-92 V85	Ksp37 - His insert transduced into NK-92 wt cells.

All expression cassettes for stably transfected NK-92 cell lines were inserted into BamHI_NotI sites of pScalps_puro vector, designed by Silje Krokeide, senior engineer at Malmberg's Group, and synthesized by Genscript Biotech Corp. Transduction and clonal expansion was carried by Silje Krokeide.

2.1.2 Panc-1 cell lines[2]

Human pancreatic cancer cell line isolated from a 56-year-old male with epithelioid carcinoma of ductal cell origin [129]. Panc-1 cells migrate primarily as singles cells and hold great capacity for motility and invasiveness [129]. The cell line used in the present project was donated from Fate Therapeutics, Inc. (San Diego, CA) to the Malmberg's Group. Two different Panc-1 cell lines were employed along the thesis as detailed in Table 2.

Table 2 - Panc-1 cell lines

Cell line	***Description***
Panc-1 wt	Wild type Panc-1 cell line
Panc-1 FGF2 $^{-/-}$	Panc-1 cell line with CRISPR/Cas9-mediated biallelic knockout of the FGF2

2.1.3 K562 cell line[2]

The K562 (ATCC, #CCL-243) are non-adherent lymphoblast cells isolated from the bone marrow of a 53-year-old patient afflicted with chronic myelogenous leukemia. These cells display a round morphology and are positive for the bcr-abl fusion gene [130]. Only the wild type K56 was used for experiments.

2.1.4 U20S cell line

Human bone osteosarcoma cell line derived from the tibia of a 15-year-old male female with osteosarcoma. Cell line characterized by its fibroblastic morphology and high chromosomal alteration [131]. Both U2OS cell lines used in the present project were donated from Jørgen Wesche's Group (OUS) to the Malmberg's Group Table 3.

Table 3 - U2OS cell lines

Cell line	***Description***
U2OS wt	Wild type U2OS cell line
U2OS FGFR1	Stably transfected cell line with Fibroblast growth factor receptor 1 (FGFR1)

2.2 Cell culture

Panc-1 and U2OS cells were cultured as adherent monolayers in sterile tissue culture flasks (Thermo Scientific, #156472) and incubated at 37 0C with 5% CO2 in a humidified incubator. Split of cells was performed twice a week once they reached ~85% confluency. The growth media composition used for each cell line is detailed in Table 4.

[2] Cells stably labeled with IncuCyte® NucLight Red (Essen, #4625) for red fluorescence.

The procedure was as described: Media was removed, and cells were washed once with Phosphate Buffered Saline (PBS, #MT21040CV), followed by the addition of trypsin-EDTA (Sigma, #T4049) for 5 to 7 minutes at 37 °C. After cell detachment, trypsin was inactivated with 1:1 volume of cell media, followed by centrifugation at 400 x g for 4 minutes. Next, the supernatant was removed and 500 µl was aliquoted in case a mycoplasma test was required. The cell pellets were resuspended in standard culture media and sub-cultured at 1:4 or 1:5 rations depending on confluency before the split.

Table 4 - Growth media used for cell line culture

Cell line	***Growth Media***	***Supplements***
NK-92	MEM α (Gibco, # 12571063)	12.5% fetal bovine serum (FBS, Sigma #F7524), 12.5% of horse serum (HS, Gibco #26050088), 100 U/mL of Penicillin-Streptomycin (Gibco, # 15140122), 2mM of L-glutamine (Gibco, #25030081), 250 µg of Amphotericin B (Gibco, #15290018), and 200 U/mL of IL-2.
Panc-1 / K562	RPMI 1640 (Lonza, # BE12-115F)	10% heat inactivated FBS (FBS, Gibco #26140079) and 100 U/mL of Penicillin-Streptomycin (Gibco, # 15140122).
U20S	Advanced DMEM (Sigma, # D8437)	10% heat inactivated FBS (FBS, Gibco #26140079) and 100 U/mL of Penicillin-Streptomycin (Gibco, # 15140122).

NK-92 cells were maintained in suspension in sterile tissue culture flasks (Thermo Scientific, 156472) with growth media described in Table 4. Split was performed 3 times a week as follows: The cell suspension was transferred to a falcon tube and centrifuged at 300 x g for 4 minutes. The supernatant was removed and 500 µl was aliquoted in a 1.5 mL Eppendorf in case a mycoplasma test was needed. Cells were then resuspended in growth media and counted twice with counting slides using 10 µl of 1:1 mixture of cell suspension and trypan blue (NanoEntek, #EVS-050). Thereupon cells were sub-cultured at a confluency of 3 x 10^5/mL and IL-2 was added according to the final culture volume.

2.3 Isolation of peripheral blood mononuclear cells

Buffy coats were purchased from healthy donors at the Oslo University Hospital Blood Bank. To extract peripheral blood mononuclear cells (PBMCs), 35 mL of peripheral blood was poured into a 50 ml falcon tube containing 10 mL of PBS, and then transferred to a 50 mL fretted spin tube (# 85450, Stemcell Technologies) with 9 mL of Lymphoprep (Axis-Shield).

The tubes were then centrifuged at 1200 x g for 10 min with the break set at level 1 out of 9. Next, the supernatant in the upper layer of the tube containing the diluted plasma was discarded. The white layer with the buffy coat in the middle of the tube was then transferred to a new sterile 50 mL tube, washed once with PBS, and centrifuged at 200 x g for 8 minutes. The resulting supernatant was discarded, and the pellet containing the PBMCs was resuspended in 30 mL of RPMI 1640 (Lonza, #BE12-115F) supplemented with 10 % FBS (Gibco, #26140079) and 100 U/mL of Penicillin-Streptomycin (Gibco, # 15140122), transferred to a T75 flask and placed in the cell incubator. A depiction of layers generated by the density gravity centrifugation can be found in Figure 5.

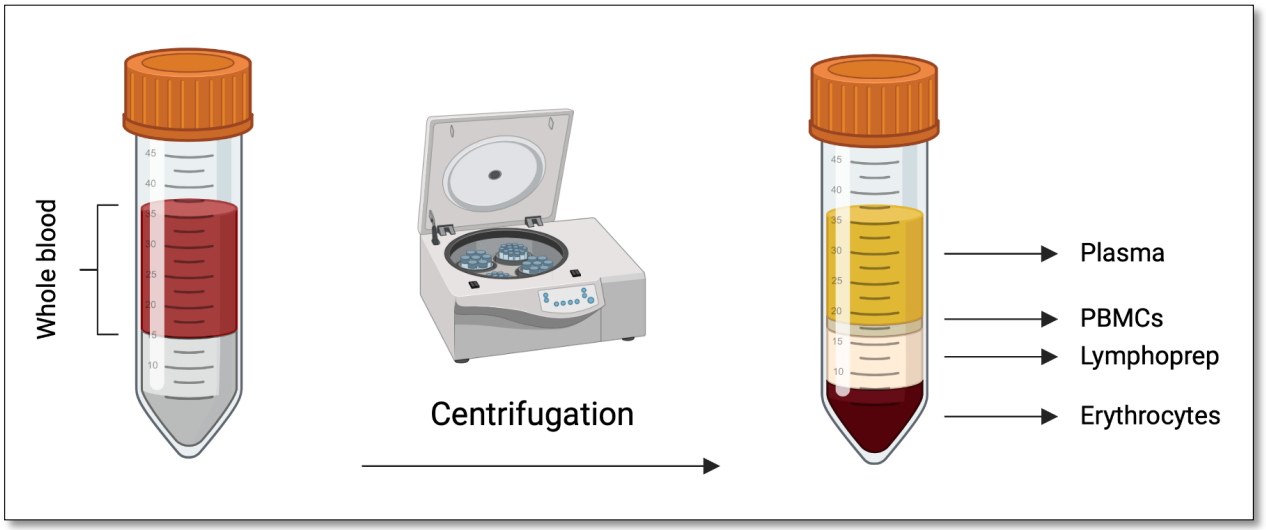

Figure 5 - Layered blood after a density gradient centrifugation

Illustration of the layers resulting from density gradient centrifugation. The tube on the left represents the diluted whole blood in PBS. While on the right is found a representation of the layer obtained after centrifugation.

2.3.1 Natural Killer cell isolation

NK cells were isolated from PBMCs with the human NK isolation kit from Miltenyi and AutoMACS Pro Separator (Miltenyi Biotech), following the protocol provided on Miltenyi's website [132]. After isolation, the cells were counted as previously described (2.2) and resuspended at a concentration of 2M cells/ml and seeded in 6-well plates (Thermo Scientific, # 140675) in RPMI 1640 (Lonza, #BE12-115F) supplemented with 10 % FBS (Gibco, #26140079), and 100 U/mL of Penicillin-Streptomycin 100 U/mL of Penicillin-Streptomycin (Gibco, # 15140122). NK cells were then rested overnight prior to use in experiments.

2.4 Flow cytometry

2.4.1 Cell staining

The desired number of PBMC-derived NK cells or NK-92 were resuspended in 200 ul of staining buffer (PBS with 2% FCS and 2mM EDTA) and plated in a V-shaped-bottom 96-well microplate (Falcon, #353263). Next, for the surface staining, cells were spun down at 500 x g for 4 minutes and resuspended in 50 µl of staining buffer with fluorochrome-conjugated antibodies and a dead-cell marker (Invitrogen, #L34957), followed by a 20-minute incubation at room temperature. The detailed information as well as concentrations used for each antibody and the dead-cell marker can be found in Table 5. After incubation for the surface staining, cells were washed twice with staining buffer, continued by fixation and permeabilization using BD Cytofix/Cytoperm (BD Bioscience, #554714).

Table 5 - List of antibodies used for Flowcytometry

Marker	***Fluorophore***	***Manufacturer***	***Catalog number***	***Concentration***
CD56	APC	BD Bioscience	IM2474U	(1:50)
Ksp37	PE	BioLegend	346603	(2:50)
Anti-His	FITC	Abcam	ab1206	(1:50)
Live/Dead (Aqua)	-	Invitrogen	L34957	(1:200)

Cells were then washed once with 1x BD Perm/Wash (BD Bioscience, #554714). Afterward, cells were resuspended in 50 µl of the intracellular staining mix of Perm/Wash with fluorochrome-

conjugated antibodies and incubated for 30-minute incubation at 4°C. After incubation, the cells were washed twice with Perm/Wash, resuspended in staining buffers, and immediately run on an LSRII flow cytometer. Cells were then run immediately on an LSRII flow cytometer (BD Bioscience). FlowJo version V10.8.1 was used for data analysis.

2.4.2 Cytokine incubation

Treatment media was prepared with a combination of cytokines IL-2 (200 U/mL) and IL-15 (10 ng/mL), in the presence or absence of Brefeldin A (BFA) (1 µl/mL of cell culture, BD Bioscience - 555029). PBMC-derived NK cells or NK-92 cells were then counted as previously described (2.2), spun down at 300 x g for 4 minutes, and resuspended at a concentration of 4 x 10^5 cells/mL with the desired treatment media. All cytokine incubation experiments were performed on 24-well plates (Corning, 3524) with a total volume of 2 mL cell suspension per replicate.

2.5 Cancer-on-a-Chip model

The chips used during the present thesis project were designed and manufactured by the Hybrid Technology Hub (HTH) from the University of Oslo. They are composed of several laser-structured polymethylmethacrylate films thermally bonded together. A visual representation of the chips used can be found in Figure 6.

The concept behind HTH's platform relies on pump-less chips with a unidirectional flow, set within a closed microfluidic circuit [133]. The flow is generated by the placement of the chips over a standard laboratory rotator (3D rotator waver, VWR Avantor, USA), where the rate of flow is tuned by the volume within the channels as well as the tilt and speed of the rotating platform. This layout grants key advantages over pump-driven platforms. For instance, air bubbles are confined to the reservoirs (Figure 6 (c)), avoiding channel blockages and minimizing cell death.

Furthermore, unlike pump-driven systems, these chips do not require flow control units and connecting tubes, providing a higher degree of scalability and lower implementation costs. Finally, another notable advantage is that polymethylmethacrylate does not absorb small molecules to the extent other commonly used materials do such as Polydimethylsiloxane [134].

Detailed information about the design, testing, and fabrication process of the chips can be found in the recent publication by Busek et al [133].

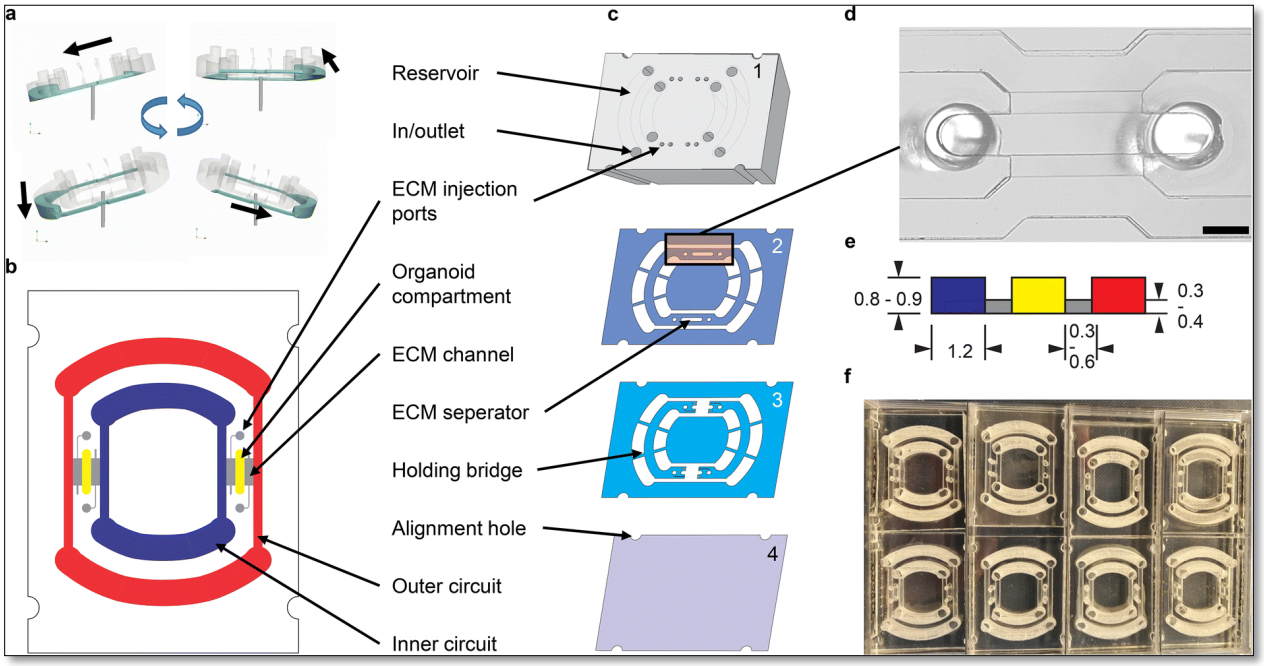

Figure 6 - Chip platform layout

a) Fluid movement generated by the 3D-tilting motion of the rotating platform. b) View from the top of the chip with the two circuits (Red: outer channel, blue: inner channel), the extracellular matrix (ECM) in gray, and the organoid chamber in yellow. c) Layered view of the chip. d) Microscopic view of the organoid chamber. Scale bar: 1 mm e) Cross-section of the chip with corresponding dimensions in mm. f) representative image of chips used in experiments. Adopted from [133].

2.5.1 Spheroid production

Tumor spheroids production was performed employing agarose microwells. 1% weight/volume agarose was diluted in PBS and melted in the microwave. The mixture was then poured into two wells of a 6-well plate, a 3D printed microwell stamp was subsequently set on top of the agarose mixture, and the gel was let to polymerize. In each given experiment, the wells employed were placed symmetrically for an even distribution of cells. The gel was then left to polymerize for ~ 20 minutes, washed twice with 2 mL of PBS, and incubated with 2 mL of panic-1 growth media for 30 minutes at 37 °C.

Media was then removed, and 750 µl of single-cell suspension of Panc-1 cells was added to each well. The cell concentration for the experiments was of 1.64 x 10^5 / mL. Cells were then spun down at 100 x g for 2 minutes, and the supernatant was afterwards carefully removed. Lastly, 2 mL of growth media was added to each well with spheroids, and the plate was transferred to a humidified incubator. Spheroids were grown for a lapse of 10 days.

2.5.2 Spheroid seeding and incubation

Prior to spheroid seeding, the chips were washed with 60% ethanol and dried under UV light for 15 minutes. On the 10th day of culture, the spheroids were removed from the microwells by carefully pipetting up and down and transferred to 0.5 mL Eppendorf tubes. After the spheroids were sedimented on the bottom of the tubes, the growth media on top was removed, leaving only ~5 µl. Next, 30 ul of Geltrex (Gibco, #A1413301) was added to resuspend the organoids. 15 µl of the Geltrex with spheroids was then transferred to each organoid chamber on the chip through the injection ports using a 20 µl filter pipet.

This process was repeated for each chip replicate. The channels were then filled either with Panc-1 media or single-cell suspension containing PBMC-derived NK cells or NK-92 cells at a concentration of 4 x 10^5 / mL and incubated for 39 hours. In all experiments the volumes introduced in the outer channel was of 350 µl and of 200 µl for the inner channel.

2.6 Immunofluorescence

2.6.1 Spheroids on the chip

Chips were washed once with PBS, followed by the addition of 4% paraformaldehyde (PFA). After incubation at room temperature for 20 minutes, the PFA was discarded, and the chips were washed twice with PBS for 10 minutes each time. Spheroids were then permeabilized with 10% FBS, 0.2% Triton-X100 solution (Sigma, #9036-19-5), and 1% dimethyl sulfoxide (DMSO) in PBS at room temperature for 2 hours. Chips were then washed twice with PBS for 5 minutes and stained overnight at 4°C with primary antibodies diluted in a solution of 1% FBS and 0.1% TritonX-100 in PBS. Detailed primary antibody layout can be found in Table 6.

Table 6 - Primary antibodies for spheroid staining

Marker	*Dilution*	*Final concentration*	*Host specie*	*Manufacturer*
E-cadherin	1:200	0.2 mg/mL	Goat	R&D systems (#AF748)
Caspase-3	1:200	1.544 mg/ml	Rabbit	Abcam (#ab32042)
DAPI	1:100	1 mg/ml	-	Invitrogen (#D1306)

On day 2 the chips were washed 3 times with PBS for 15 minutes. The spheroids were then stained for 2 hours at room temperature with secondary antibodies and DAPI stain in a solution of 1% FBS and 0.1% TritonX-100 in PBS. Lastly, secondary antibodies were aspirated, and the chips were washed 3 times with PBS. Samples were then either stored at 4 °C or immediately taken for imaging. The Volumes used in all cases were of 200 µl for the inner channel and 300 µl for the outer channel. Detailed Secondary antibody layout can be found in Table 7.

Table 7 - Secondary antibodies for spheroid staining

Target	*Dilution*	*Final concentration*	*Fluorophore*	*Manufacturer*
Anti-goat	1:200	2 mg/mL	AF488	Invitrogen (#A32814)
Anti-rabbit	1:200	2 mg/ml	AF635	ThermoFisher (#A-31577)

2.6.2 Cell cultured on coverslips

For the FGF2 secretion experiments, Panc-1 cells were counted and seeded on a µ-slide 18-well coverslip (ibidi, #81816) at a density of $0.01x10^6$ cells/mL. The coverslip was then kept in the incubator overnight to allow cell attachment.

On the second day, the media was removed and the cells were washed once with PBS. Cells were then fixated with 4% PFA for 10 min at room temperature, followed by two washes with PBS for 1 minute. Afterward, the cells were stained with unconjugated anti-FGF2 (Invitrogen, #MA1-24682, Mouse) for 20 minutes at 4°C in a solution of 10% FBS in PBS. Cells on the coverslips

were then washed three times with PBS for 1 minute and immediately incubated with DAPI (Invitrogen, #D1306) and anti-mouse antibody conjugated with Alexa Fluor® 647 (Jackson ImmunoResearch, #115-605-003) in a solution of 1% FBS in PBS for 15 minutes. After incubation, the cells were washed three times with PBS (1 minute/wash) and stained with CellBrite Cytoplasmic Membrane Dye (Biotium, #30021) according to the protocols provided by the manufacturer for labeling fixed cells. Lastly, stained cells were stored overnight at 4 °C and taken for imaging the day after.

2.7 CRISPR gene knockout

Synthetic guide RNAs (sgRNAs) targeting the FGF2 gene and the Cas9 protein were ordered from Synthego (Synthego V2-kit). The electroporation procedure was followed according to the protocol for Panc-1 cells provided by Lonza (SE Cell Line 4D-Nucleofector™ X Kit S, #: V4XC-1032) [135]. The position of the sgRNAs on the FGF2 gene are found in Figure 7, whilst the guide sequences are attached on the Appendix (5.1.1).

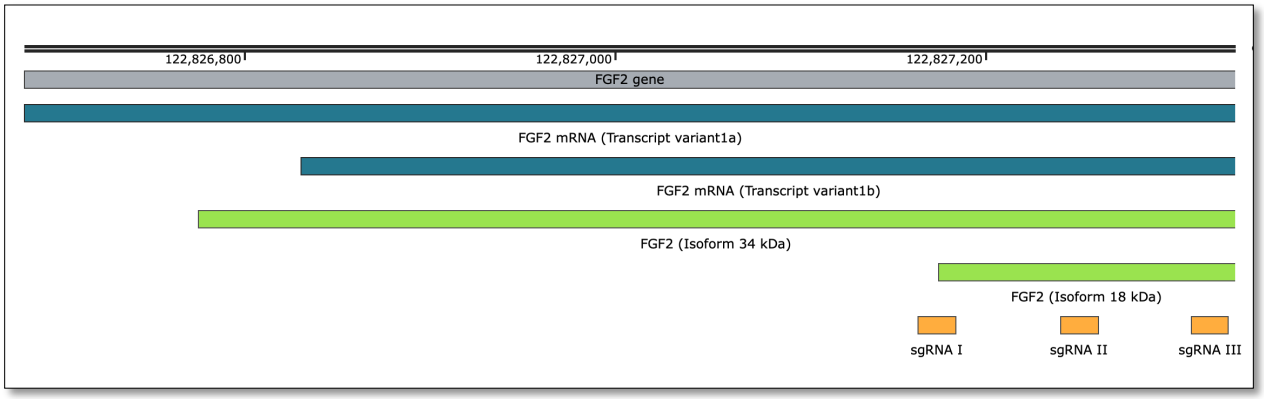

Figure 7 - sgRNAs binding sites on the FGF2 gene

Depiction of sgRNAs targeting the FGF2 gene on exon 1 (in gray). Their position (orange) is such that the Cas9-sgRNA complexes (RNPs) generate double-strand breaks encompassing both the mRNA transcripts (dark blue), as well as the respective peptide sequences (green).

The summary of the procedure was as follows: sgRNAs and Cas9 (ribonucleoprotein, RNP) were assembled at a 9:1 ratio in an Eppendorf tube according to Table 8. RNPs were then incubated for 10 minutes at room temperature. Panc-1 cells were next counted and resuspended at a density of 1.5 x 10^5 cells / 5 µl in electroporation buffer (Lonza, SE Cell Line Nucleofector Solution).

The 5 µl cell suspension was added to 15 µl of assembled RNP and transferred to a single well of a 16-well strip nucleocuvette. The latter was then placed in the core unit of a 4D-Nucleofector (Lonza, #AAF-1003X) and run with pulse code CK-116. At the end of the run, cells were recovered by adding 80 µl of pre-warmed Panc-1 media and pipetting up and down, followed by transfer to a 12-well plate for culture with a total of 1.5 ml of growth media. Cells were cultured for 5 days until enough material was available for genotyping.

Table 8 - RNP assembly solution

Component	**Volume (µl)**
Electroporation buffer	8
sgRNA (100 pmol/µl)	1.8
MQ water	4.2
Cas9 (20 pmol/µl)	1
Total volume	***15***

2.7.1 gDNA isolation of FGF2$^{-/-}$ Panc-1 cells

Approximately 0.5 x 10^5 cells were pelleted, and genomic DNA (gDNA) isolation proceeded according to the NucleoSpin Tissue protocol (Macherey-Nagel, # 740952.50) [136]. gDNA was eluted in 50 µl of MQ water and stored at 4 °C prior to use for polymerase chain reaction (PCR). A NanoDrop ND-1000 UV-Vis spectrophotometer (ThermoFisher) was used to estimate gDNA quality with a required minimum DNA concentration of 50 ng/µl and the 260/280 and 260/230 ratios of > 1.8.

2.7.2 Genotyping of FGF2$^{-/-}$ Panc-1 cells

Forward and reverse genotyping primers were designed by Snap Gene V. 6.2.2., and placed flanking the sgRNAs binding sites (Figure 6). Their respective sequences as well es relevant features can be found on the Appendix (5.1.2). Phusion high-fidelity DNA polymerase (New England Biolabs, #M0530) was used for the PCR. The components of the reaction setup (5.1.3), as well as the cycling conditions (5.1.4), can be found on the Appendix.

Gel electrophoresis with the PCR product was run on a 1.5% agarose gel and imaged on an iBright CL1500 imager (ThermoFisher, #A44114). gDNA from Panc-1 wt cells was used as control. Lastly, samples with clear gel bands were purified according to the manufacturer's protocol (Macherey-Nagel, #740609.250) and sent for sanger sequencing provided by Eurofins Genomics (Germany). Incoming sequences were analyzed with Synthego ICE Analysis tool.

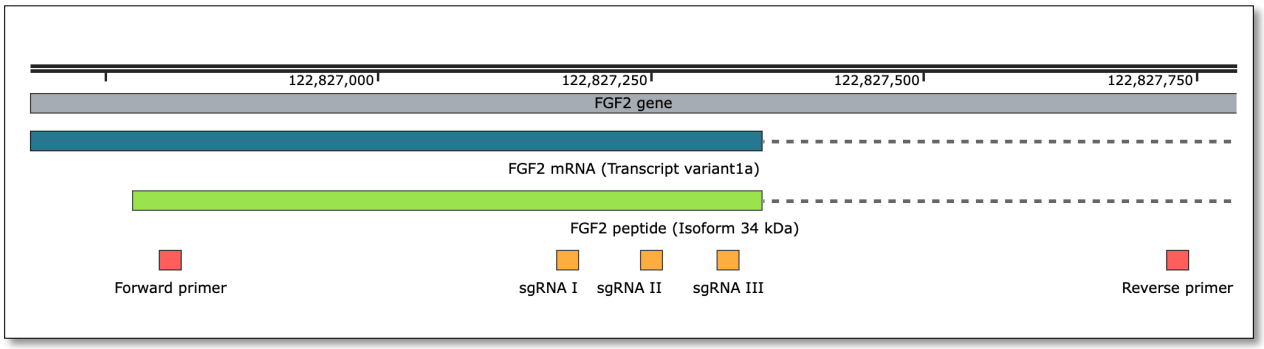

Figure 8 - Positions of FGF2 -/- genotyping primers

Primers (in red) flanking the sgRNAs with a theoretical amplicon size of 903 base pairs. Adapted from Figure 7.

2.8 Western Blot

2.8.1 Cell lysate generation

Panc-1 wt and Panc-1 FGF2$^{-/-}$ cells were spun down at room temperature for 5 minutes and the supernatant was discarded. This step was repeated once with PBS. RIPA lysis buffer (Pierce, #89900) was then added at a concentration of 0.1 x 10^5 cells/µl, cells were then gently resuspended with a pipette and incubated on ice for 30 minutes.

Afterward, cells were disrupted by vortexing, and homogenization with a 22-G needle, followed by another incubation on ice for 30 minutes. Lastly, the lysate was centrifuged at 10 000 x g for 10 minutes at 4°C. The supernatant containing the protein was transferred to a new 1.5 mL Eppendorf tube and stored at -80°C freezer or taken directly for measuring protein concentration.

2.8.2 Protein concentration measurement

Protein standard preparation with a working range of 125 - 2000 µg/ml was prepared according to the manufacturer's instructions (Pierce, #23275). 10 ul of sample and standards were both pipetted into a flat-bottom 96-well plate in replicates. 200 ul of the WR reagent (Pierce, #23275) was added to each used well. Three additional wells containing only RIPA lysis buffer were included for background subtraction. The plate was then incubated at 37°C for 30 minutes, and the results were obtained using an absorbance microplate reader (Tecan, Sunrise).

2.8.3 Gel electrophoresis and blotting

Samples were prepared by diluting the protein lysates with MQ water such that the protein concentrations were equal among them. The total volume per sample was 20 µl. 5 ul of sample buffer (Invitrogen, #NP0008) and 2 µl of reducing agent (Invitrogen, #NP0009) were added and heated at 70°C for 10 minutes. Next, the tubes were quickly spun down and applied to a NuPage Bis-Tris 4 – 12% gradient gel (Invitrogen, #NP0322BOX). 5 µl of protein standard was also applied (Invitrogen, #LC5925) to help estimate the size and concentration of the proteins separated in a gel.

The gel electrophoresis was run at constant volt (150V) for ~ 1 hour in a gel chamber (Invitrogen, #EI0001). Immediately after, the gel was placed in a dry blotting transfer stack (Invitrogen, #IB401002) and carried into an iBlot2 dry blotting device (Invitrogen, #IB21002S) for protein transfer. The transfer was confirmed by the presence of the ladder on the nitrocellulose membrane.

2.8.4 Antibody detection and enhanced chemiluminescence visualization

The nitrocellulose membrane was blocked for 1 hour at room temperature with 5% non-fat skimmed milk in tris-buffered saline (TBS) with 0.1% Tween (Sigma, #9005-64-5). Incubation with primary antibodies was overnight at 4C and with secondary antibodies for 2 hours at room temperature. The membranes were washed three times for 5 minutes with 0.1% Tween - TBS in between antibody incubations. After the last wash, the SuperSignal West Dura chemiluminescence substrate was added (ThermoFisher, #34075), and signals were detected with an iBright CL1500 (ThermoFisher, #A44114). Primary and secondary antibodies used for western blot are detailed below (Table 9).

Table 9 - Antibodies used for western blot experiments

Target	*Dilution*	*Host*	*Conjugate*	*Manufacturer*
Anti-FGF2	1:2000	Mouse	Unconjugated	Invitrogen (#MA1-24682)
Anti-FGFR1	1:1000	Rabbit	Unconjugated	Cell signaling (# 9740)
Anti-mouse	1:10 000	Horse	HRP	Cell signaling (#7076)
Goat anti-Rabbit	1:10 000	Goat	HRP	Invitrogen (#31460)

2.9 Reverse transcription-quantitative PCR

RNA purification proceeded according to the RNeasy Micro Kit protocol (Qiagen, #74004). The amount and quality of RNA were estimated with a NanoDrop ND-1000 UV-Vis spectrophotometer (ThermoFisher). A ratio of 2 - 2.2 was considered satisfactory for both ratios 260/280 and 260/230.

RNA samples were diluted with RNase-free water (Qiagen, #74004) to 100 ng of total RNA in 2 µl. MQ water was used as a negative control in all experiments. Each sample was diluted 10-fold five times in total for standard curve generation. KiCqStart One-Step Probe (Sigma-Aldrich, #KCQS07) was used for the reverse transcription-quantitative PCR (rt-qPCR) assay, with TaqMan probes labeled with a fluorescein amidite (FAM) dye targeting the genes of interest (FGF1 – FGF2) (ThermoFisher, #4331182), and with VIC-labeled probes targeting the gene of reference Beta-2 microglobulin (B2M) (ThermoFisher, #4448489).

The composition of each reaction used for the experiments and the cycling conditions can be found in the Appendix (5.2.1-5.2.2). Samples were then transferred to a transparent 96-well PCR plate (Labcon, #3977-520-000-9, sealed, and performed with an Applied Biosystems 7500 real-time PCR system (ThermoFisher). The results were analyzed in Microsoft Excel using the delta cycle threshold (Ct) method.

2.10 Incucyte killing Assay

A day prior to the start of the experiment (Day -1), a 96-well flat bottom plate (ThermoFisher, #165306) destinated for killing assays with the K562 cell line, was coated with 50 µl/well of a

0,01% poly-L-ornithine solution (Sigma, #P4957), and incubated at room temperature for 1 hour. The solution was then removed from the wells and the plate was allowed to dry for 40 minutes. K562 cells were subsequently counted as previously described, resuspended at a density of 0.05 x 10^5 / 100 µl of media, added to the coated wells and transferred to an incubator for attachment overnight.

On day 0, Panc-1 cells were counted and resuspended at a density of 0.10 x 10^5 / 100 µl of media. The cells were then transferred to uncoated wells and let to adhere for 2 hours at 37°C. On the same day, the NK-92 cells (effector cells) were counted and resuspended at concentrations of 0.20 x 10^5 / 100 µl, 0.50 x 10^5 / 100 µl, or 1.00 x 10^5 / 100 µl, corresponding to the effector-target ratios (ET) of 2:1, 5:1 and 10:1 respectively. In addition, each ET ratio was treated with or without cytokines: IL-2 (500 IU) and IL-15 (10 ng/mL). 100 µl of effector cells were seeded into the appropriate wells and left at room temperature for 15 minutes to allow for even settling of the cells.

The plates were then placed into an IncuCyte live-cell analysis system (Sartorius, #4647) and scheduled for scan intervals of 1 hour for a total of 39 hours. The images were taken in replicates for each given well. For all experiments, the measurements were based on total red object integrated intensity per image (RCU x µm²/Image) retrieved from either Panc-1 or K562 target cells stably transfected with IncuCyte® NucLight Red (Essen, #4625). Lastly, the results were analyzed with the IncuCyte Basic Analyzer software according to the instructions provided by the manufacturer. Experiments with each target cell line (Panc-1 or K562) were analyzed with the same parameters.

2.11 Statistical analysis

All quantitative data are presented with respective statistical tests dependent on normality of distribution. The significance was set as $p < 0.05$, and analysis carrier in Prism 9 version 9.5.1 (GraphPad, USA).

3 Results

3.1 Confirmation of FGF1 and FGF2 mRNA transcription in the Panc-1 cell line

According to published data, the Panc-1 cell line is positive for FGF1 and FGF2. Nonetheless, cell lines can display phenotypic variation depending on the source and conditions they have been acquired from [137]. Therefore, RNA base levels of expression for both genes were analyzed through rt-qPCR.

For this purpose, standard curves were established for each target gene and the corresponding housekeeping gene B2M (Figure 10,Figure 11). In both cases the R^2 coefficient obtained was > 95%, indicating an appropriate fit of the experimental data onto the linear regression. To estimate the relative expression of FGF1 and FGF2 to B2M the delta cycle threshold (Δ Ct) method was employed. However, the difference in Ct values for B2M among the 10-fold dilutions was not close to the expected 3.32 in all cases [3]. Therefore, for the Δ Ct calculation, dilutions 1:1 and 1:10 were chosen based on the overall closest approximation to 3.32: 3.10 for samples amplified for B2M and FGF1 and 2.36 for B2M and FGF2 (Figure 9).

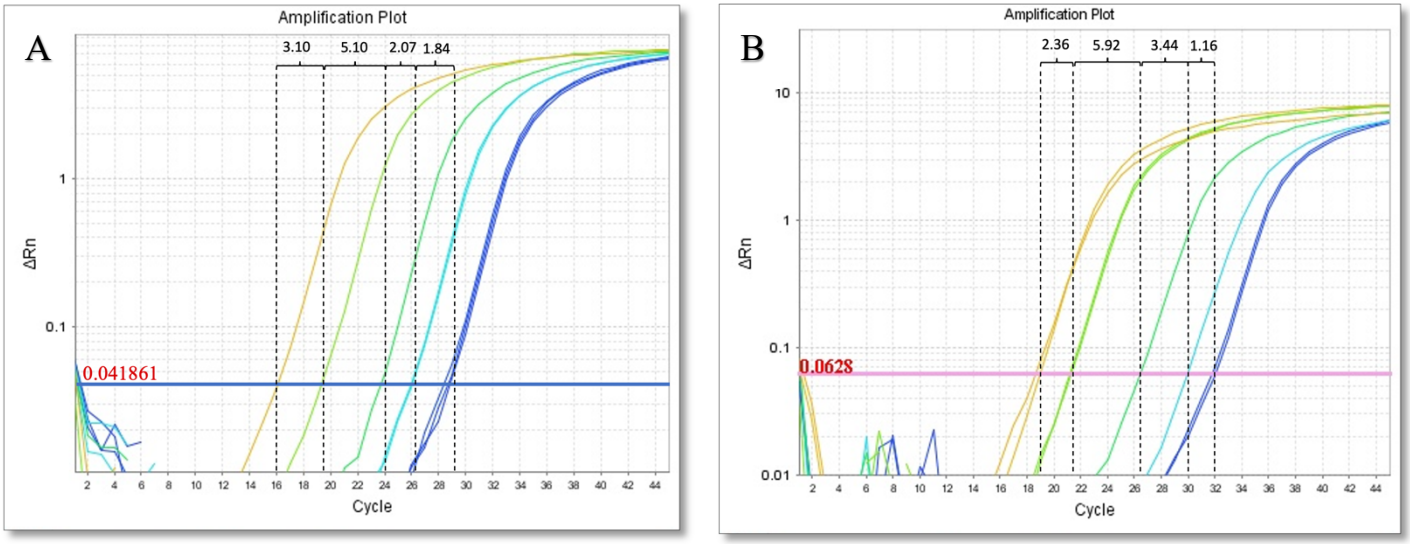

Figure 9 - B2M amplification curves

Amplification curves for the housekeeping gene B2M run with FGF1 (A) and B2M run with FGF2 (B). Dilutions from left to right, with curves for non-diluted samples in yellow (left), and the highest dilution in dark blue (1:10 000, right). Dotted lines mark the points used for calculating differences in Ct. In red is the signal threshold for each sample.

[3] 3.32 difference in Ct between the 10-fold dilutions assumes 100% primer efficiency and DNA duplicating each cycle.

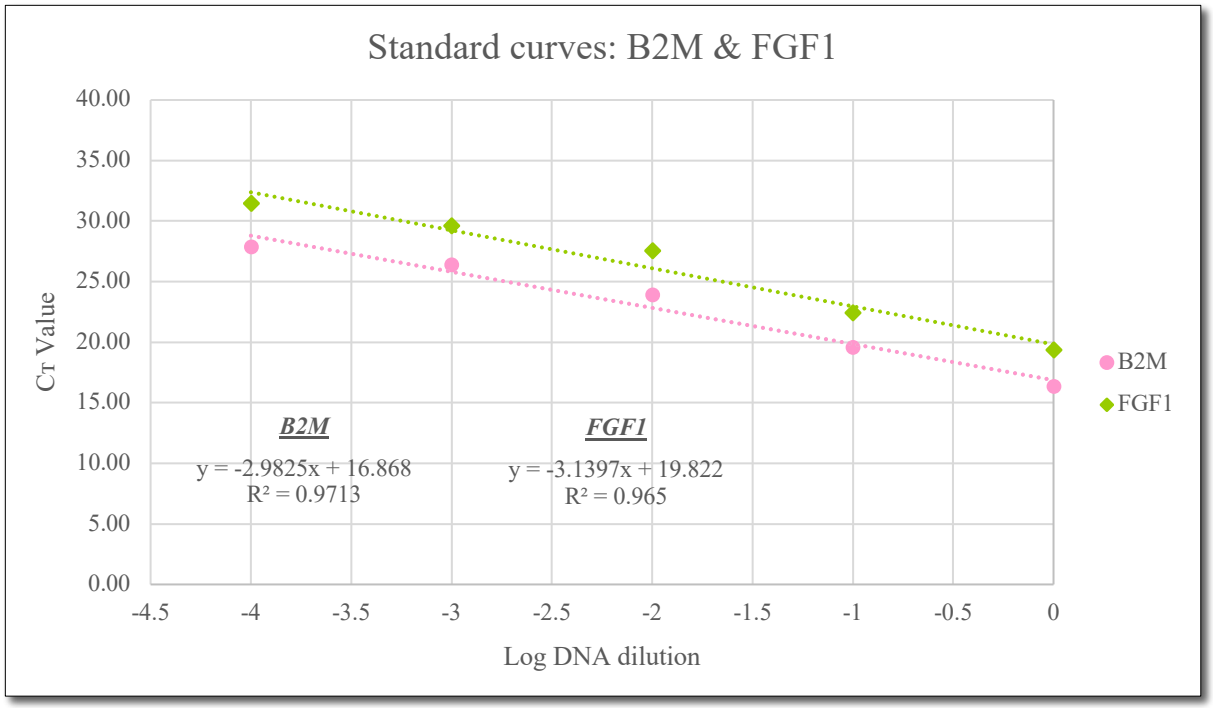

Figure 10 - Standard curve of B2M and FGF1

Dilutions go from left to right, with non-diluted samples on 0 and dilution 1:10 000 on -4 (X-axis). Each dot on the graph represents the Ct average value of three replicates.

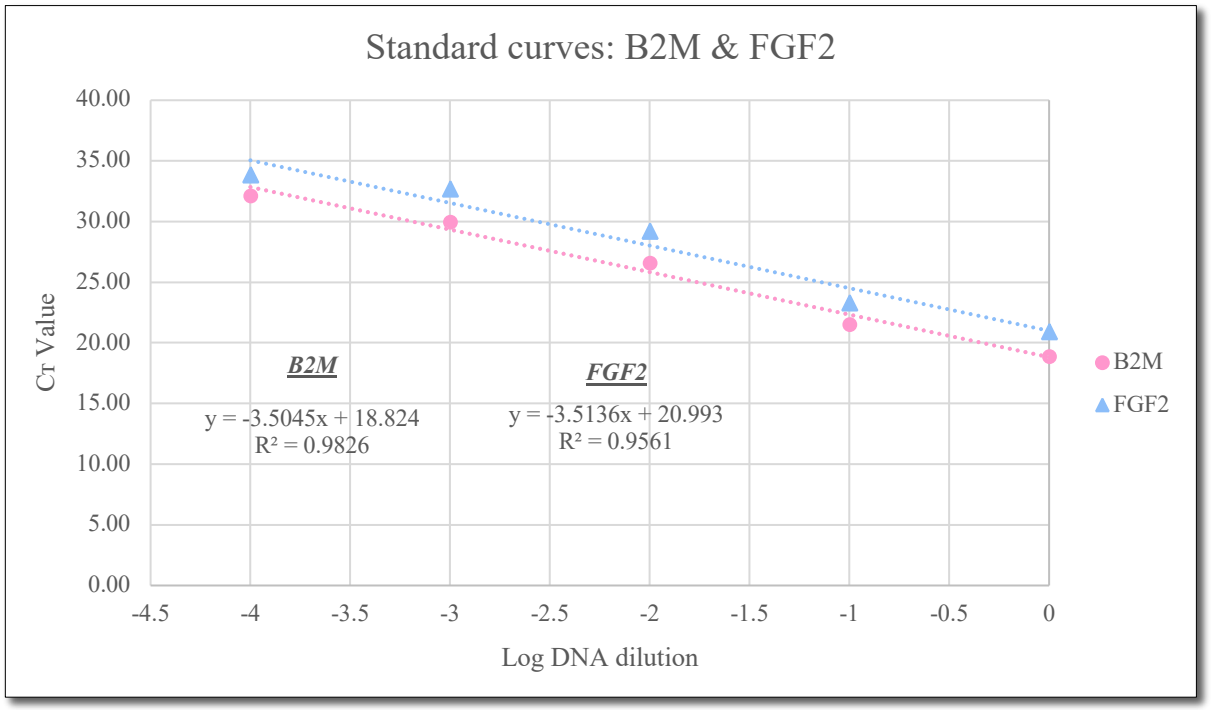

Figure 11 - Standard curve for B2M and FGF2

Dilutions go from left to right, with non-diluted samples on 0 and dilution 1:10 000 on -4 (X-axis). Each dot on the graph represents the Ct average value of three replicates.

As expected, the results from the rt-qPCR confirmed the expression of FGF1 and FGF2 in the Panc-1 cell line. By the same token, the Δ Ct calculation showed also the expected higher expression of FGF2 than FGF1 relative to B2M, where FGF2 expression corresponded to 26% (Table 11) of the B2M, while FGF1 corresponded to 13% (Table 10). Amplification curves of the FGF1 and FGF2 genes can be found in the Appendix (5.3).

Table 10 - Δ Ct calculation for FGF1

Dilution	*B2M Ct*	*FGF1 Ct*	*Δ Ct*	$2^{-\Delta Ct}$	*Fold difference*	*Average fold difference*
1:1	16.38	19.37	-2.99	0.13	7.92	7.62 *(13%)*
1:10 000	19.59	22.46	-2.87	0.14	7.32	

Table 11 - Δ Ct calculation for FGF2

Dilution	*B2M Ct*	*FGF2 Ct*	*Δ Ct*	$2^{-\Delta Ct}$	*Fold difference*	*Average fold difference*
1:1	18.87	20.97	-2.10	0.23	4.27	3.89 *(26%)*
1:10 000	21.52	23.33	-1.81	0.29	3.51	

3.2 Confirmation of FGF2 and Ksp37 binding

The Jørgen Wesche's group (Institute of Cancer Research, Oslo) focuses on the study of sarcoma development and the implications FGFs plays in this process. Hence the signals strongly pointing at a possible binding of FGF2 and Ksp37 (1.4) motivated them to execute tests that could provide experimental evidence in this matter. To this end, they perform the in-vitro translation of Ksp37 with rabbit reticulocyte lysate and ^{35}S-Methionine, followed by pulldown with glutathione magnetic beads (glutathione-S-transferase, GST) tagged with FGF2, and the use of autoradiography as experimental readout. ^{35}S-Methionine is a beta-emitting radioisotope commonly used for metabolic labeling to track the biosynthesis of proteins [138]. An overview of the procedure is depicted in Figure 12.

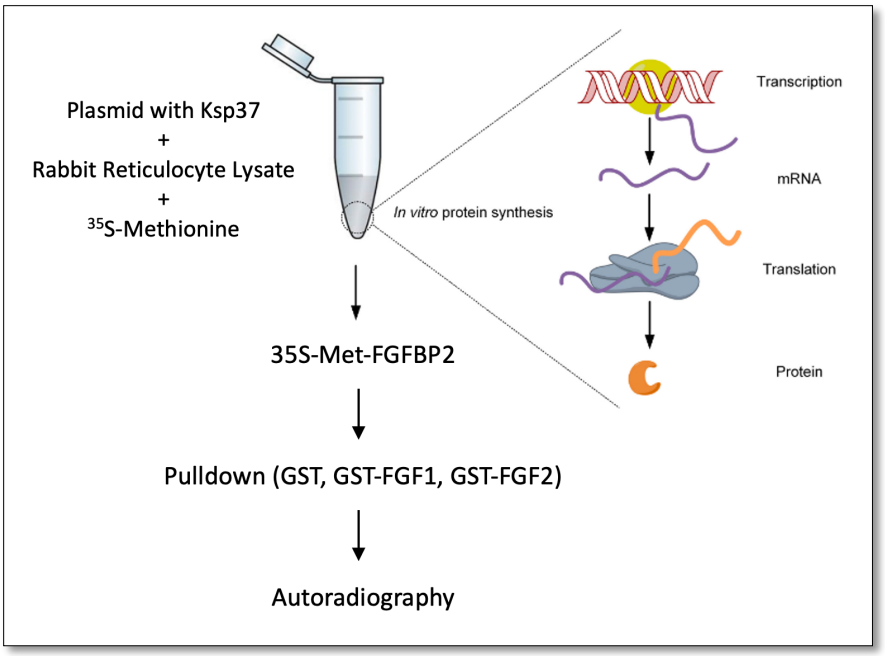

Figure 12 - In-vitro translation of Ksp37 with ^{35}S-Methionine

Image depicting the in-vitro protein synthesis of radiolabeled Ksp37 and the subsequent pulldown with GST-tag beads. Illustration adapted from design provided by Wesche's group.

As can be appreciated in Figure 13, two independent experiments showed a notably higher concentration of ^{35}S-Methionine present on the GST beads tagged with FGF2, as compared to the same bead tag with FGF1, implying thus a greater amount of labelled Ksp37. Therein delivering experimentally confirmation for the interaction between FGF2 and Ksp37.

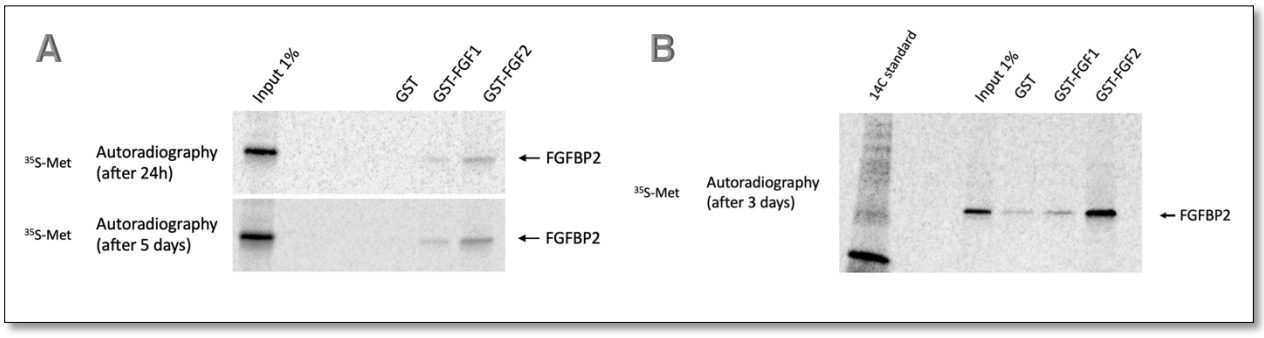

Figure 13 - FGF2 - Ksp37 binding experiments results

SDS-PAGE followed by autoradiography analysis of pull-down samples. (A) Experiment #1 with two different time points for the Autoradiography: 24 hours and 5 days after. (B) Experiment #2 with Autoradiography taken 3 days after. 1% of 35 S-labeled Ksp37 used in the pull-down reactions was loaded as the input control (Input 1%). Image adapted from Wesche Group scientist Ellen M. Haugsten, Ph.D.

3.3 CRISPR/Cas9-mediated knock-out of FGF2 in Panc-1 cell line

Bearing in mind the confirmed expression of FGF2 in the Panc-1 cell line and the experimental evidence showing FGF2 binding to Ksp37, the generation of a homozygous FGF2 $^{-/-}$ line was the subsequent objective. Consequently, Panc-1 cells were electroporated with the Cas9/sgRNA complex targeting the FGF2 gene, and cultured until enough material was available for gDNA isolation. The latter was then used for genotyping through PCR and gel electrophoresis. However, despite proving several pairs of primers and different PCR cycling conditions, the assays failed to generate reliable bands on the agarose gels.

Sample	*B2M Ct*	*FGF2 Ct*	*Δ Ct*	*ΔΔ Ct*	*2^-ΔΔCt*	*Fold Change*
Panc-1 wt 1	17.14	22.51	5.38	-0.19	1.14	1.03
Panc-1 wt 2	18.03	23.29	5.26	-0.31	1.24	
Panc-1 wt 3	17.19	23.25	6.06	0.50	0.71	
Panc-1 FGF2 -/- 1	17.12	24.39	7.27	1.70	0.31	0.34
Panc-1 FGF2 -/- 2	17.24	23.88	6.64	1.07	0.48	
Panc-1 FGF2 -/- 3	17.15	24.75	7.60	2.03	0.24	
Control Average Ct			***5.57***			

Table 12 - ΔΔ Ct calculation for FGF2 expression on Panc-1 FGF2 $^{-/-}$ cell line

Under those circumstances, rt-qPCR was chosen as an alternative method to validate the FGF2 knockout at the transcript level. As the ΔΔ Ct analysis results show in Table 12, the number of FGF2 mRNA transcripts present in the Panc-1 FGF2 $^{-/-}$ cell line showed case a 69% (*Fold change*) downregulation compared to those obtained in the Panc-1 wt. Thereupon suggesting a partially successful gene knockout in the Panc-1 FGF2 $^{-/-}$ line.

3.4 FG2 knockout validation at the protein level

To further validate the FGF2 knockout, protein from Panc-1 cells was isolated and measured to perform a western blot assay. As shown in Figure 14, the wt sample exhibited the expected three protein variants detected by the FGF2 antibody as indicated by the manufacturer (lines 5 and 6). On the contrary, Panc-1 FGF2-/- candidate #2 (lines 3 and 4) showed only one band with an approximate weight of 21kDa (line 3). FGF2 -/- candidate #1 on the other hand, displayed only a very fading line, also corresponding to an approximate weight of 21kDa (line 1).

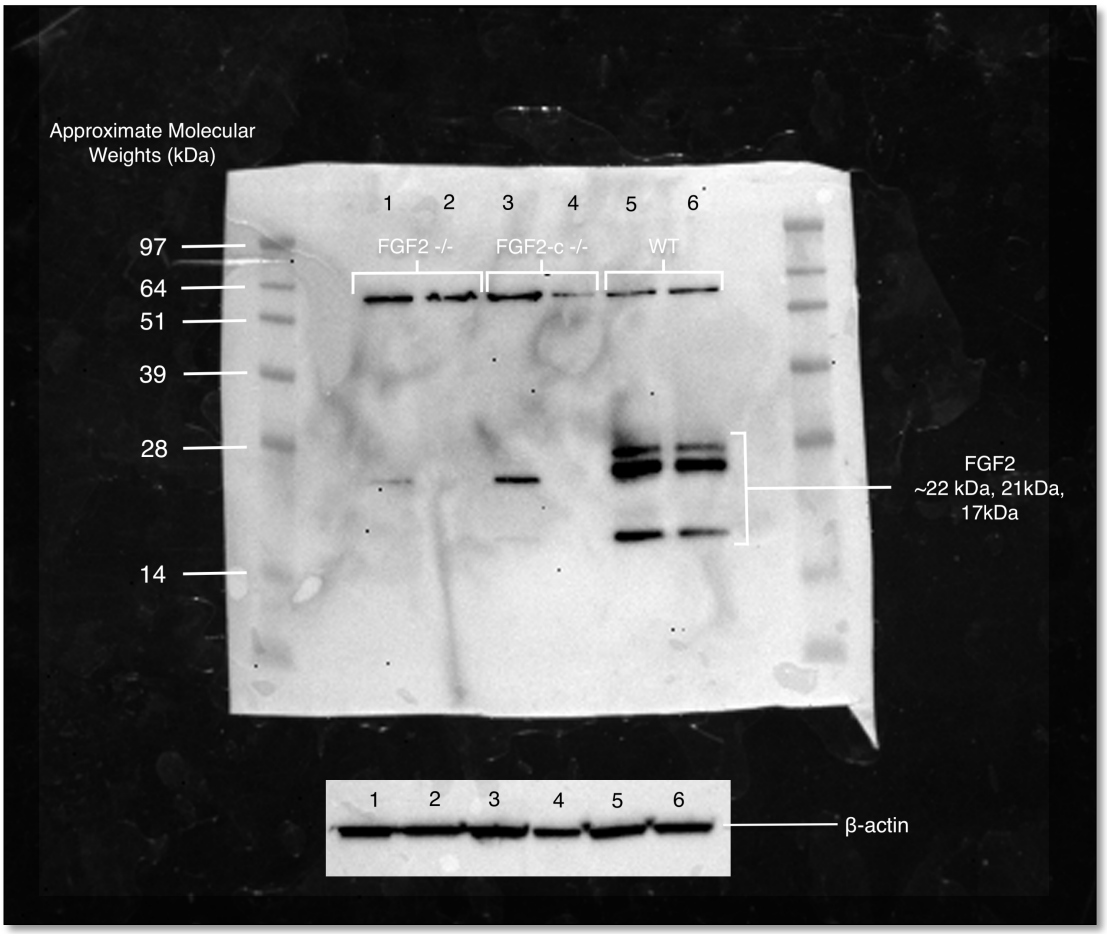

Figure 14 - Western blot results from Panc-1 FGF2$^{-/-}$ cells

*Western blot was performed using an anti-FGF2 monoclonal antibody (2.8.4). Two different protein concentrations were used, each sample had a line with 16 µg of total protein (left) and a second line with a total of 8 µg (right). 17 kDa, 21 kDa, and 22 kDa bands corresponding to FGF2 were detected on the wt sample at both protein concentrations (lines 5 and 6). Panc-1 FGF2-/- candidates number #1 and #2 showed only two weaker bands of 21kDa on the lines with the highest amount of protein: line 1 for candidate #1 and line 3 for candidate #2. Beta-actin (*β-actin*) bands at the bottom were used as loading control.*

Based on these results, two more rounds of protein isolation and western blot were performed on Panc-1 FGF2$^{-/-}$ candidate #1, which provided additional support to validate the FGF2 knockout. The images can be found on the appendix (5.4). The Panc-1 FGF2-/- candidate #1 was affirmed as the most fitting knockout model for subsequent experiments, taking into account the PCR results as well as corroborative evidence from Western blot analyses confirming the FGF2 knockout[4].

3.5 Ksp37 secretion in NK-92 cell lines

Non-published data from work by Kishan Kumar and Axel Berg-Larsen at the Malmberg group, have provided compelling evidence for the secretion of Ksp37 from PBMC-derived NK cells upon cytokine stimulation. Moreover, their results have also demonstrated that Ksp37 secretion is highly sensitive to cell confluency. Therefore, determining that the NK-92 cell lines over-expressing Ksp37 could indeed secret it was imperative for the project. Herein three different cell lines were tested as stated in the methods section (2.1.1), and a snap of Kishan and Axel's results regarding Ksp37 secretion can be found in the appendix (5.5).

3.5.1 The NK-92 V51 cell line does not show signs of secreting Ksp37

The NK-92 V51 cell line expressing a Ksp37 protein tagged with GFP in the N terminal was the first one to be tested. The cells were treated overnight with IL-15 and IL-15 together with BFA, stained with antibodies, and the results were retrieved through a flow cytometer. Unlike primary NK cells, however, a reduction of the median fluorescence intensity (MFI) on the Ksp37 channel was not observed in the cells treated with only IL-15 (Figure 15). Furthermore, the introduction of BFA did not seem to increase the intracellular amount of Ksp37 either, strongly suggesting a lack of secretion. The experiment was repeated in three different instances with similar results among them, and thus the NK-92 V51 cell line was discarded from further experiments. The expression vector used for the present, as well as for lines NK-92 V84 and V85, cell line can be found in the appendix section 5.6.

[4] Herein is worth noting that, unlike the NK-92 clone cell lines, the Panc-1 FGF2$^{-/-}$ candidates were batches of electroporated cells. In that sense, the presence of remaining FGF2 bands is indicative of the cell batch heterogeneity, given that CRISPR/Cas9 editing efficiency is way below 100% on average [135] [136].

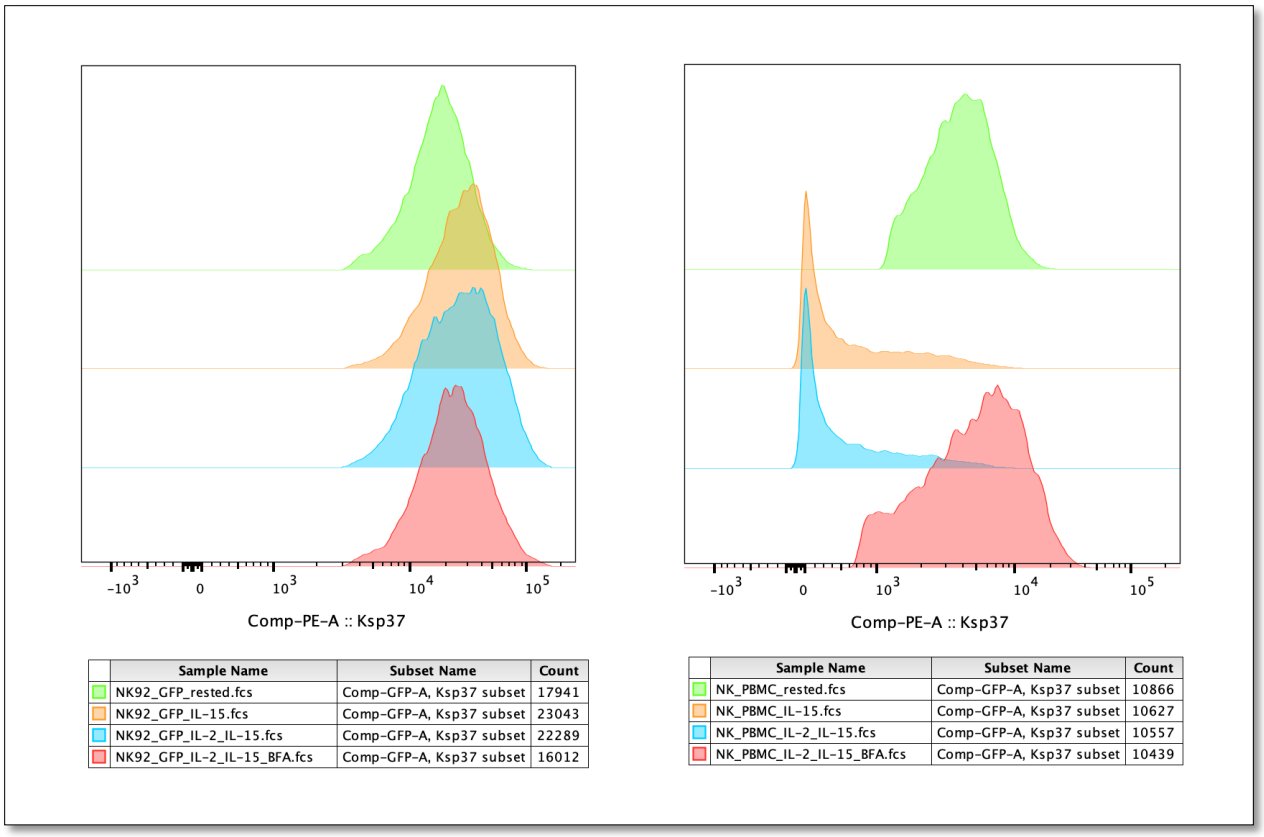

Sample Name	Subset Name	Count
NK92_GFP_rested.fcs	Comp-GFP-A, Ksp37 subset	17941
NK92_GFP_IL-15.fcs	Comp-GFP-A, Ksp37 subset	23043
NK92_GFP_IL-2_IL-15.fcs	Comp-GFP-A, Ksp37 subset	22289
NK92_GFP_IL-2_IL-15_BFA.fcs	Comp-GFP-A, Ksp37 subset	16012

Sample Name	Subset Name	Count
NK_PBMC_rested.fcs	Comp-GFP-A, Ksp37 subset	10866
NK_PBMC_IL-15.fcs	Comp-GFP-A, Ksp37 subset	10627
NK_PBMC_IL-2_IL-15.fcs	Comp-GFP-A, Ksp37 subset	10557
NK_PBMC_IL-2_IL-15_BFA.fcs	Comp-GFP-A, Ksp37 subset	10439

Figure 15 - Stimulation of NK-92 V51 cell with Il-15

Representative flow cytometry histogram overlay plot showing no MFI decrease on the PE channel (Ksp37) in NK-92 V51 cells (left as NK92_GFP) treated with IL-15 (orange and blue histograms). In contrast, to the right are found the results from primary NK cells used as positive controls, with a clear Ksp37 shedding upon IL-15 stimulation (orange and blue histograms). The experiment was repeated in three different instances with the NK-92 V51 line.

3.5.2 NK-92 V84 and V85 cells lines constitutively secrete Ksp37

Following the unsuccessful results with the V51 cell line, the focus shifted toward the NK-92 cells expressing a His-tagged Ksp37 protein. The rationale behind it was that the much larger GFP tag (27 kDa compared to 0.8 kDa of the 6x-His tag) could be detrimental to Ksp37 transport, post-translational modification, and secretion. Accordingly, the NK-92 V84 (V84) and NK-92 V85 (V85) were stimulated with IL-15 to test for Ksp37 secretion. In that regard, both cell lines underwent the same treatments, and the results were acquired under the same instrument conditions.

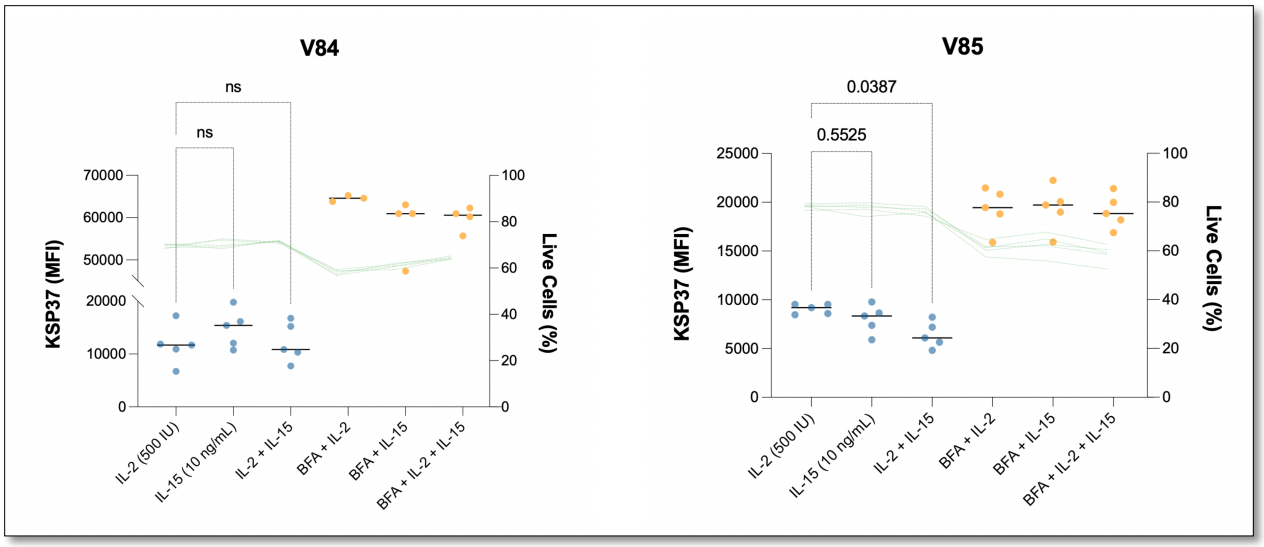

Figure 16 - Stimulation of NK-92 V84 and NK-92 V85 cells with Il-15

The blue color represents the cells treated without BFA; orange color represents the cells treated with BFA. The green lines indicate the percentage of viable cells in each sample after the treatments. For the V85 cell lines, there is a statistically significant decrease in MFI in the group treated with IL-2 and IL-15 when compared to the samples treated with IL-2 only. All samples were run on the same experiment, each dot represents a biological replicate.

Figure 16 shows the MFI values on the Ksp37 channel obtained from the IL-15 incubation experiments. Among the cells treated without BFA, there is no significant MFI reduction upon IL-15 exposure on the V84 cell line. As for the V85, there is a statistically significant difference between the only IL-2 treatment when compared to IL-2 together with IL-15. This difference however does not reach the extent to which primary NK cells secret Ksp37 when exposed to the same cytokine concentration (10 ng/mL).

Despite these facts, the results obtained from the cells treated with BFA (orange) show an approximate 3-fold (V84) to 2-fold (V85) fluorescence intensity increase on the Ksp37 channel when compared to the groups without BFA (blue). Furthermore, this observation also becomes apparent by a clear shift to the right in the x-axis of the cells treated with BFA (Figure 17). All things considered, these results strongly suggest a constitutively Ksp37 shedding that comes to a halt when cell transport is inhibited, in this case through hindering vesicle formation at the Golgi apparatus.

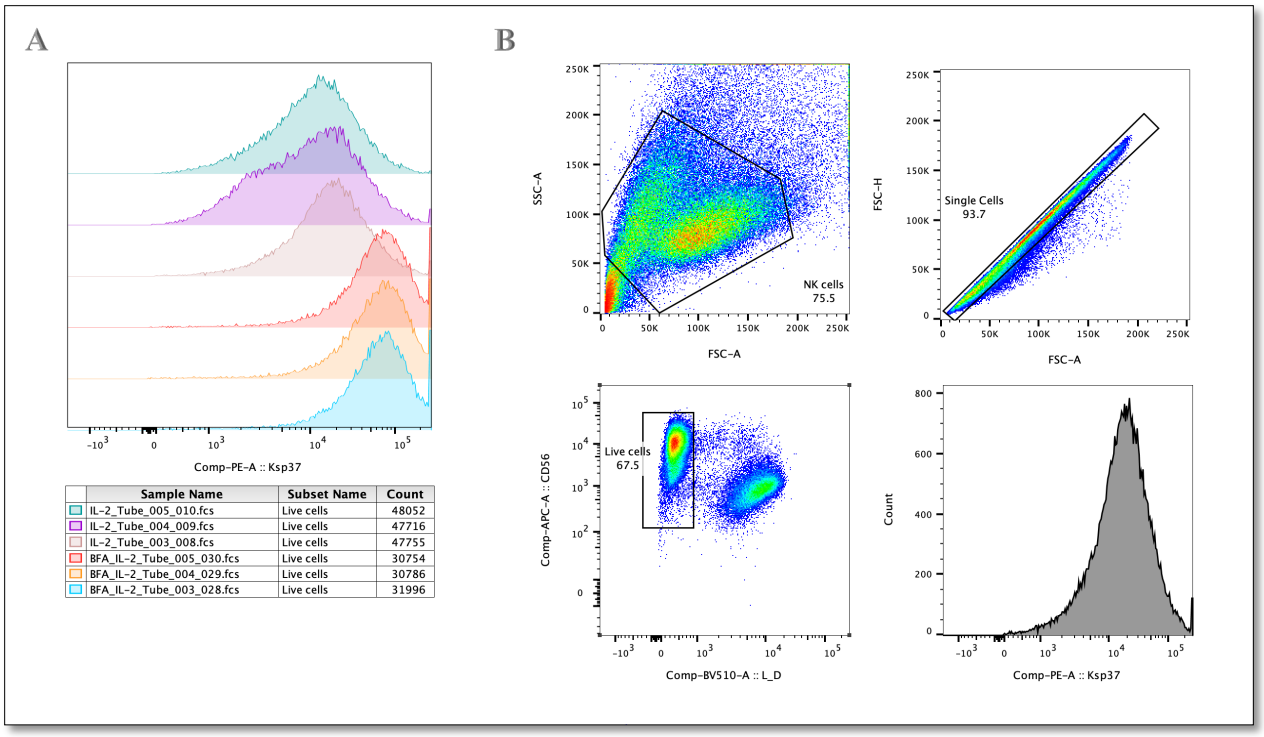

Figure 17 - Histogram overlay of V84 samples and corresponding gating strategy

(A) Histograms half offset of representative samples from V84 cell line treated with and without BFA. (B) Example of the gating strategy employed for flow cytometry data analysis of Ksp37 secretion experiments (Figure 18).

3.5.3 The NK-92 wt cell line is negative for Ksp37 expression

One of the major hurdles during the experimental design of the project was the establishment of a reliable negative control for Ksp37. A concern that was expelled after including the NK-92 wt cell line in the IL-15 incubation experiments. As Figure 18 shows, regardless of exposing the cells to BFA, there is no significant increase in the intracellular levels of Ksp37 with respect to the cells incubated only with IL-2. Moreover, the fluorescence intensity retrieved on the PE channel (Ksp37) lies very close to zero, especially when compared with a Ksp37-positive cell line such as NK-92 V51 (Figure 19). In sum, the results obtained from the IL-15 incubation of NK92 wt cells were consistent enough to rely on the NK-92 wt cell line as a negative control for the subsequent killing assays.

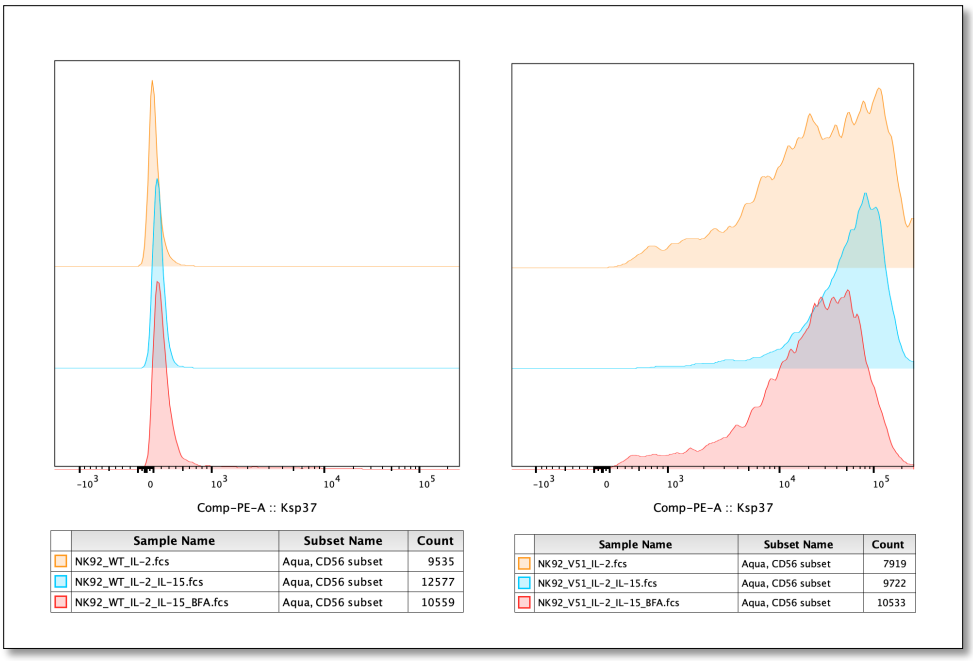

	Sample Name	Subset Name	Count
	NK92_WT_IL-2.fcs	Aqua, CD56 subset	9535
	NK92_WT_IL-2_IL-15.fcs	Aqua, CD56 subset	12577
	NK92_WT_IL-2_IL-15_BFA.fcs	Aqua, CD56 subset	10559

	Sample Name	Subset Name	Count
	NK92_V51_IL-2.fcs	Aqua, CD56 subset	7919
	NK92_V51_IL-2_IL-15.fcs	Aqua, CD56 subset	9722
	NK92_V51_IL-2_IL-15_BFA.fcs	Aqua, CD56 subset	10533

Figure 18 - Representative histogram of results from Ksp37 secretion experiments with the NK-92 wt line

To the left are the histograms obtained for the NK-92 wt line, and on the right-hand side, those obtained from the NK-92 V51 cell line used as a positive control. The curves in orange show the cells incubated only with IL-2, in blue IL-2 in combination with IL-15, and the red curves show the results from the incubation with IL-2, IL-15, and BFA. Two independent experiments were carried for the test of Ksp37 in the NK-92 wt line.

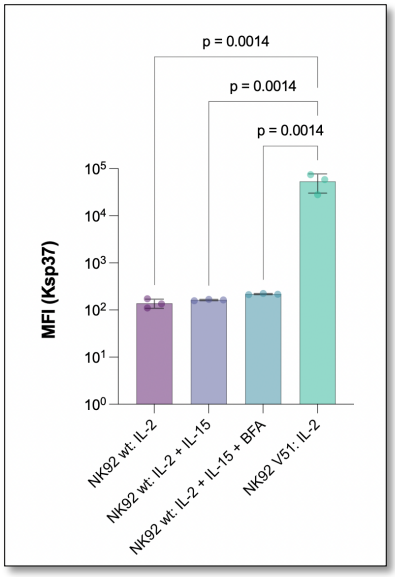

Figure 19 - Summary of Ksp37 secretion results on the NK-92 cell line

One-way ANOVA results comparing the Ksp37 MFI of NK-92 V51 cells incubated only with IL-2 as a positive control to NK-92 wt cells incubated with (1) IL-2, (2) IL-2 together with IL-15, and (3) both cytokines combined with BFA. Significance was found in all three comparisons. All samples were run on the same experiment, each dot represents a biological replicate.

3.6 Mosaic cytotoxicity results among NK-92 Ksp37-expressing cell lines

As previously mentioned (1.4), Ksp37 is almost exclusively expressed in cytotoxic lymphocytes. Furthermore, in CD16+ NK cells, this protein is co-expressed with perforin, a key molecule in granule-mediated cytotoxicity [101]. Consequently, after establishing the capability of the NK-92 V84 and V85 to secrete high amounts of Ksp37 (Figure 15), with NK-92 wt line being negative for the same protein, the subsequent step in the project was to test for difference in cytotoxicity among the three NK-92 cell lines (V84, V85 and wt).

For this purpose, the effector cells (NK-92) were co-cultured with both Panc-1 cell lines (wt and FGF2 -/-) in the presence of IL-2 and IL-15 as described in section 2.10. As shows, however, the overall diminishing of red fluorescence, used as an indicator of target cell killing, did not follow a homogenous pattern among the effector cell lines across the different targets[5]. For instance, the NK-92 wt line displayed the highest lytic activity towards Panc-1 wt cells (Figure 21, A). Meanwhile, the analogous scenario was not observed in the experiments with Panc-1 FGF2$^{-/-}$ cells as targets, where NK-92 V84 presented the highest level of killing (Figure 21, A). Regarding the NK-92 V85 line, it showed significantly less lysis of both target cell lines compared with the response observed for the NK-92 wt line, and reduced killing of Panc-1 FGF2 -/- cells in contrast with the NK-92 V84 line.

Nevertheless, when the differential killing is assessed from the effector cell line perspective, for the NK-92 wt line it is possible to observe a significantly higher amount of activity over the Panc-1 wt line as a target in comparison to the Panc-1 FGF2 -/- line (Figure 21, B). A similar pattern appears to show for the NK-92 V85 cell lines, where the total red fluorescence reduction registered seems higher for the Panc-1 wt cells compared to the Panc-1 FGF2 -/-. However, these differences are not significant for either of the Ksp37 over-expressing cell lines.

[5] For illustration purposes, the data displayed on the charts have been simplified. The results with the complete set of conditions and ET ratios can be found in the Appendix 5.7.

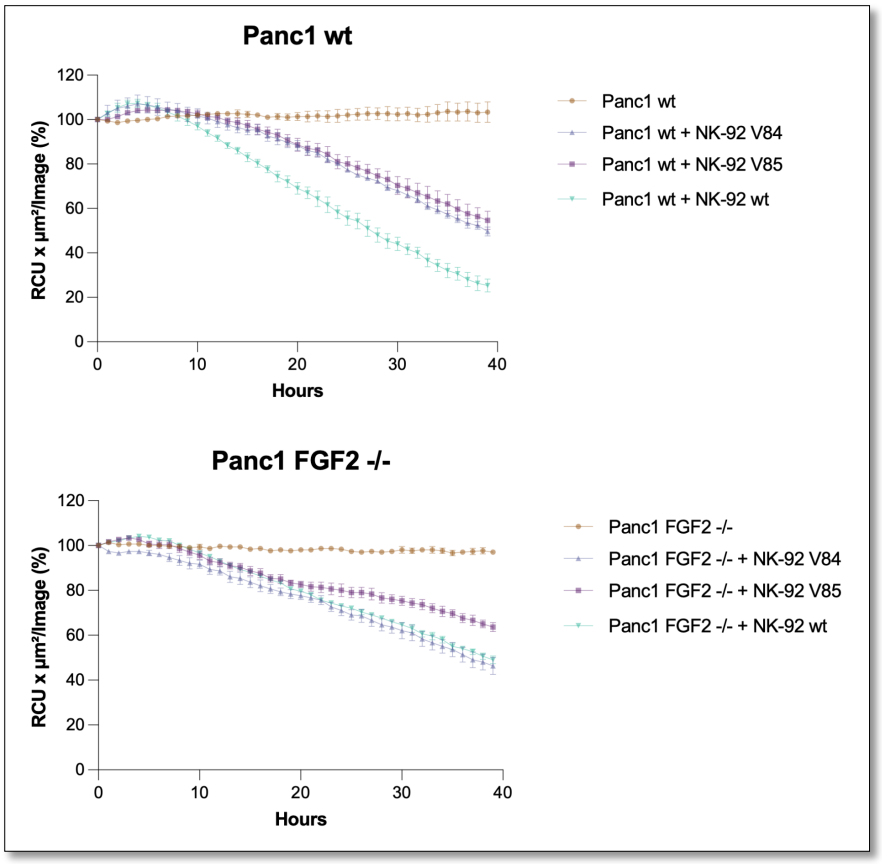

Figure 20 - Incucyte cell killing assay with Panc-1 lines

Red fluorescent Panc-1 cell lines were co-cultured with NK-92 cells and analyzed using the IncuCyte basic analyzer software. All cells were seeded at the same density for each experiment at an ET ration of 2:1. For the construction of the graphs, each RCU x um/image value was normalized to time 0 and then to the controls (target cells only). All samples were stimulated with IL-2 and IL-15. All samples were run on the same experiment, each dot represents the average result of three biological replicate.

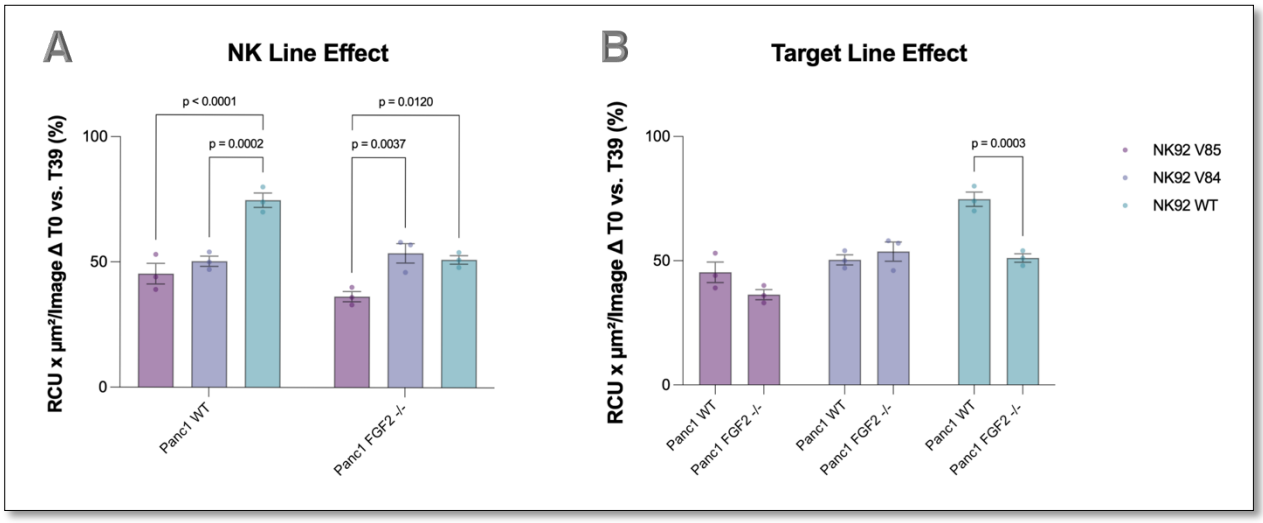

Figure 21 - Total reduction in red fluorescence of Panc-1 cells between time points 0 and 39

The statistical analysis of the results described in Figure 20. (A) Comparison of the percentage of killed target cells registered between the three NK-92 cell lines. (B) Contrast of the amount of killing detected between the Panc-1 wt and FGF2 -/- lines for each effector cell line. P-values were determined by two-way ANOVA.

3.7 Killing assay results with the K562 line as a target reflects observations in Panc-1

A frequently used method to elicit NK cell activation is through their co-culture with HLA-null cells. In this regard, the K562 cells are one of the most commonly employed cell lines, lacking expression of MHC class-I A, B, and C on their surface [139, 140]. This absence renders the K562 cells incapable of engaging the inhibitory KIRs on the surface of NK cells, allowing rather the engagement of activating receptors with their ligands to activate NK cells [141]. In addition, NK cells have demonstrated promising results in the targeting of hematological malignancies [142], efficacy that has not been reflected to the same degree in the treatment of solid tumors (1.3.1). All the above reasons why the K562 cell line was incorporated as positive control during the Incucyte killing experiments.

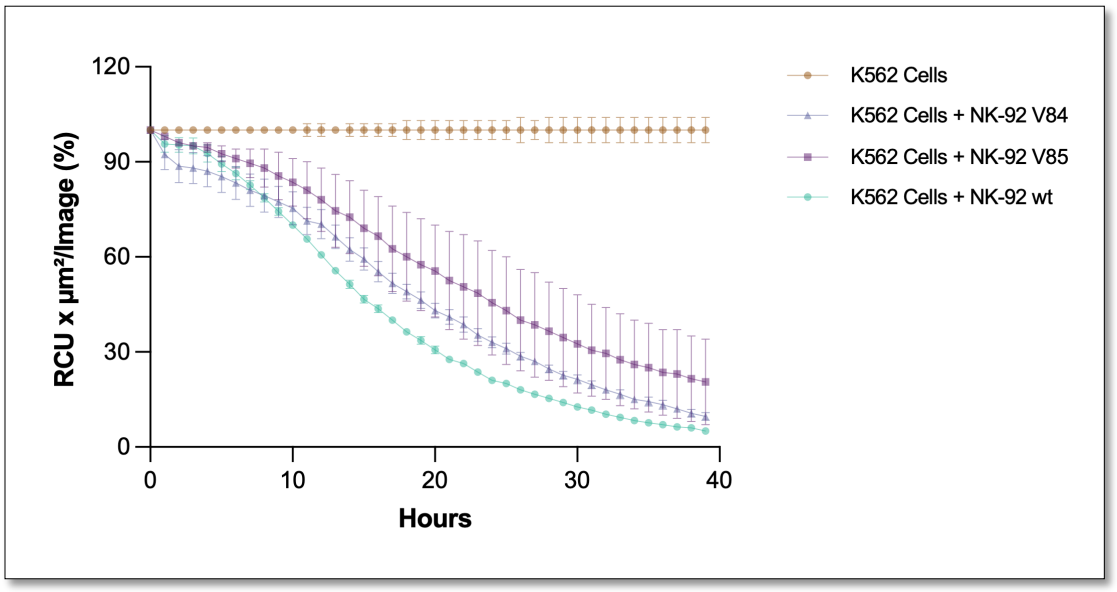

Figure 22 - Incucyte cell killing assay with K562 cell line

Red fluorescent K562 cell lines were co-cultured with NK-92 cells and analyzed using the IncuCyte basic analyzer software. All cells were seeded at the same density as described in 2.10. For the construction of the graphs, each RCU x um/image value was normalized to time 0 and then to the controls (target cells only). All samples were run on the same experiment. Groups were run in triplicates; the dots represent the mean and the bars the standard error.

As expected, the amount of red fluorescence from the K562 cells, compared with time point 0, achieved levels considerably below 20% (Figure 22), representing approximately 1.5 to 2 times lower than those observed with the Panc-1 lines (Figure 21). Confirming thus the adequacy of K562 cells as positive controls for cytotoxic assays with NK cells.

As Figure 24 depicts (B), these differences were particularly pronounced in the groups treated with IL-2 and IL-15, with all treated effector cell lines displaying a reduction in red fluorescence greater than 80%. A scenario that found its counterpart in the experiments with Panc-1 cells, where, except for the NK-92 V85 line, both NK-92 V84 and NK-92 wt demonstrated higher lytic activity in the presence of cytokines (Figure 24, A). What is more, despite the presence of statistically significant differences (Figure 23), the trend observed in the Incucyte experiments with Panc-1 wt cells, whereby the NK-92 wt exerted higher cytotoxic activity (Figure 21, A), was also observed with the K562 cells. A fact that was especially marked in the group of cells cultured only with growth media[6].

In summary, the cytotoxicity appeared to be intrinsically lower in NK92 cells overexpressing Ksp37. This finding is somewhat unexpected and needs confirmation in further experiments. It is possible that the growth kinetics of the target cells during the assay affect the outcomes. These results may also be affected by subcloning of the NK92 lines and further experiments are required to formally prove a pro-tumor effect of Ksp37 secretion.

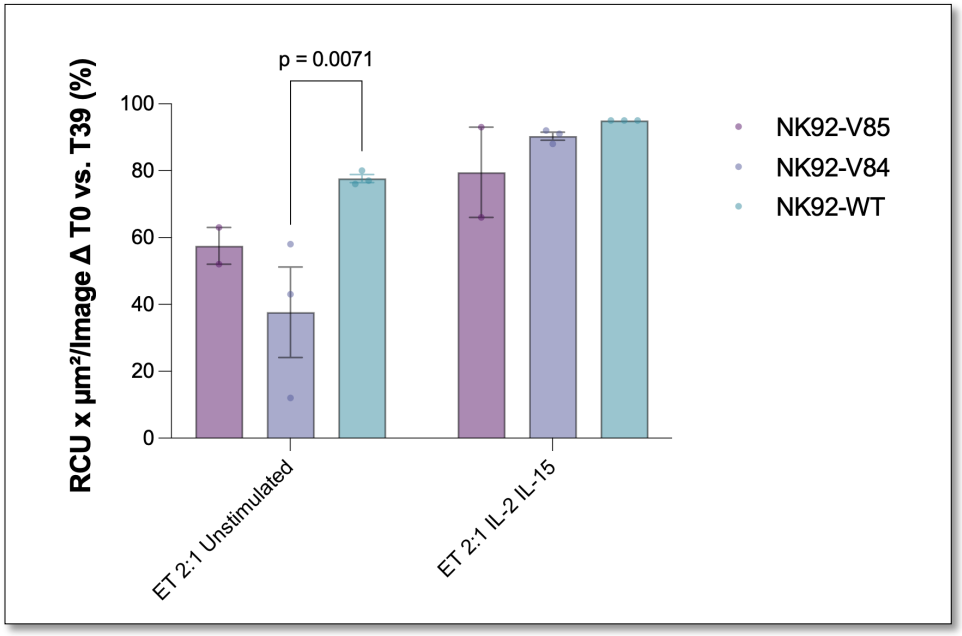

Figure 23 – Total red fluorescence reduction of K562 between time points 0 and 39. *Statistical analysis of the results described in Figure 22, contrasting the target cell killing registered between the three NK-92 cell lines. P-values were determined by two-way ANOVA.*

[6] As with the case of experiments with the Panc-1 cells, the results from all the conditions tested with the K562 cell can be found on 5.7.4.

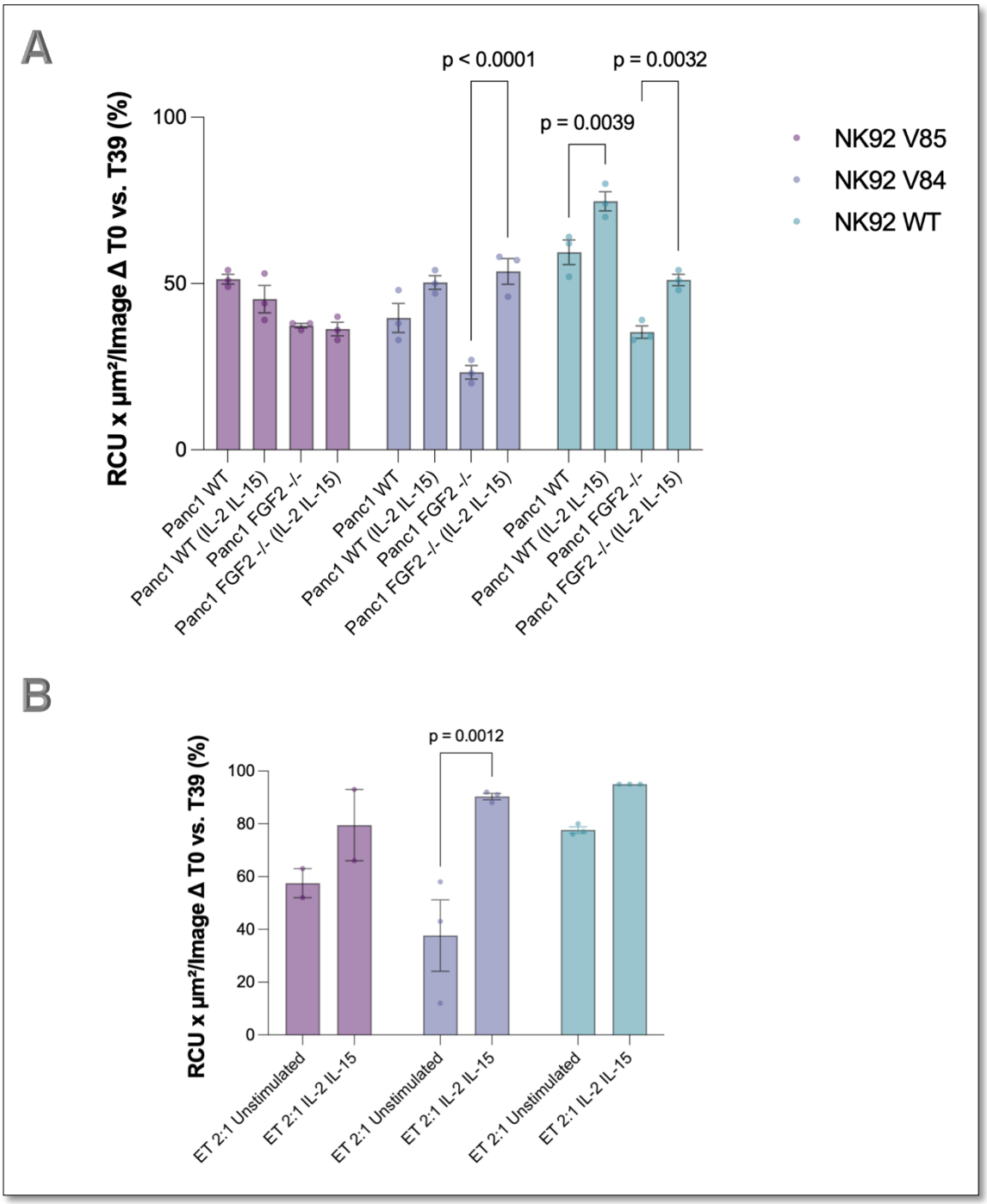

Figure 24 - Effect of cytokines in target cell lysis.

Statistical analysis of the results described in Figure 22 contrasting the effects of IL-2 and IL-15 in target cell lysis. (A) Pairwise comparison of the effect on the killing of Panc-1 cells. (B) Pairwise comparison of the effect on the killing of K562. Results from the three NK-92 cell lines are shown. Each dot represents a biological replicate. P-values were determined by two-way ANOVA.

3.8 Microfluidic system does not impair viability of NK-92 cells

As previously stated (1.5), the inclusion of microfluidics in a 3D setting was mainly driven by an intent to mimic closer the physiological conditions in which Ksp37 could play a role. Nonetheless, before proceeding to execute the cytotoxic assays, it was essential to test if the model in and of itself held any influence on the viability of NK-92 or the secretion of Ksp37.

For this purpose, two flow conditions were tested (High and low) on the NK-92 V85 cell line, as determined by the tilt of the rotating platform. Likewise, static controls were also included, with volumes corresponding to the inner (200 ul) and outer (350 ul) channels of the chip. As Table 12 shows, the cell viability, measured both with trypan blue and the Live/Dead aqua dye (flow cytometry, 2.4.1), before (93%) and after incubation of NK-92 cells on the chip was very close to each other with minimal variation.

Conditions	*Location / Volume*	*Trypan Dye*	*Live/Dead (Aqua)*
High flow	Inner Channel	90%	94%
	Outer Channel	85%	97%
Low Flow	Inner Channel	90%	
	Outer Channel	89%	
Static controls	200 ul	91%	88%
	350 ul	88%	88%
Initial viability		***93%***	

Table 13 – Results of NK-92 V85 cell viability upon 24 hours chip incubation

In light of the viability results, it was decided to proceed forward with the high flow setting, hence the spontaneous Ksp37 secretion was also assessed by flow cytometry under this condition. As Figure X shows, the Ksp37 MFI values showed no significant variation, regardless of the channel in which the NK-92 cell were seeded. All in all, these results corroborated the suitability of the model for the use of NK-92 cells in the context of Ksp37.

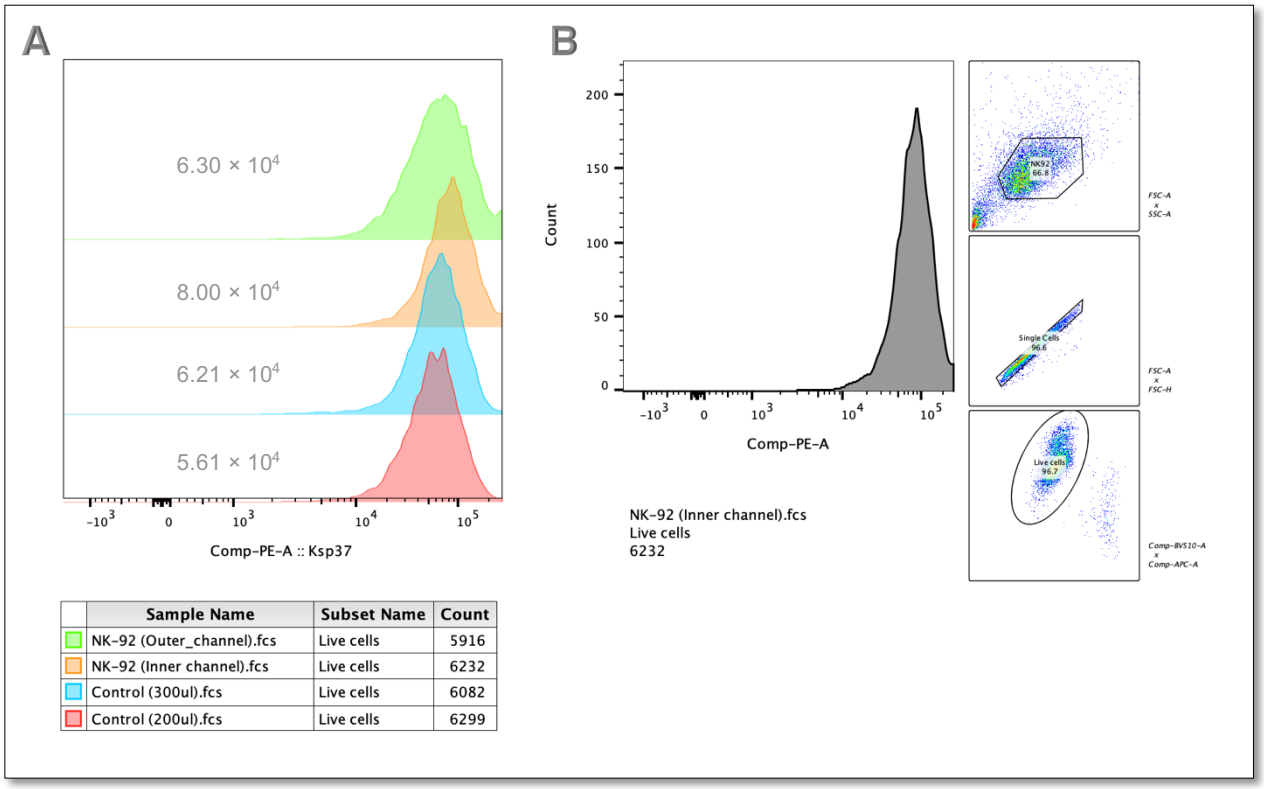

Figure 25 - Histogram overlay of NK-92 V85 cells and corresponding gating strategy.

(A) Histograms half offset of representative samples from V84 cell line incubated on the chips for 24 hours. (B) Example of the gating strategy employed for flow cytometry data analysis. MFIs are shown in exponential notation on gray for each sample. The experiment was carried a single time with two biological replicates per treatment.

3.9 NK-92 lytic activity over Panc-1 cells is not observed in the microfluidic chip model

On the face of the Incucyte results, whereby a higher amount of lytic activity over the Panc-1 wt cells, compared to Panc-1 FGF2-/-, was observed for the NK-92 V85 and NK-92 wt cell lines (Figure 21), and bearing in mind the time constraints due to the labor-intensive nature of the technology, it was decided to proceed only with Panc-1 wt cells as a target for the experiments on the microfluidic chips. For this purpose, a total of 8 chips were employed, with two chips for each group: Panc-1 wt cells alone as negative controls, and Panc-1 wt co co-cultured with each one of the three NK-92 lines (V84, V85, and wt). Moreover, each chip counts with two organoid chambers (Figure 6) where spheroid target cells can be seeded independently, generating an aggregate of 4 replicates per treatment group.

The experimental readout for target cell lysis was obtained through the immunofluorescence staining of cleaved caspase-3, a cysteine–aspartic acid protease responsible for most of the proteolysis during apoptosis [143]. However, as Figure 26 shows, nearly all target cells were negative for cleaved-caspase 3. Further, most of the signals detected for the marker in question were an overt result of unspecific binding (Figure 26, B-D). Demonstrating thus a lack of responsiveness from the NK-92 effector cell lines towards Panc-1 wt spheroids in a microfluidic context.

Notwithstanding, a noticeable pattern that arose after the co-culture period was the pronounced difference in migration patterns between the Panc-1 wt cells cultured alone, compared with the cells co-culture with NK-92, regardless of the cell line. As Figure 27 (A) illustrates, the Panc-1 wt cells in monoculture displayed a marked proliferation outside the organoid chamber and towards the channels containing NK-92 cell growth media. In contrast, the Panc-1 cells co-cultured with NK-92 cells exhibited signs of proliferation (C-D), nonetheless without any trace of infiltration into the channels.

Finally, the NK 92 cells were harvested after the incubation period with the aim of assessing any potential changes in the intracellular levels of Ksp37. The latter included NK92 cells in static culture employed as controls, that were cultured at the same confluency as those in the chips. For this purpose, cells were stained and scrutinized through flow cytometry as described in section 2.4. As the results portrayed in Figure 28 show, the MFI retrieved on the Ksp37 channel, both for lines NK-92 V84 and V85, revealed higher levels on the cells incubated on the chips (co-cultured with Panc-1 spheroids) with respect to the ones in static controls, suggesting thus a decrease in the amount of Ksp37 secretion. Finally, in congruency with the results obtained in the secretion experiments (3.5.3), the NK-92 wt cells were all negative for Ksp37 between the cells deployed in the experiments and the ones used as controls.

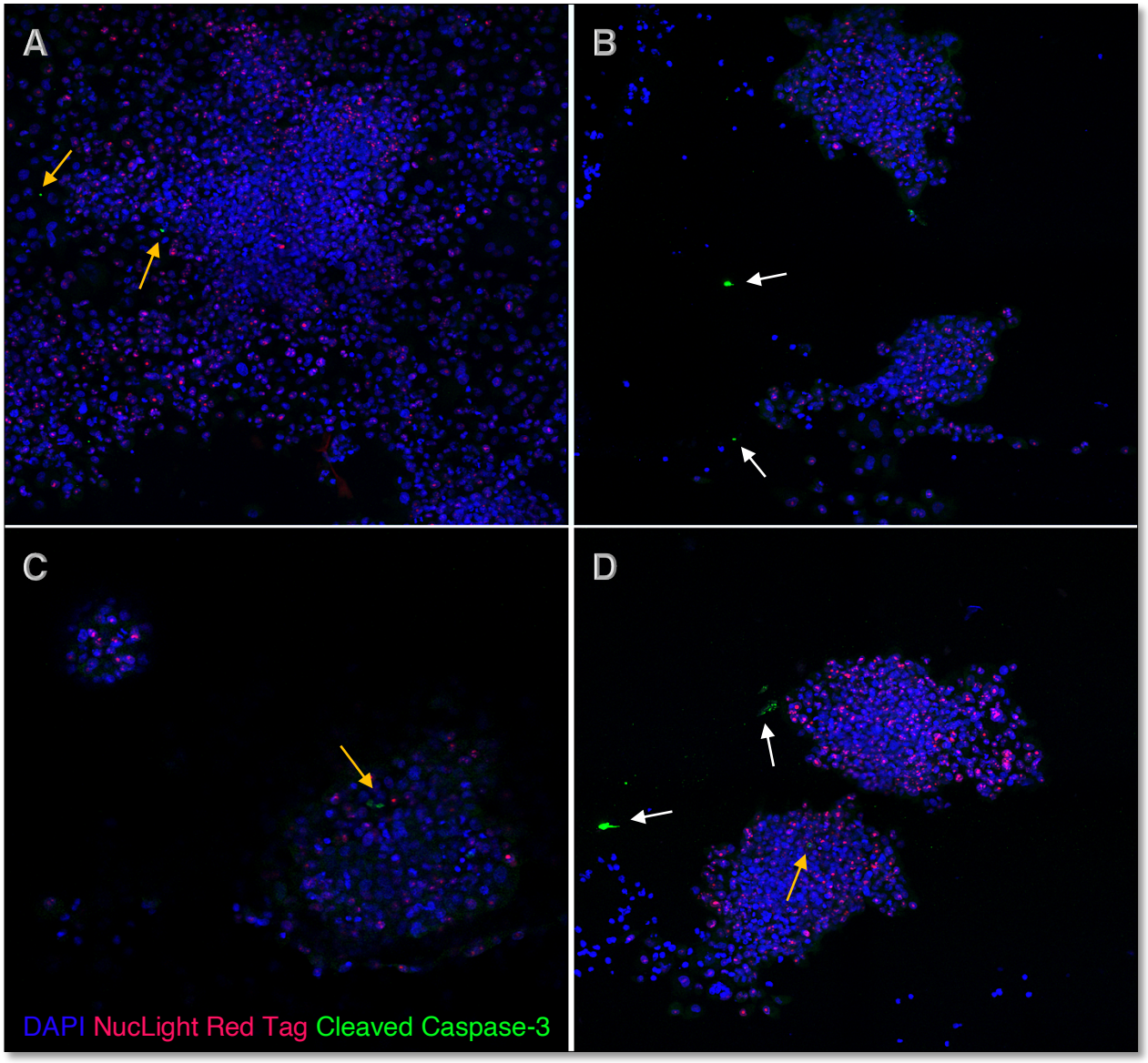

Figure 26 - Immunostaining of Panc-1 spheroids

(A) Spheroids cultured alone. (B) Spheroids co-cultured with NK-92 V84 cells. (C) Spheroids co-cultured with NK-92 wt. (D) Spheroids cocultured with NK-92 V85. All cells were nuclear counterstained stained with DAPI (blue) and cleaved caspase-3 (green). The NucLight Red Tag present on the cells was also captured. Orange arrows point at cleaved caspase-3 positive cells, while white arrows indicate unspecific binding. Differences in cell proliferation outside the spheroids can also be observed when comparing Panc-1 cells cultured alone (A) to Panc-1 cells cultured with NK-92 cells (B-D). The experiment was conducted a single time with 4 replicates per treatment.

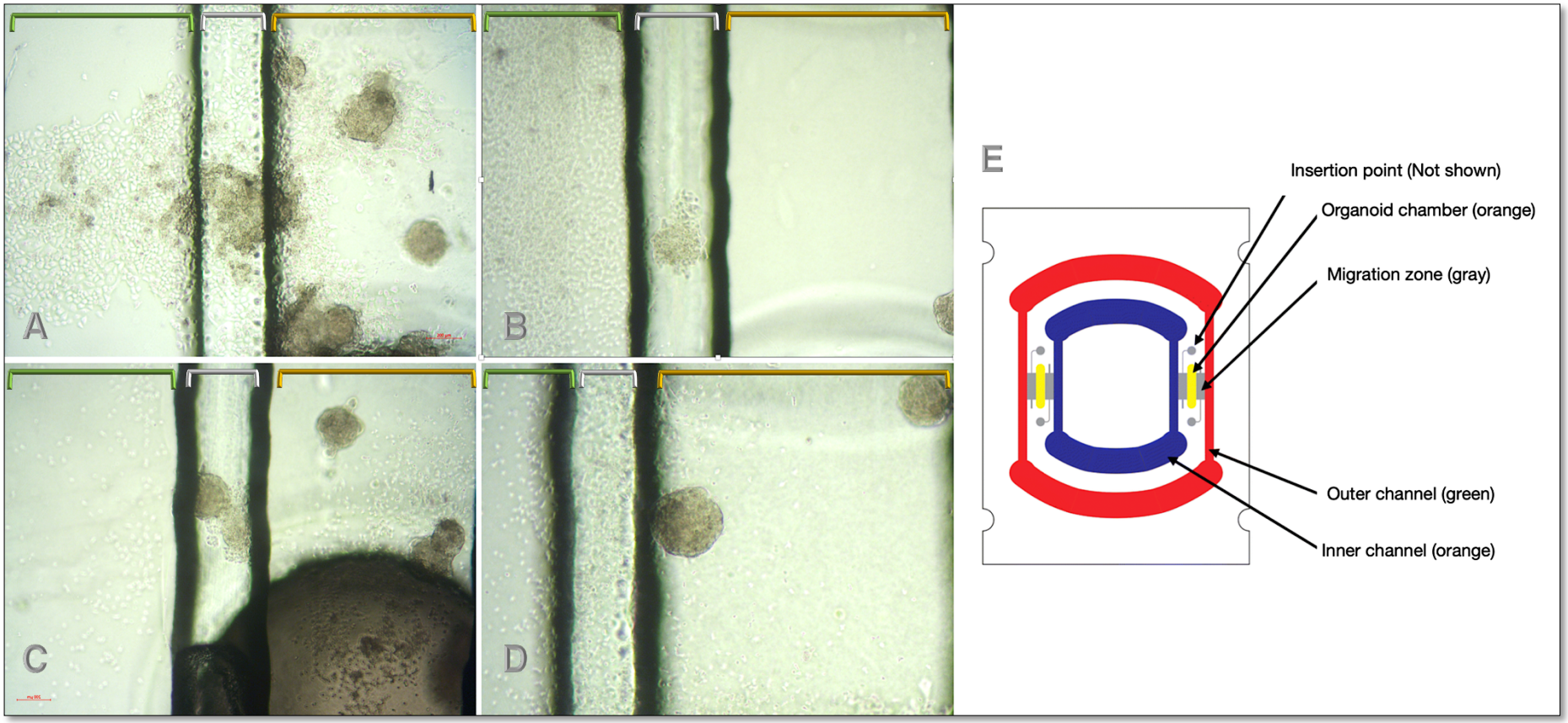

Figure 27 - Panc-1 wt spheroids 39 hours after co-culture with NK-92 cells.

(A) Spheroids cultured alone. (B) Spheroids co-cultured with NK-92 V84 cells. (C) Spheroids co-cultured with NK-92 wt. (D) Spheroids cocultured with NK-92 V85. (E) Chip layout indicating the colors representing each compartment. NK-92 cells can be appreciated on the chip channels in B, C, and D (orange bracket). Green and gray brackets delineate the organoid chambers and migration zones respectively. Images were taken with a bright-field microscope at 4x magnification. In picture A a visible infiltration and attachment of Panc-1 cells can be appreciated in the channel, an event that was not observed in spheroids co-culture with NK-92 cells.

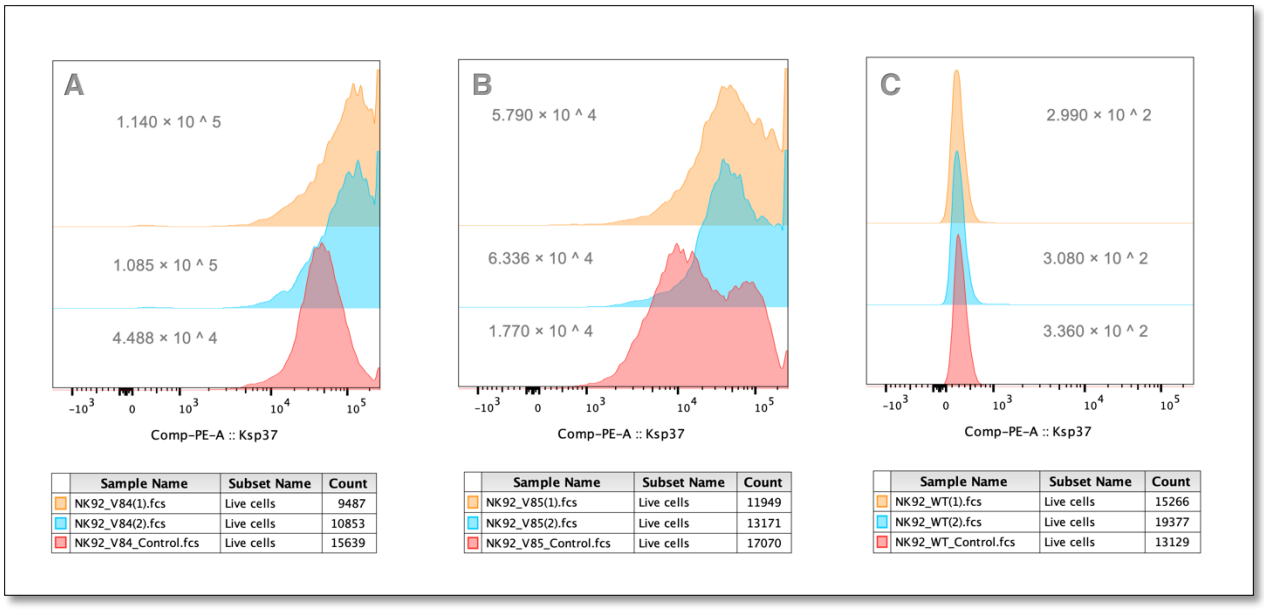

Sample Name	Subset Name	Count
NK92_V84(1).fcs	Live cells	9487
NK92_V84(2).fcs	Live cells	10853
NK92_V84_Control.fcs	Live cells	15639

Sample Name	Subset Name	Count
NK92_V85(1).fcs	Live cells	11949
NK92_V85(2).fcs	Live cells	13171
NK92_V85_Control.fcs	Live cells	17070

Sample Name	Subset Name	Count
NK92_WT(1).fcs	Live cells	15266
NK92_WT(2).fcs	Live cells	19377
NK92_WT_Control.fcs	Live cells	13129

Figure 28 - Intracellular Ksp37 histograms of NK-92 cells determined by flow cytometry.

(A) NK-92 V84. (B) NK-92 V85. (C) NK-92 wt. MFIs are shown in exponential notation on gray for each sample.

4 Discussion

The main goal of the project was to investigate the implication of Ksp37 in NK cell-mediated cytolysis of pancreatic cancer cells in the context of FGF2. To attain this objective, I employed genetically modified NK-92 cell lines expressing Ksp37 at a levels above the baseline for the corresponding wild-type strain. Further, through flow cytometry, it was possible to establish the constitutive secretion of Ksp37 regardless of stimulation with IL-15. As a third element, it was possible to determine the suitability of the microfluidic platform, developed by the Hybrid Technology Hub, for the use of NK-92 cells as an immune component in experiments on a tumor-on-a-chip system. Lastly, from a cell target perspective, both expression and subsequent gene knockout of FGF2 were confirmed at the transcript and the protein level, respectively.

The observations obtained from the immune cell-killing assays did not provide a direct correlation between the levels of Ksp37 secretion and the registered cytotoxicity towards Panc-1 cells. A situation exemplified by the registered of similar, and higher cytotoxicity in some instances, exhibited by NK-92 wild-type cells, compared to the Ksp37 overexpressing lines NK-92 V84 and V85. This fact diverges to some extent from previous results acquired by ex-post-docs at the Malmberg lab Kishan Kumar and Axel Berg-Larsen, whereby the use of Ksp37 treated media in scratch wound healing assays, treated HEK293 cells displayed lower proliferation rates than the cells treated only with growth media (5.5.3). Nonetheless, despite Panc-1 and HEK293 cells sharing similar HLA profiles and epithelial morphology [144-147], herein it is worth bearing in mind that comparisons across different cell lines are very challenging to draw. A caveat that is particularly relevant for the case of Ksp37 given the lack of published data directly evaluating its cytotoxicity.

The lack of Ksp37 secretion responsiveness upon IL-15 stimulation, observed in all three NK-92 cell lines evaluated, constituted another unexpected event. For instance, the registered absence of increased fluorescence after treatment with BFA in the NK-92 V51 carrying the GFP-Kps37 fusion protein could have arisen due to the relatively large size of GFP (27 kDa) in respect to its fusion partner (28 kDa before post-translational modifications). Interfering perhaps with the proper

folding [148], intracellular trafficking [149, 150], and secretion of Ksp37 [151]. Moreover, protein overexpression can also obstruct the research of cellular feedback to physiological stimuli given the large copy number of the fluorescent target, overloading thus the readout of methods relying on fluorescence variation such as flow cytometry [152]. Thirdly, despite all three NK-92 cell lines (V51, V84, and V85) sharing the same spleen focus-forming virus (SFFV) promoter (5.6) for the transgene expression of Ksp37, lentiviral vector insertions are largely unpredictable. Hence, the expression levels of the inserted Ksp37 gene could differ among the clonal cell lines depending on the chromosomal location where the integration has taken place [153]. These conjectures are undoubtedly not mutually exclusive. It would not be far-fetched to speculate that a blend of these three factors could contribute to the results obtained with the NK-92 V51 cell line.

Herein it is relevant to note that Kishan Kumar and Axel Berg-Larsen were also presented with similar obstacles confirming Ksp37 secretion. Although in a different NK-92 cell line, generated by adenovirus-mediated gene delivery and with the fluorescent tag on the C-terminus, the expressed Ksp37 protein also carried GFP as a fusion partner. As shown in Figure 5.5.1 (D), the western blot bands obtained with an anti-GFP antibody accurately corresponded in size to the Ksp37-GFP construct (65 kDa). However, the bands displayed no substantial difference between the cells treated with IL-15 as opposed to the non-treated cells. In addition, the signal obtained from the cell lysate was ostensibly more prominent than the supernatant samples. All in all, these observations strongly hint at the lack of appropriateness of GFP as a fluorescent reporter for the expression of Ksp37 in NK-92 cells.

Notwithstanding, these potential explanations are not directly transferable to the NK-92 lines V84 and V85, considering for instance the much smaller molecular weight of the 6x-His tag (0.8 kDa). Despite that, a point of similarity with the V51 cell line is found in the futility to elicit visible protein shedding upon stimulation with IL-15. One possible reason could be inefficient protein processing, considering that both (*i*) the size difference between the polypeptide and the secreted form of Ksp37, (*ii*) as well as results from its translation in-vitro, strongly suggest the requirement for specific post-translational modifications. [101]. Hence, its overexpression may be overwhelming the cellular machinery responsible for such modifications.

An alternative explanation for the lack of response to IL-15 by all three NK-92 lines could be found in the biological commonalities this cytokine shares with IL-2. Both cytokines are structurally related and bind to receptors with shared downstream signal transduction pathways [154, 155]. Additionally, the complexes they form with their cognate receptors, Interleukin-2 receptor and Interleukin-15 receptor, are topologically almost indistinguishable [156]. These similarities are reflected in the influence they exert over NK cells, whereby both cytokines are capable of inducing NK cell proliferation and enhancing cytotoxicity [155]. Consequently, the Ksp37 secretion IL-15 provokes on primary NK cells could be overshadowed by the presence of IL-2, which represents an essential component of the growth media required for NK-92 cell culture.

Irrespective of the unsuccessful stimulation with IL-15, the NK-92 V84 and V85 cells treated with BFA clearly demonstrated intracellular aggregation of Ksp37. Providing in that sense an indirect confirmation of constitutive synthesis and secretion of Ksp37 by the V84 and V85 cell lines in the presence of IL-2. An observation that is in agreement with previous reports on PBMC-derived CD16+ NK cells, as well as for CD4+, CD8+, and γδ+ T cells [101].

4.1 Bringing FGF2 into the picture: Moment of reckoning for Panc-1

The foremost criterion for selecting the Panc-1 cell line as the target for the present project was its known expression of FGF2 (3.1). With that in mind, the following questions arose: Is Ksp37 capable of binding to FGF2? And if so, is FGF2 secreted by Panc-1 cells and thus able to interact with Ksp37? Theoretical grounds at first provided support for a positive answer to the first question (1.4), which will later be reinforced by experimental evidence provided by Jørgen Wesche's lab (3.2). The second question, however, emerged as a much sturdier challenge.

As the western blot results showed (Figure 14), the Panc-1 cell line was not only positive for FGF2 but also for the ~17 kDa isoform that is known to be secreted [157]. Despite of that, published results demonstrating FGF2 secretion by Panc-1 cells are quite limited. The best evidence thus far has been brought forward by Hardikar et al. [158]. Nonetheless, the absence of a membrane marker on the immunofluorescence images provided, combined with the considerable size of the cytoplasmatic region and cell membrane protrusions in Panc-1 cells (5.7.5), renders the statement

of FGF2 secretion frail. The latter reason why I sought to replicate the experiment, as shown in Appendix 5.8, this time however with the inclusion of a membrane marker. The resulting images displayed what most likely represented unspecific antibody binding for FGF2, without visible differences between the different cell lines (wt vs. FGF2 $^{-/-}$).

Given the lack of conclusiveness, the results were not included in the main body of the manuscript. Nevertheless, it does raise the question of whether the observed absence of a positive correlation between the amount of Ksp37 secreted and cytolytic activity (Figure 21) could be partially explained by a missing interaction of FGF2 with Ksp37. To some extent, this would be in line with the higher cytotoxic capacity the NK-92 wt line exerted over the NK-92 V85 line, both for Panc-1 wt and FGF2-/- lines as targets, and over the NK-92 V84 line with Panc-1 wt cells as the target (Figure 21). Furthermore, the poorer performance of the Ksp37 overexpressing cell lines is also consistent with the reports linking protein overexpression and the potential for pathological changes in the host cells [159-161]. Opening thus the question of whether the Ksp37 overexpression in and of itself could be in some degree detrimental to the NK-92 cells, for instance by driving promiscuous unspecific interactions with other proteins as proposed by Vavouri et al. [159].

Lastly, the results obtained from the cytotoxic experiments in the microfluidic chips with NK-92 wild-type cells are more challenging to dissect, given in part to the system's complexity. However, the timeline employed of 1 day and 15 hours could constitute one major variable. For instance, most of the published experiments on tumor-on-a-chip models rely on co-culture time frames of 3 to 7 days [126, 162, 163]. Thus, the incubation time, in this case, could be representing a limiting factor for the effector cells to migrate through the gel and physically engage with the Panc-1 cells. In addition to this, the E:T ratios commonly used to assess natural killer cell cytotoxicity in microfluidic models range from 10:1 to 15:1 in most cases [162-164]. The latter represented a factor that was discussed during the experimental design part of the project. However, given the layout of the microfluidic platform employed, establishing a reliable method to control the number of spheroids seeded in the chips was not feasible given the timeframe of the project. Therefore, conceivably the confluency of 3.0 x 10^5 NK-92 cells / mL of media used in the chips was not adequate to trigger an observable response.

4.2 Concluding remarks

Natural killer cell-based immunotherapies are surging as promising domains of clinical research. Largely due to the reported manageable safety profiles and encouraging signs of efficacy, particularly in patients with hematological malignancies. If the field of NK cell therapy ought to continue thriving, however, there are pressing hurdles that are vitally important to address. Among them, two of the most pivotal matters are perhaps, on the one hand, (*i*) the lack of understanding on how to deal with immunosuppressive factors such as hypoxic conditions, limited glucose availability, and immunosuppressive cells present in the tumor microenvironment. (*ii*) And on the other hand, how to overcome the scarcity of growth factors needed for NK cell proliferation and persistence in-vivo such as IL-15 and IL-2. Both queries could benefit from a finer comprehension of NK cell biology, the reason why basic research efforts to incorporate knowledge of yet unknown elements of NK cells represent a dominant worth pursuing.

The overexpression models used in the present project render a simple yet reliable fashion to secrete Ksp37 protein into the media. A tool that could be used to explore the function of Ksp37 through a more reductionistic approach, such as the initiative of Kishan Kumar and Axel Berg-Larsen to generate conditioned media for proliferation experiments (5.5.3). The latter could help to circumvent the noise generated by factors such as cell heterogeneity, viability, and physiological changes intrinsic to the expression system. Moreover, the confirmed binding of Ksp37 to FGF2 opens up a path for a more targeted approach to deciphering the biological relevance of Ksp37. Significant correlations have been found between serum FGF2 levels and tumor invasives, size, and metastatic lesions in patients with colorectal, esophageal, liver, renal, and testicular cancers. In this regard, target cell lines derived from FGF2-sensitive cancer types could establish a clearer view of whether the FGF2-Ksp37 interaction is ultimately beneficial or detrimental during the cancer development process.

All in all, this project has provided preliminary evidence for (i) the capacity of Ksp37 to physically interact with FGF2, (ii) the lack of direct cytolytic involvement of Ksp37, and (iii) the suitability of pumpless microfluidic chip systems for studying NK cells in a dynamic 3D context. Insights that carry the potential for bringing forth a better understanding of FGF2 dysregulation in cancer development and perhaps even additional tools to address it.

5 Appendix

5.1 CRISPR gene KO of FGF2$^{-/-}$ in Panc-1 cells

5.1.1 sgRNAs sequences targeting FGF2

sgRNA I	CCGCAGGGACCAUGGCAGCC
sgRNA II	GGGUCCUUGAAGUGGCCGGG
sgRNA III	ACGGCCGAGUUGACGGGGUC

Note: Trans-activating CRISPR RNA (tracrRNA) sequences are not provided by Synthego.

5.1.2 Primer sequences for genotyping

Primer	Sequences (5′ to 3′)	GC%	Tm	Length
Forward primer	GTAGAAGATGTGACGCCGCG	60%	61	20 bp
Reverse primer	TTCCTGTCTTTGTCCCCGGG	60%	61	20 bp

5.1.3 PCR reaction setup

Component	Volume	Final concentration
MQ water	22 µl	
5X Phusion HF Buffer	10 µl	1X
10 mM dNTPs	1 µl	200 µM
5 µM Forward Primer	5 µl	0.5 µM
5 µM Reverse Primer	5 µl	0.5 µM
Template DNA	2.5 µl	< 250 ng
DMSO	1.5 µl	3%
Phusion DNA Polymerase	0.5 µl	1 U
Total	*50 µl*	

5.1.4 PCR cycling conditions

Step	Temperature	Time
Initial Denaturation	98°C	30 seconds
35 Cycles	98°C 72°C	10 seconds 30 seconds
Final extension	72°C	7 minutes
Hold	4°C	∞

5.2 rt-qPCR

5.2.1 rt-qPCR reaction composition

Component	Volume
KiCqStart 2x mix	2.50 µl
Reference gene assay	0.25 µl
Target gene assay	0.25 µl
Diluted RNA	2.00 µl
Total volume	*5.00 µl*

5.2.2 rt-qPCR cycling conditions

Step	Temperature	Time
cDNA synthesis	50°C	10 minutes
Initial Denaturation	95°C	1 minutes
PCR cycling (45 cycles)	95°C 60°C	10 seconds 30 seconds (data collection step)

5.3 rt-qPCR in Panc-1 cells

5.3.1 Amplification curves for FGF1 and B2M

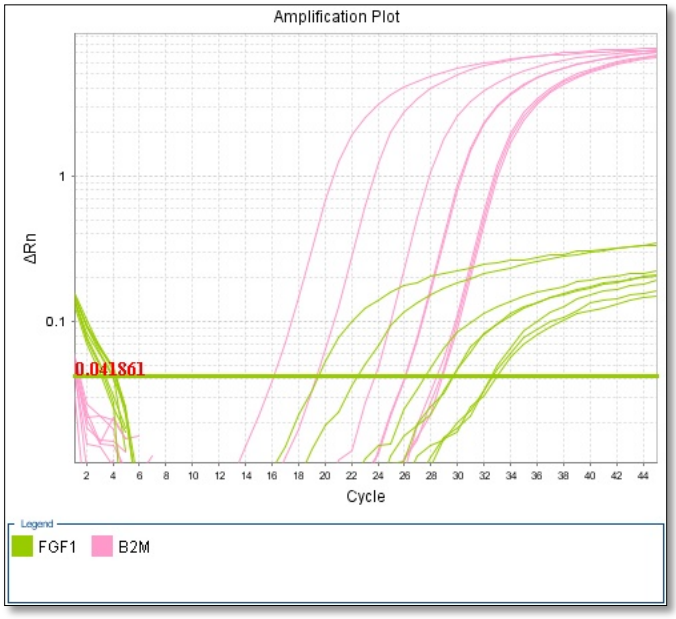

5.3.2 Amplification curves for FGF2 and B2M

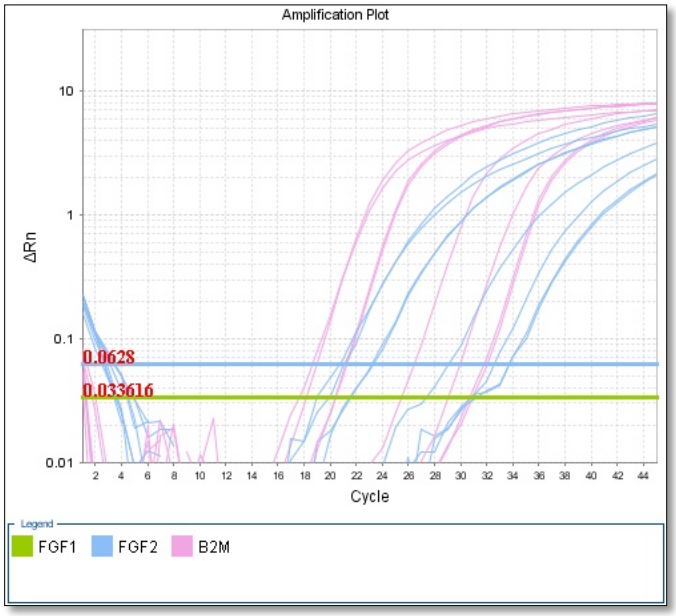

Note: Despite the presence of the FGF1 threshold line (green), the calculations involving FGF2 and the corresponding B2M were performed with their set threshold: 0.0628.

5.4 Western blots of FGF2 in Panc-1 cells

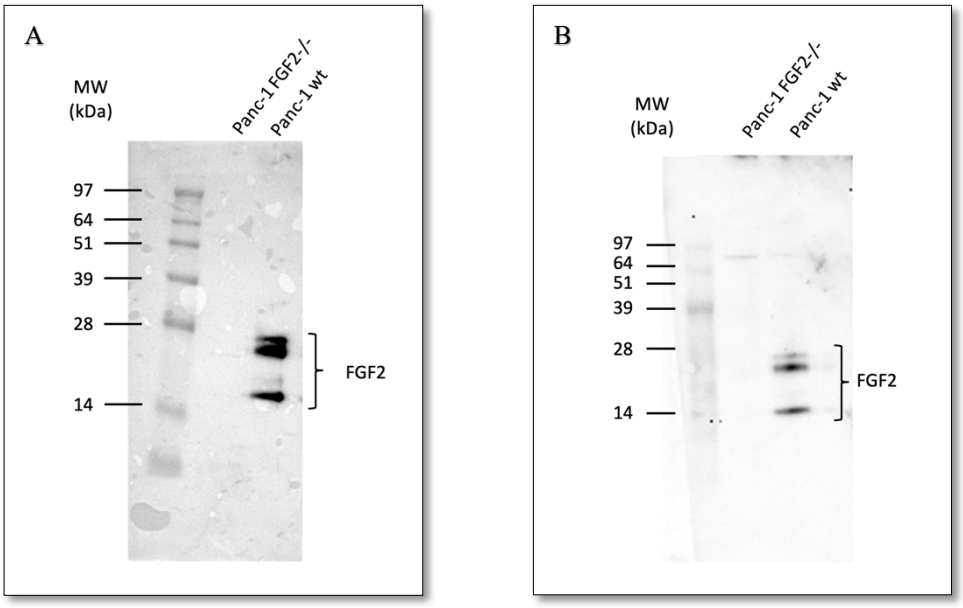

Note: The gel electrophoresis in both cases was run with the same ladder (2.8.3). However, the transfer of blot B was not as efficient compared to A, and thus the blur ladder.

5.5 Ksp37 secretion data (Unpublished data)

5.5.1 Intracellular Ksp37 level upon IL-15 stimulation

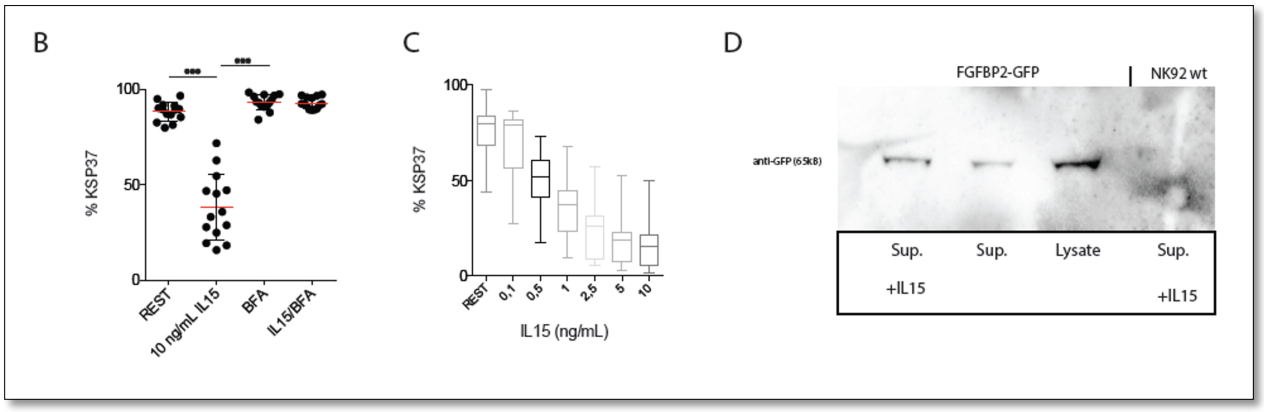

5.5.2 KSP37 levels relate to cell density and cell interaction in culture (No IL-15 added)

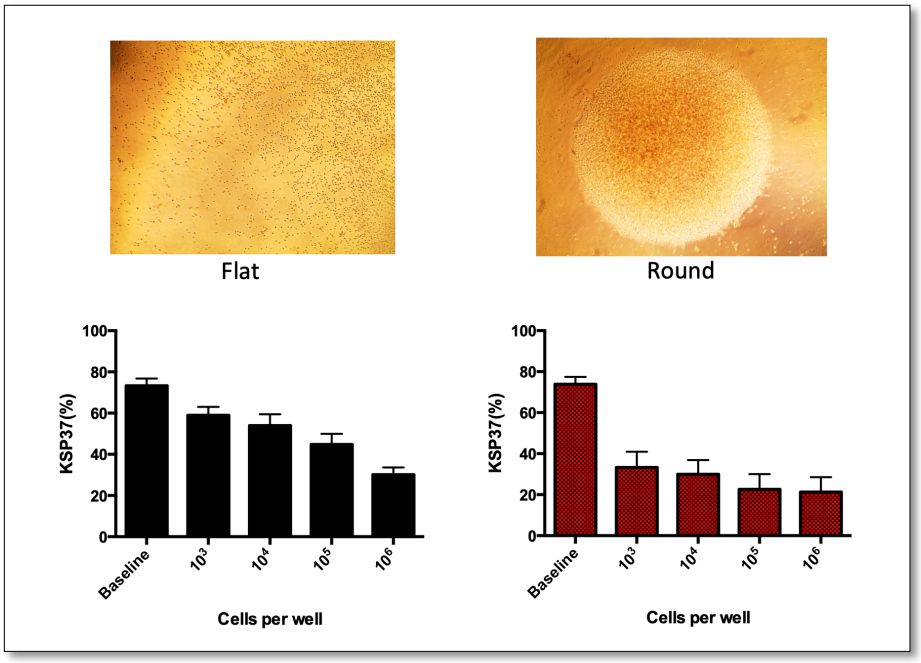

5.5.3 Incucyte scratch wound healing assay with HEK293 cells

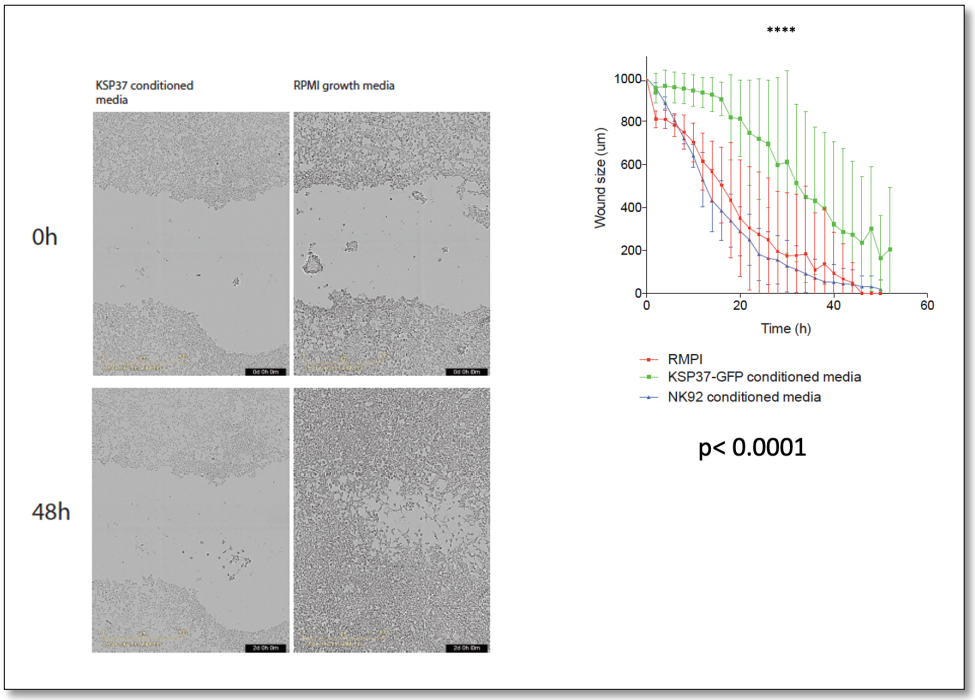

5.6 Expression vectors in NK-92 cell lines

5.6.1 NK-92 V51 (GFP-Ksp37)

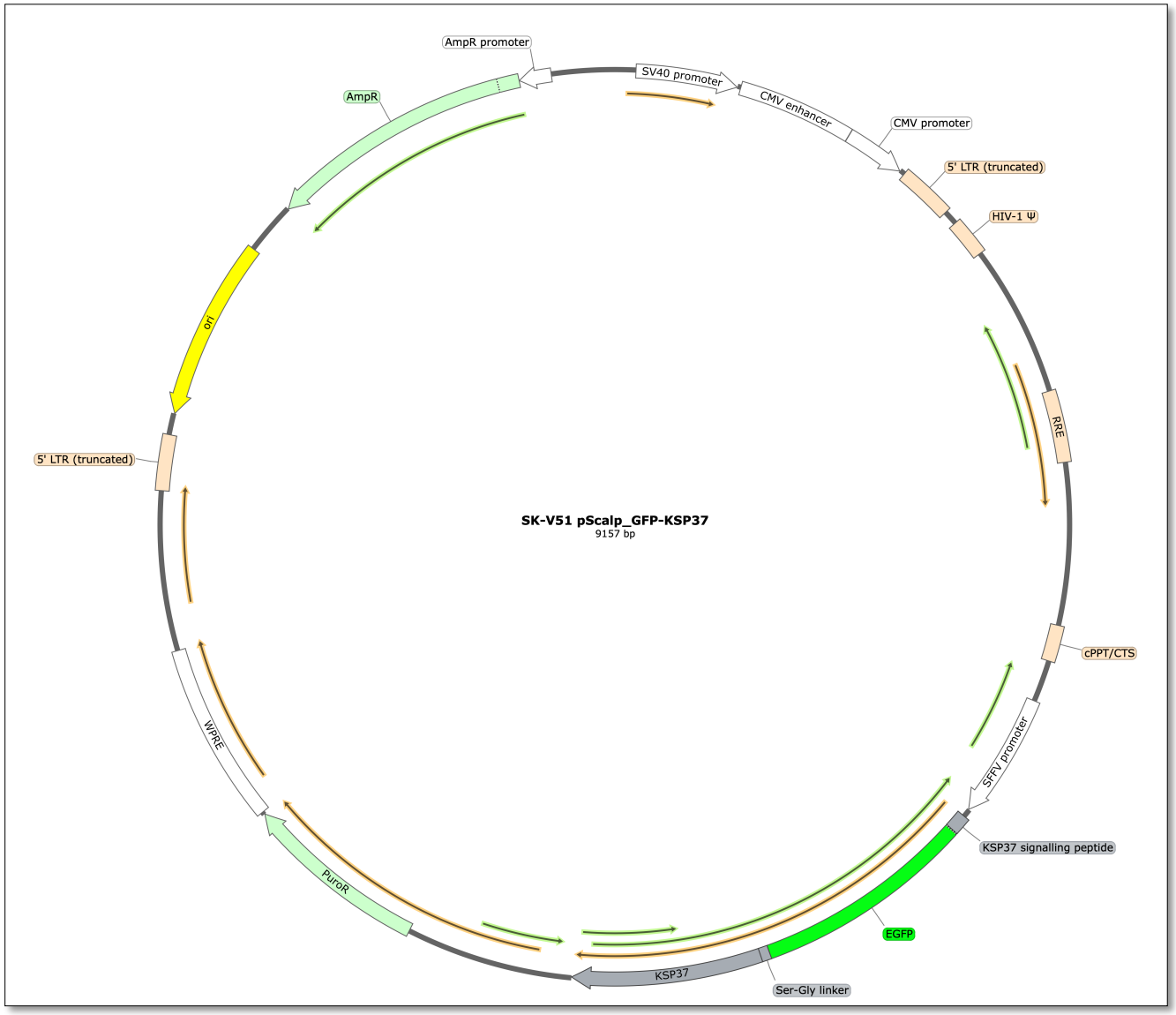

5.6.2 NK-92 V84 (His-Ksp37)

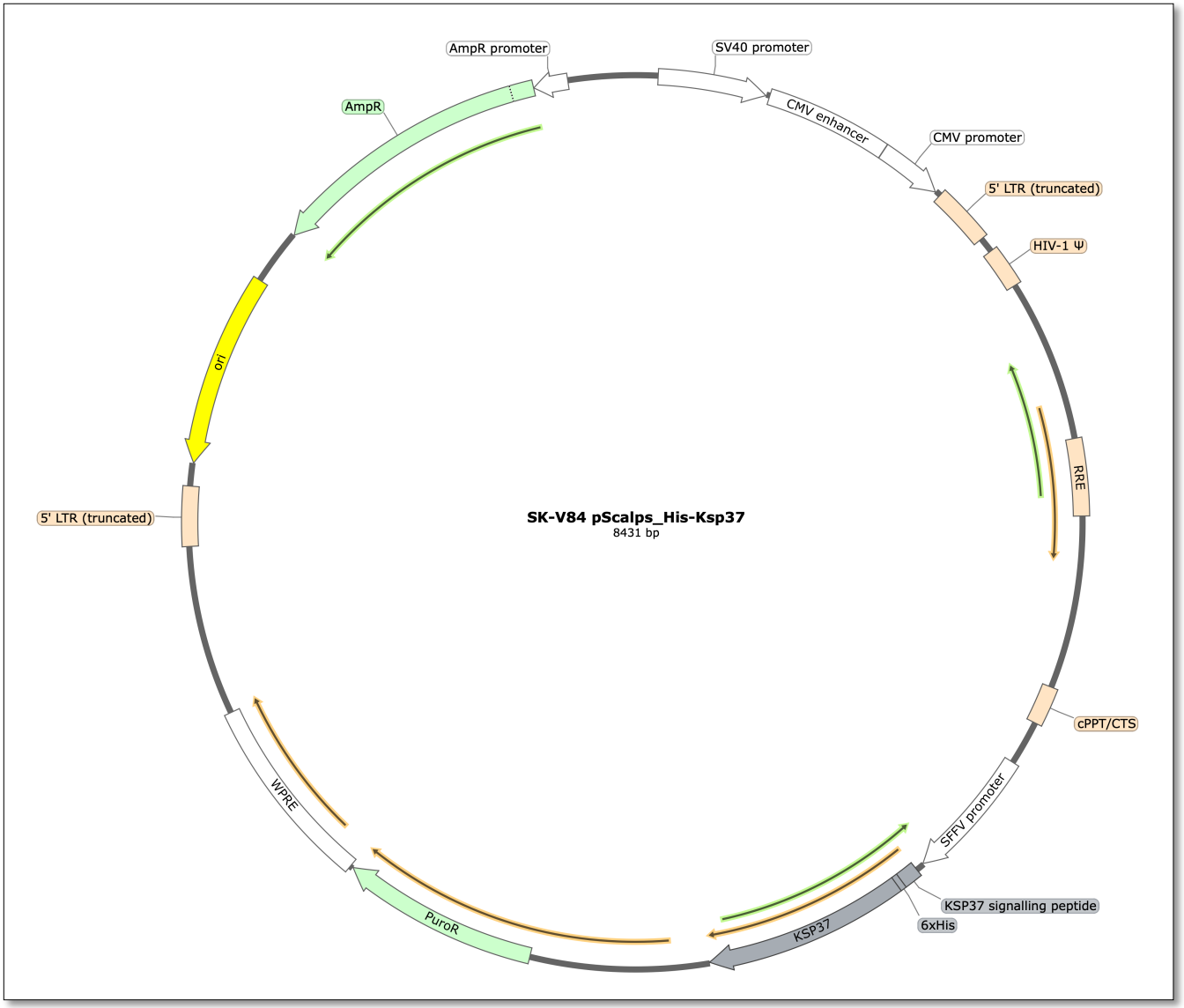

5.6.3 NK-92 V85 (Ksp37-His)

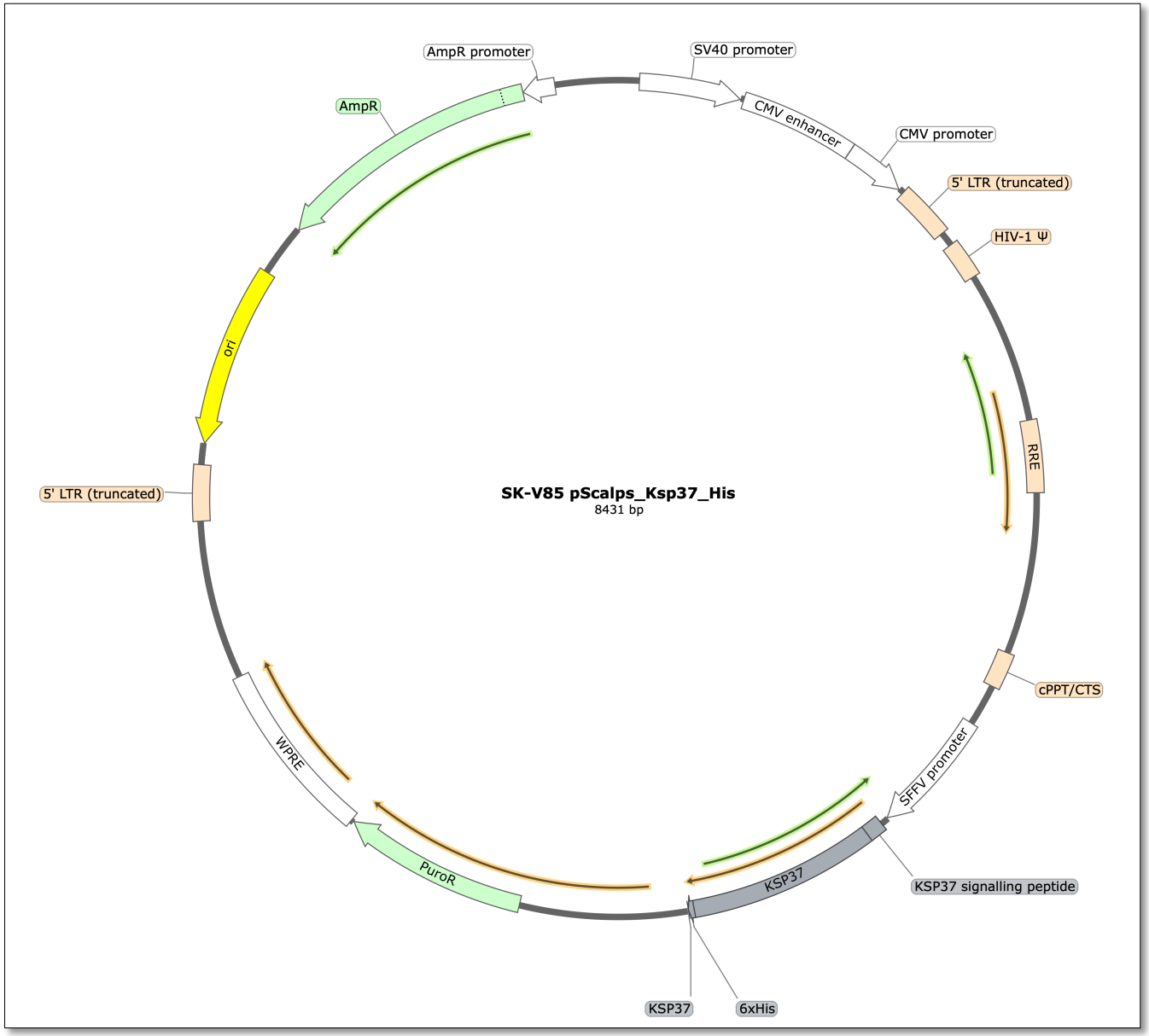

5.7 Incucyte killing assay results

Below a Complete overview of conditions tested during the IncuCyte killing assays for each one of the effector cell lines can be found. Target cells in their corresponding media or with the addition of IL-2 and IL-15 were used as negative controls. Each condition was tested on replicates. All data shown have been normalized to time 0 and then to the corresponding controls.

5.7.1 NK-92 V84

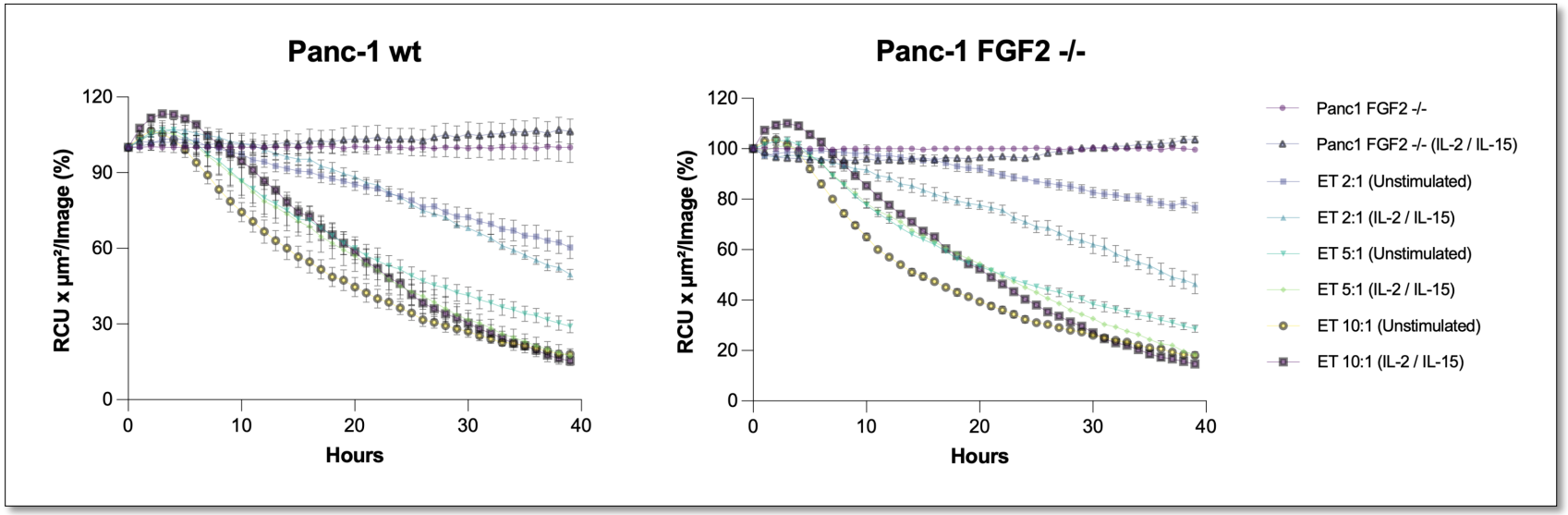

5.7.2 NK-92 V85

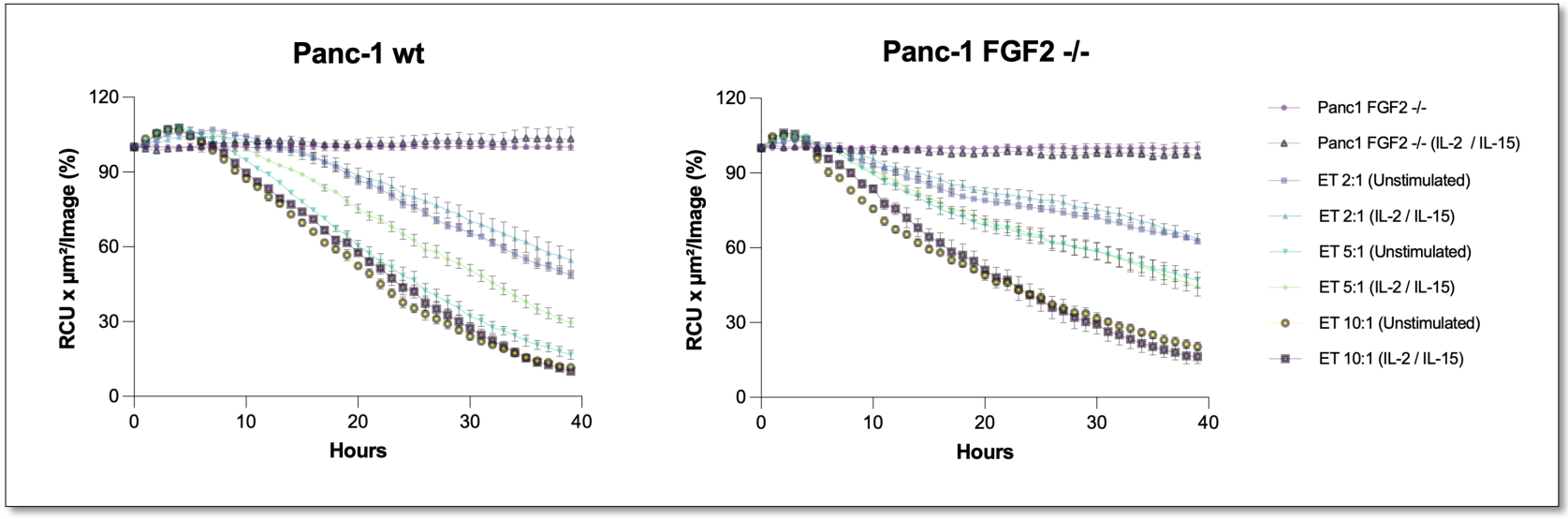

5.7.3 NK-92 wt

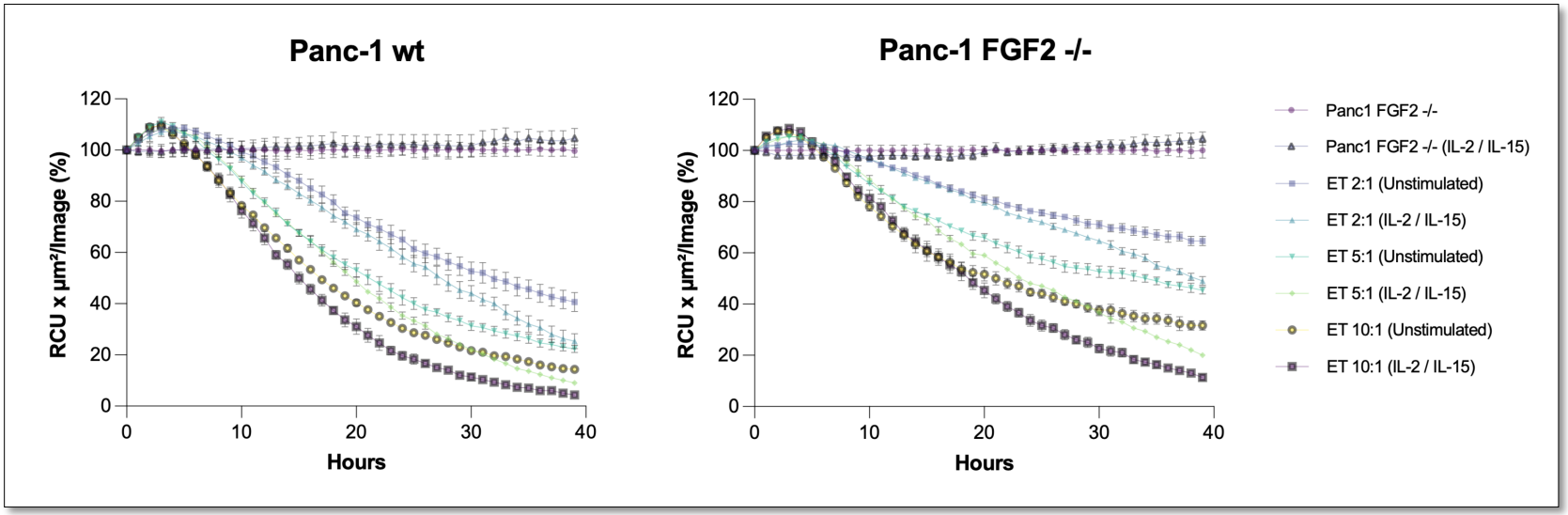

5.7.4 Incucyte results with the K562 cell line

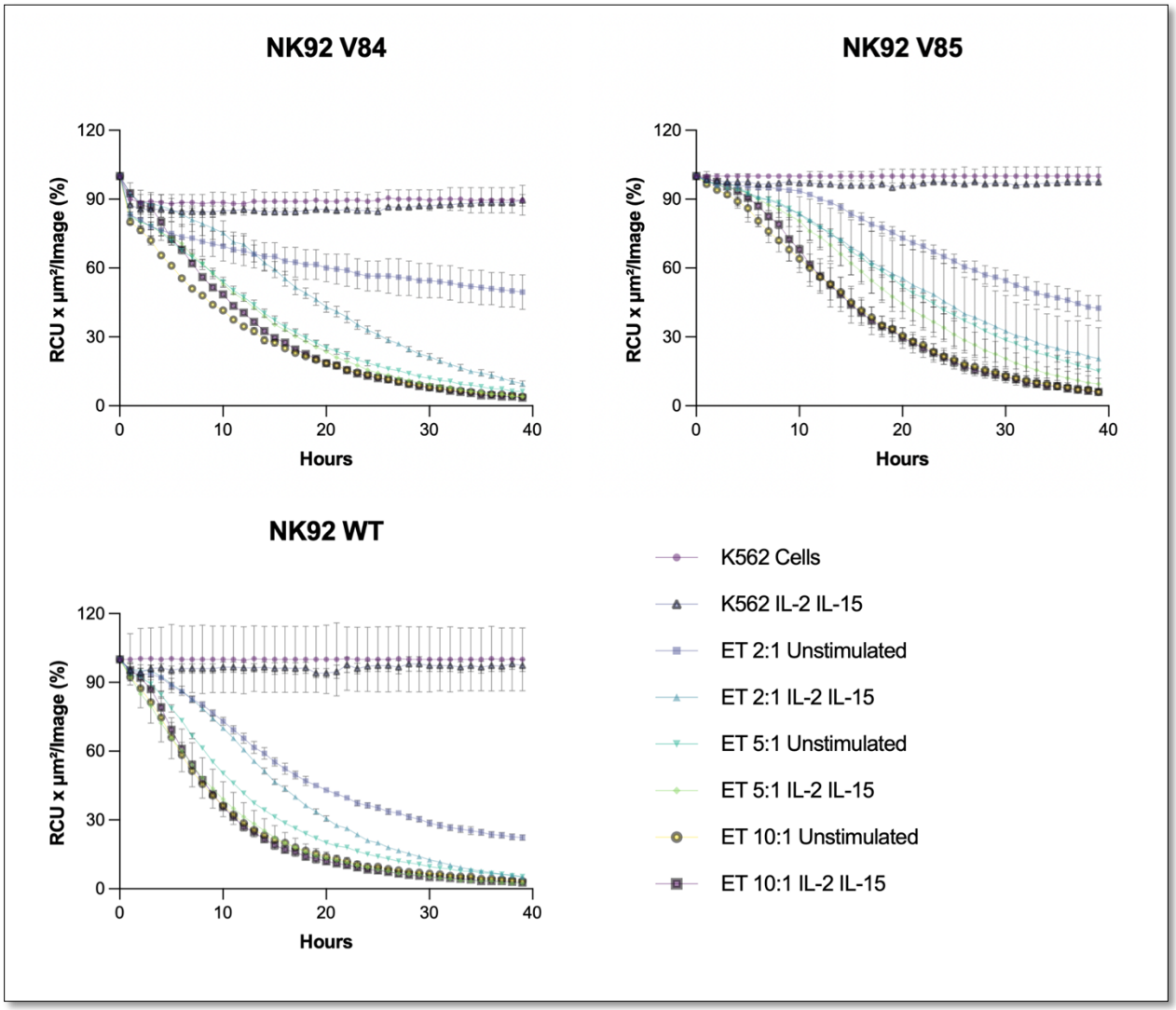

5.7.5 Representative image of attached Panc-1 cells in a 96-well plate

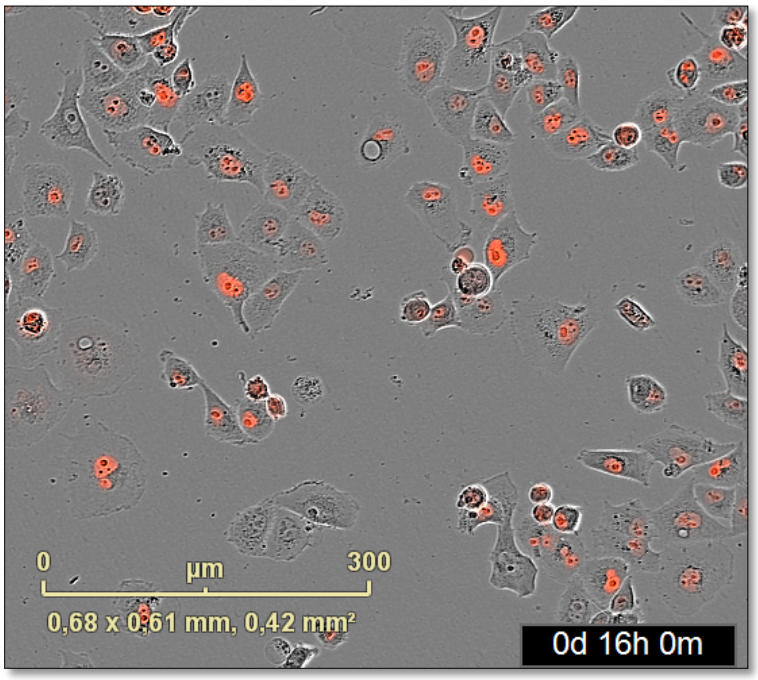

Note: Red fluorescence stems from the NucLight Red tag in the nucleus of cells.

5.8 Immunostaining of Panc-1 cells

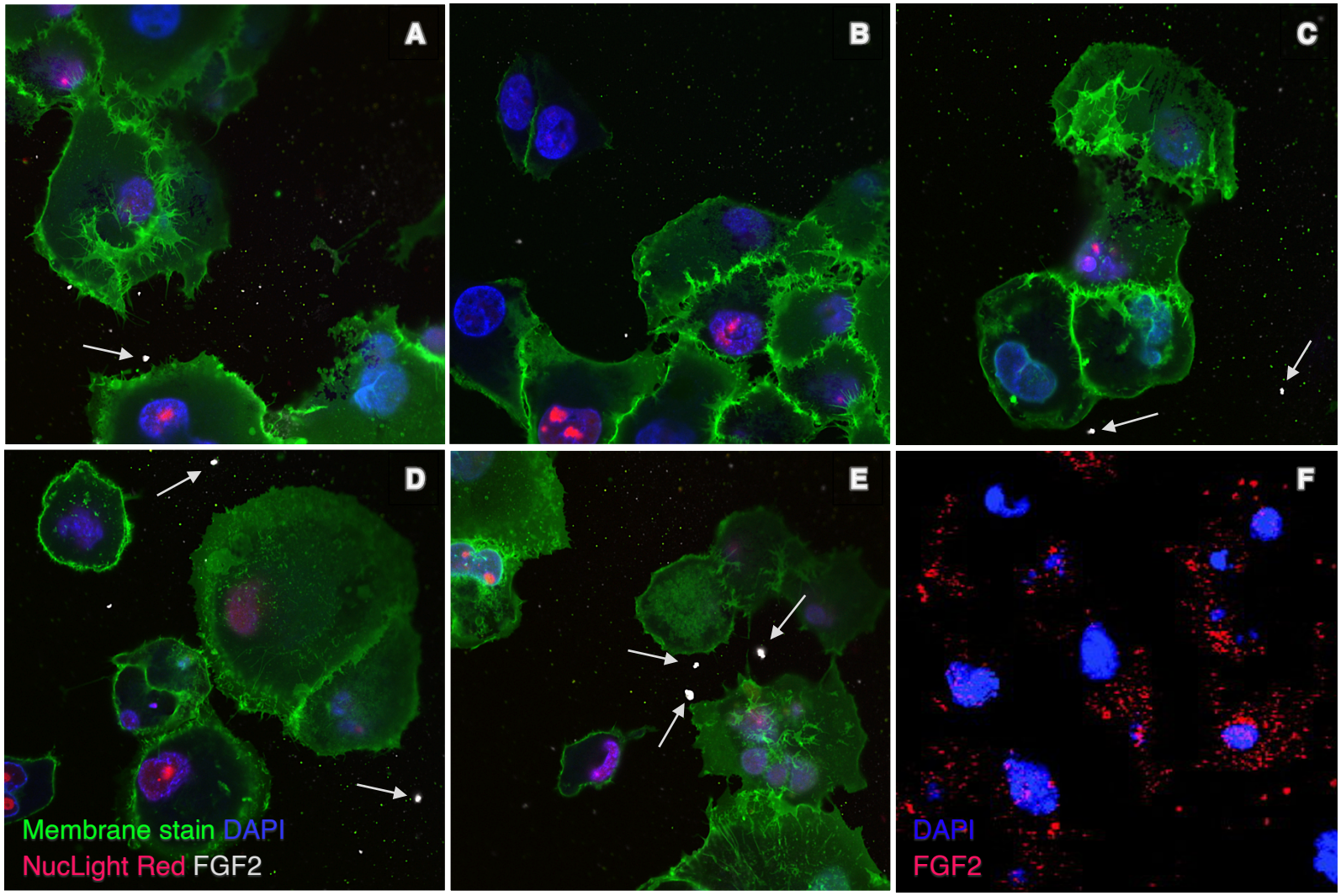

Confocal microscopy images from Panc-1 wt cells (A – C) and Panc-1 FGF2-/- cell (D – E) incubated in serum-free media for 2 hours. All images were taken from the extracellular matrix plane. (F) Image from FGF2 secretion experiment adopted from Hardikar et al. [158]. White arrows point at the most prominent unspecific aggregates of anti-mouse secondary antibody (# 715-605-151, Jackson ImmunoResearch) for primary anti-FGF2 (#MA1-24682, ThermoFisher).

6 Bibliography

1. Goodier, M.R., A.-S. Wolf, and E.M. Riley, *Differentiation and adaptation of natural killer cells for anti-malarial immunity.* Immunological Reviews, 2020. **293**(1): p. 25-37.
2. Abbas, A.K., et al., *Cellular and molecular immunology*. Tenth edition. ed. 2021, Amsterdam: Elsevier.
3. Thompson, M.R., et al., *Pattern recognition receptors and the innate immune response to viral infection.* Viruses, 2011. **3**(6): p. 920-40.
4. Hernandez, C., P. Huebener, and R.F. Schwabe, *Damage-associated molecular patterns in cancer: a double-edged sword.* Oncogene, 2016. **35**(46): p. 5931-5941.
5. McNab, F., et al., *Type I interferons in infectious disease.* Nature Reviews Immunology, 2015. **15**(2): p. 87-103.
6. Alberts B, J.A., Lewis J, et al., *Molecular Biology of the Cell*, in *Lymphocytes and the Cellular Basis of Adaptive Immunity*. 2002, Garland Science: New York.
7. Wu, S.-Y., et al., *Natural killer cells in cancer biology and therapy.* Molecular Cancer, 2020. **19**(1): p. 120.
8. Trinchieri, G., *Biology of natural killer cells.* Adv Immunol, 1989. **47**: p. 187-376.
9. Chan, A., et al., *CD56bright Human NK Cells Differentiate into CD56dim Cells: Role of Contact with Peripheral Fibroblasts.* The Journal of Immunology, 2007. **179**(1): p. 89-94.
10. Ferlazzo, G. and C. Münz, *NK cell compartments and their activation by dendritic cells.* J Immunol, 2004. **172**(3): p. 1333-9.
11. Robertson, M.J., et al., *Human natural killer cell adhesion molecules. Differential expression after activation and participation in cytolysis.* J Immunol, 1990. **145**(10): p. 3194-201.
12. Zamai, L., et al., *Kinetics of in vitro natural killer activity against K562 cells as detected by flow cytometry.* Cytometry, 1998. **32**(4): p. 280-5.
13. Eberl, G., et al., *Innate lymphoid cells: A new paradigm in immunology.* Science, 2015. **348**(6237): p. aaa6566.
14. Ljunggren, H.-G. and K. Kärre, *In search of the 'missing self': MHC molecules and NK cell recognition.* Immunology Today, 1990. **11**: p. 237-244.
15. Raulet, D.H., *Missing self recognition and self tolerance of natural killer (NK) cells.* Seminars in Immunology, 2006. **18**(3): p. 145-150.
16. Deauvieau, F., et al., *Human natural killer cells promote cross-presentation of tumor cell-derived antigens by dendritic cells.* International Journal of Cancer, 2015. **136**(5): p. 1085-1094.
17. Vivier, E., et al., *Functions of natural killer cells.* Nature Immunology, 2008. **9**(5): p. 503-510.
18. Christine A. Biron, et al., *NATURAL KILLER CELLS IN ANTIVIRAL DEFENSE: Function and Regulation by Innate Cytokines.* Annual Review of Immunology, 1999. **17**(1): p. 189-220.
19. Long, E.O., et al., *Controlling natural killer cell responses: integration of signals for activation and inhibition.* Annu Rev Immunol, 2013. **31**: p. 227-58.
20. Yokoyama, W.M. and B.F.M. Plougastel, *Immune functions encoded by the natural killer gene complex.* Nature Reviews Immunology, 2003. **3**(4): p. 304-316.

21. Pegram, H.J., et al., *Activating and inhibitory receptors of natural killer cells.* Immunology & Cell Biology, 2011. **89**(2): p. 216-224.
22. Sivori, S., et al., *Human NK cells: surface receptors, inhibitory checkpoints, and translational applications.* Cell Mol Immunol, 2019. **16**(5): p. 430-441.
23. Campbell, K.S. and A.K. Purdy, *Structure/function of human killer cell immunoglobulin-like receptors: lessons from polymorphisms, evolution, crystal structures and mutations.* Immunology, 2011. **132**(3): p. 315-25.
24. Rothbard, J.B. and M.L. Gefter, *Interactions between immunogenic peptides and MHC proteins.* Annu Rev Immunol, 1991. **9**: p. 527-65.
25. Heijmans, C.M.C., N.G. de Groot, and R.E. Bontrop, *Comparative genetics of the major histocompatibility complex in humans and nonhuman primates.* International Journal of Immunogenetics, 2020. **47**(3): p. 243-260.
26. Robinson, J., et al., *The IPD and IMGT/HLA database: allele variant databases.* Nucleic Acids Research, 2014. **43**(D1): p. D423-D431.
27. Siemaszko, J., A. Marzec-Przyszlak, and K. Bogunia-Kubik, *NKG2D Natural Killer Cell Receptor-A Short Description and Potential Clinical Applications.* Cells, 2021. **10**(6).
28. Groh, V., et al., *Broad tumor-associated expression and recognition by tumor-derived gamma delta T cells of MICA and MICB.* Proc Natl Acad Sci U S A, 1999. **96**(12): p. 6879-84.
29. Cosman, D., et al., *ULBPs, novel MHC class I-related molecules, bind to CMV glycoprotein UL16 and stimulate NK cytotoxicity through the NKG2D receptor.* Immunity, 2001. **14**(2): p. 123-33.
30. Carretero, M., et al., *The CD94 and NKG2-A C-type lectins covalently assemble to form a natural killer cell inhibitory receptor for HLA class I molecules.* Eur J Immunol, 1997. **27**(2): p. 563-7.
31. Braud, V.M., et al., *HLA-E binds to natural killer cell receptors CD94/NKG2A, B and C.* Nature, 1998. **391**(6669): p. 795-9.
32. Mota, G., et al., *Interaction of human immunoglobulin G with CD16 on natural killer cells: ligand clearance, FcgammaRIIIA turnover and effects of metalloproteinases on FcgammaRIIIA-mediated binding, signal transduction and killing.* Scand J Immunol, 2004. **59**(3): p. 278-84.
33. Dixon, K.J., J. Wu, and B. Walcheck, *Engineering Anti-Tumor Monoclonal Antibodies and Fc Receptors to Enhance ADCC by Human NK Cells.* Cancers (Basel), 2021. **13**(2).
34. Long, E.O., *Ready for prime time: NK cell priming by dendritic cells.* Immunity, 2007. **26**(4): p. 385-7.
35. Walzer, T., et al., *Natural-killer cells and dendritic cells: "l'union fait la force".* Blood, 2005. **106**(7): p. 2252-8.
36. Luevano, M., A. Madrigal, and A. Saudemont, *Transcription factors involved in the regulation of natural killer cell development and function: an update.* Front Immunol, 2012. **3**: p. 319.
37. Abel, A.M., et al., *Natural Killer Cells: Development, Maturation, and Clinical Utilization.* Frontiers in Immunology, 2018. **9**.
38. Kondo, M., I.L. Weissman, and K. Akashi, *Identification of clonogenic common lymphoid progenitors in mouse bone marrow.* Cell, 1997. **91**(5): p. 661-72.
39. Rosmaraki, E.E., et al., *Identification of committed NK cell progenitors in adult murine bone marrow.* Eur J Immunol, 2001. **31**(6): p. 1900-9.

40. Huntington, N.D., C.A.J. Vosshenrich, and J.P. Di Santo, *Developmental pathways that generate natural-killer-cell diversity in mice and humans.* Nature Reviews Immunology, 2007. **7**(9): p. 703-714.
41. Bai, L., et al., *Liver type 1 innate lymphoid cells develop locally via an interferon-γ-dependent loop.* Science, 2021. **371**(6536).
42. Scoville, S.D., A.G. Freud, and M.A. Caligiuri, *Modeling Human Natural Killer Cell Development in the Era of Innate Lymphoid Cells.* Front Immunol, 2017. **8**: p. 360.
43. Yu, J., A.G. Freud, and M.A. Caligiuri, *Location and cellular stages of natural killer cell development.* Trends Immunol, 2013. **34**(12): p. 573-82.
44. Kim, S., et al., *In vivo developmental stages in murine natural killer cell maturation.* Nat Immunol, 2002. **3**(6): p. 523-8.
45. Mace, E.M., et al., *Mutations in GATA2 cause human NK cell deficiency with specific loss of the CD56(bright) subset.* Blood, 2013. **121**(14): p. 2669-77.
46. Björkström, N.K., et al., *Expression patterns of NKG2A, KIR, and CD57 define a process of CD56dim NK-cell differentiation uncoupled from NK-cell education.* Blood, 2010. **116**(19): p. 3853-3864.
47. Cooper, M.A., et al., *Human natural killer cells: a unique innate immunoregulatory role for the CD56(bright) subset.* Blood, 2001. **97**(10): p. 3146-51.
48. Jacobs, R., et al., *CD56bright cells differ in their KIR repertoire and cytotoxic features from CD56dim NK cells.* Eur J Immunol, 2001. **31**(10): p. 3121-7.
49. Béziat, V., et al., *NK cell terminal differentiation: correlated stepwise decrease of NKG2A and acquisition of KIRs.* PLoS One, 2010. **5**(8): p. e11966.
50. Caligiuri, M.A., *Human natural killer cells.* Blood, 2008. **112**(3): p. 461-9.
51. Lopez-Vergès, S., et al., *CD57 defines a functionally distinct population of mature NK cells in the human CD56dimCD16+ NK-cell subset.* Blood, 2010. **116**(19): p. 3865-3874.
52. Mujal, A.M., R.B. Delconte, and J.C. Sun, *Natural Killer Cells: From Innate to Adaptive Features.* Annual Review of Immunology, 2021. **39**(1): p. 417-447.
53. Gumá, M., et al., *Expansion of CD94/NKG2C+ NK cells in response to human cytomegalovirus-infected fibroblasts.* Blood, 2006. **107**(9): p. 3624-31.
54. Gumá, M., et al., *Imprint of human cytomegalovirus infection on the NK cell receptor repertoire.* Blood, 2004. **104**(12): p. 3664-71.
55. Wagner, J.A. and T.A. Fehniger, *Human Adaptive Natural Killer Cells: Beyond NKG2C.* Trends Immunol, 2016. **37**(6): p. 351-353.
56. Rölle, A. and P. Brodin, *Immune Adaptation to Environmental Influence: The Case of NK Cells and HCMV.* Trends Immunol, 2016. **37**(3): p. 233-243.
57. Goodridge, J.P., B. Önfelt, and K.-J. Malmberg, *Newtonian cell interactions shape natural killer cell education.* Immunological Reviews, 2015. **267**(1): p. 197-213.
58. Kim, S., et al., *Licensing of natural killer cells by host major histocompatibility complex class I molecules.* Nature, 2005. **436**(7051): p. 709-13.
59. Raulet, D.H. and R.E. Vance, *Self-tolerance of natural killer cells.* Nat Rev Immunol, 2006. **6**(7): p. 520-31.
60. Elliott, J.M. and W.M. Yokoyama, *Unifying concepts of MHC-dependent natural killer cell education.* Trends Immunol, 2011. **32**(8): p. 364-72.
61. Yokoyama, W.M. and S. Kim, *Licensing of natural killer cells by self-major histocompatibility complex class I.* Immunol Rev, 2006. **214**: p. 143-54.

62. Höglund, P. and P. Brodin, *Current perspectives of natural killer cell education by MHC class I molecules.* Nat Rev Immunol, 2010. **10**(10): p. 724-34.
63. Elliott, J.M., J.A. Wahle, and W.M. Yokoyama, *MHC class I-deficient natural killer cells acquire a licensed phenotype after transfer into an MHC class I-sufficient environment.* J Exp Med, 2010. **207**(10): p. 2073-9.
64. Joncker, N.T., et al., *Mature natural killer cells reset their responsiveness when exposed to an altered MHC environment.* J Exp Med, 2010. **207**(10): p. 2065-72.
65. Liao, N.S., et al., *MHC class I deficiency: susceptibility to natural killer (NK) cells and impaired NK activity.* Science, 1991. **253**(5016): p. 199-202.
66. de la Salle, H., et al., *Homozygous human TAP peptide transporter mutation in HLA class I deficiency.* Science, 1994. **265**(5169): p. 237-41.
67. Höglund, P., et al., *Recognition of beta 2-microglobulin-negative (beta 2m-) T-cell blasts by natural killer cells from normal but not from beta 2m- mice: nonresponsiveness controlled by beta 2m- bone marrow in chimeric mice.* Proc Natl Acad Sci U S A, 1991. **88**(22): p. 10332-6.
68. Schreiber, R.D., L.J. Old, and M.J. Smyth, *Cancer immunoediting: integrating immunity's roles in cancer suppression and promotion.* Science, 2011. **331**(6024): p. 1565-70.
69. Dhodapkar, M.V., et al., *Vigorous premalignancy-specific effector T cell response in the bone marrow of patients with monoclonal gammopathy.* J Exp Med, 2003. **198**(11): p. 1753-7.
70. Hollenbeak, C.S., et al., *Increased incidence of melanoma in renal transplantation recipients.* Cancer, 2005. **104**(9): p. 1962-7.
71. Penn, I., *Post-transplant malignancy: the role of immunosuppression.* Drug Saf, 2000. **23**(2): p. 101-13.
72. So, T., et al., *Haplotype loss of HLA class I antigen as an escape mechanism from immune attack in lung cancer.* Cancer Res, 2005. **65**(13): p. 5945-52.
73. Medema, J.P., et al., *Blockade of the granzyme B/perforin pathway through overexpression of the serine protease inhibitor PI-9/SPI-6 constitutes a mechanism for immune escape by tumors.* Proc Natl Acad Sci U S A, 2001. **98**(20): p. 11515-20.
74. Zitvogel, L., A. Tesniere, and G. Kroemer, *Cancer despite immunosurveillance: immunoselection and immunosubversion.* Nature Reviews Immunology, 2006. **6**(10): p. 715-727.
75. Huang, Y., et al., *Turning on/off tumor-specific CTL response during progressive tumor growth.* J Immunol, 2005. **175**(5): p. 3110-6.
76. Zhou, G., et al., *Reciprocal changes in tumor antigenicity and antigen-specific T cell function during tumor progression.* J Exp Med, 2004. **200**(12): p. 1581-92.
77. Sakaguchi, S., *Naturally arising CD4+ regulatory t cells for immunologic self-tolerance and negative control of immune responses.* Annu Rev Immunol, 2004. **22**: p. 531-62.
78. Finn, O.J., *A Believer's Overview of Cancer Immunosurveillance and Immunotherapy.* J Immunol, 2018. **200**(2): p. 385-391.
79. Liu, E., et al., *Use of CAR-Transduced Natural Killer Cells in CD19-Positive Lymphoid Tumors.* N Engl J Med, 2020. **382**(6): p. 545-553.
80. Donskov, F. and H.v.d. Maase, *Impact of Immune Parameters on Long-Term Survival in Metastatic Renal Cell Carcinoma.* Journal of Clinical Oncology, 2006. **24**(13): p. 1997-2005.

81. Gannon, P.O., et al., *Characterization of the intra-prostatic immune cell infiltration in androgen-deprived prostate cancer patients.* Journal of Immunological Methods, 2009. **348**(1): p. 9-17.
82. Delahaye, N.F., et al., *Alternatively spliced NKp30 isoforms affect the prognosis of gastrointestinal stromal tumors.* Nature Medicine, 2011. **17**(6): p. 700-707.
83. Cursons, J., et al., *A Gene Signature Predicting Natural Killer Cell Infiltration and Improved Survival in Melanoma Patients.* Cancer Immunology Research, 2019. **7**(7): p. 1162-1174.
84. Denkert, C., et al., *Tumour-infiltrating lymphocytes and prognosis in different subtypes of breast cancer: a pooled analysis of 3771 patients treated with neoadjuvant therapy.* Lancet Oncol, 2018. **19**(1): p. 40-50.
85. Larsen, S.K., Y. Gao, and P.H. Basse, *NK cells in the tumor microenvironment.* Crit Rev Oncog, 2014. **19**(1-2): p. 91-105.
86. Zwirner, N.W., C.I. Domaica, and M.B. Fuertes, *Regulatory functions of NK cells during infections and cancer.* J Leukoc Biol, 2021. **109**(1): p. 185-194.
87. Myers, J.A. and J.S. Miller, *Exploring the NK cell platform for cancer immunotherapy.* Nature Reviews Clinical Oncology, 2021. **18**(2): p. 85-100.
88. Hatjiharissi, E., et al., *Increased natural killer cell expression of CD16, augmented binding and ADCC activity to rituximab among individuals expressing the Fc{gamma}RIIIa-158 V/V and V/F polymorphism.* Blood, 2007. **110**(7): p. 2561-4.
89. Smyth, M.J., M. Taniguchi, and S.E.A. Street, *The Anti-Tumor Activity of IL-12: Mechanisms of Innate Immunity That Are Model and Dose Dependent1.* The Journal of Immunology, 2000. **165**(5): p. 2665-2670.
90. Vyakarnam, A., et al., *Human clones with natural killer function can activate B cells and secrete B cell differentiation factors.* Eur J Immunol, 1985. **15**(6): p. 606-10.
91. Becker, J.C., et al., *Human natural killer clones enhance in vitro antibody production by tumour necrosis factor alpha and gamma interferon.* Scand J Immunol, 1990. **32**(2): p. 153-62.
92. Blanca, I.R., et al., *Human B cell activation by autologous NK cells is regulated by CD40-CD40 ligand interaction: role of memory B cells and CD5+ B cells.* J Immunol, 2001. **167**(11): p. 6132-9.
93. Whitmire, J.K., J.T. Tan, and J.L. Whitton, *Interferon-gamma acts directly on CD8+ T cells to increase their abundance during virus infection.* J Exp Med, 2005. **201**(7): p. 1053-9.
94. Whitmire, J.K., et al., *Direct interferon-gamma signaling dramatically enhances CD4+ and CD8+ T cell memory.* J Immunol, 2007. **179**(2): p. 1190-7.
95. Bird, L., *NK cells set a prime example.* Nature Reviews Immunology, 2004. **4**(12): p. 924-924.
96. Iyoda , T., et al., *The CD8+ Dendritic Cell Subset Selectively Endocytoses Dying Cells in Culture and In Vivo.* Journal of Experimental Medicine, 2002. **195**(10): p. 1289-1302.
97. Sauter, B., et al., *Consequences of Cell Death: Exposure to Necrotic Tumor Cells, but Not Primary Tissue Cells or Apoptotic Cells, Induces the Maturation of Immunostimulatory Dendritic Cells.* Journal of Experimental Medicine, 2000. **191**(3): p. 423-434.
98. Albert, M.L., B. Sauter, and N. Bhardwaj, *Dendritic cells acquire antigen from apoptotic cells and induce class I-restricted CTLs.* Nature, 1998. **392**(6671): p. 86-89.

99. Moretta, A., *Natural killer cells and dendritic cells: rendezvous in abused tissues.* Nature Reviews Immunology, 2002. **2**(12): p. 957-965.
100. Taetzsch, T., V.L. Brayman, and G. Valdez, *FGF binding proteins (FGFBPs): Modulators of FGF signaling in the developing, adult, and stressed nervous system.* Biochimica et Biophysica Acta (BBA) - Molecular Basis of Disease, 2018. **1864**(9, Part B): p. 2983-2991.
101. Ogawa, K., et al., *A Novel Serum Protein That Is Selectively Produced by Cytotoxic Lymphocytes.* The Journal of Immunology, 2001. **166**(10): p. 6404.
102. Kita, Y., et al., *Novel therapeutic vaccines [(HSP65 + IL-12)DNA-, granulysin- and Ksp37-vaccine] against tuberculosis and synergistic effects in the combination with chemotherapy.* Human Vaccines & Immunotherapeutics, 2013. **9**(3): p. 526-533.
103. Zhang, W., et al., *Effect of FGF-binding protein 3 on vascular permeability.* J Biol Chem, 2008. **283**(42): p. 28329-37.
104. Liu, Z., et al., *Potential biomarkers of acute myocardial infarction based on weighted gene co-expression network analysis.* BioMedical Engineering OnLine, 2019. **18**(1): p. 9.
105. McKean, D.M., et al., *Loss of RNA expression and allele-specific expression associated with congenital heart disease.* Nature Communications, 2016. **7**(1): p. 12824.
106. HAYANO, C., et al., *Accumulation of CD16+ Cells with Secretion of Ksp37 in Decidua at the End of Pregnancy.* American Journal of Reproductive Immunology, 2002. **48**(1): p. 57-62.
107. Turner, N. and R. Grose, *Fibroblast growth factor signalling: from development to cancer.* Nature Reviews Cancer, 2010. **10**(2): p. 116-129.
108. Elgaaen, B.V., et al., *POLD2 and KSP37 (FGFBP2) Correlate Strongly with Histology, Stage and Outcome in Ovarian Carcinomas.* PLOS ONE, 2010. **5**(11): p. e13837.
109. Yamanaka, R., et al., *Identification of expressed genes characterizing long-term survival in malignant glioma patients.* Oncogene, 2006. **25**(44): p. 5994-6002.
110. Alonso, S., et al., *Peripheral blood leucocytes show differential expression of tumour progression-related genes in colorectal cancer patients who have a postoperative intra-abdominal infection: a prospective matched cohort study.* Colorectal Disease, 2017. **19**(5): p. O115-O125.
111. Liu, X., et al., *Tumor-on-a-chip: from bioinspired design to biomedical application.* Microsystems & Nanoengineering, 2021. **7**(1): p. 50.
112. Berrouet, C., et al., *Comparison of Drug Inhibitory Effects ([Formula: see text]) in Monolayer and Spheroid Cultures.* Bull Math Biol, 2020. **82**(6): p. 68.
113. Gould, S.E., M.R. Junttila, and F.J. de Sauvage, *Translational value of mouse models in oncology drug development.* Nat Med, 2015. **21**(5): p. 431-9.
114. Mak, I.W., N. Evaniew, and M. Ghert, *Lost in translation: animal models and clinical trials in cancer treatment.* Am J Transl Res, 2014. **6**(2): p. 114-8.
115. WADMAN, M. *FDA no longer needs to require animal tests before human drug trials*. 2023 [cited 2023; Available from: https://www.science.org/content/article/fda-no-longer-needs-require-animal-tests-human-drug-trials.
116. Nuwer, R. *US agency seeks to phase out animal testing*. 2022 [cited 2023; Available from: https://www.nature.com/articles/d41586-022-03569-9.
117. Mehta, P., et al., *Microfluidics meets 3D cancer cell migration.* Trends Cancer, 2022. **8**(8): p. 683-697.

118. Yang, X., et al., *Nanofiber membrane supported lung-on-a-chip microdevice for anti-cancer drug testing.* Lab on a Chip, 2018. **18**(3): p. 486-495.
119. Sciancalepore, A.G., et al., *A bioartificial renal tubule device embedding human renal stem/progenitor cells.* PLoS One, 2014. **9**(1): p. e87496.
120. Wilmer, M.J., et al., *Kidney-on-a-Chip Technology for Drug-Induced Nephrotoxicity Screening.* Trends in Biotechnology, 2016. **34**(2): p. 156-170.
121. Herland, A., et al., *Distinct Contributions of Astrocytes and Pericytes to Neuroinflammation Identified in a 3D Human Blood-Brain Barrier on a Chip.* PLoS One, 2016. **11**(3): p. e0150360.
122. Brown, J.A., et al., *Recreating blood-brain barrier physiology and structure on chip: A novel neurovascular microfluidic bioreactor.* Biomicrofluidics, 2015. **9**(5): p. 054124.
123. Deosarkar, S.P., et al., *A Novel Dynamic Neonatal Blood-Brain Barrier on a Chip.* PLoS One, 2015. **10**(11): p. e0142725.
124. Bennet, D., et al., *A microengineered human corneal epithelium-on-a-chip for eye drops mass transport evaluation.* Lab on a Chip, 2018. **18**(11): p. 1539-1551.
125. Dodson, K.H., et al., *Retina-on-a-chip: a microfluidic platform for point access signaling studies.* Biomedical Microdevices, 2015. **17**(6): p. 114.
126. Ni, B.-S., C. Tzao, and J.-H. Huang, *Plug-and-Play In Vitro Metastasis System toward Recapitulating the Metastatic Cascade.* Scientific Reports, 2019. **9**(1): p. 18110.
127. Zhang, X., et al., *Cancer-on-a-Chip: Models for Studying Metastasis.* Cancers (Basel), 2022. **14**(3).
128. Maki, G., et al., *Factors regulating the cytotoxic activity of the human natural killer cell line, NK-92.* J Hematother Stem Cell Res, 2001. **10**(3): p. 369-83.
129. Deer, E.L., et al., *Phenotype and genotype of pancreatic cancer cell lines.* Pancreas, 2010. **39**(4): p. 425-35.
130. McGahon, A.J., et al., *Downregulation of Bcr-Abl in K562 cells restores susceptibility to apoptosis: characterization of the apoptotic death.* Cell Death Differ, 1997. **4**(2): p. 95-104.
131. Niforou, K.M., et al., *The proteome profile of the human osteosarcoma U2OS cell line.* Cancer Genomics Proteomics, 2008. **5**(1): p. 63-78.
132. Miltenyi Biotec. *NK Cell Isolation Kit human*. 2020; Available from: https://static.miltenyibiotec.com/asset/150655405641/document_geh73eknot6qnfnk6pp6hbu92o?content-disposition=inline.
133. Busek, M., et al., *Pump-less, recirculating organ-on-a-chip (rOoC) platform.* Lab on a Chip, 2023. **23**(4): p. 591-608.
134. Toepke, M.W. and D.J. Beebe, *PDMS absorption of small molecules and consequences in microfluidic applications.* Lab on a Chip, 2006. **6**(12): p. 1484-1486.
135. Lonza. *4D-Nucleofector Transfection Protocol for PANC-1 cells*. 2017; Available from: https://bioscience.lonza.com/lonza_bs/CH/en/download/product/asset/34810.
136. Macherey-Nagel. *Genomic DNA from Tissue: User Manual*. 2022; Available from: https://www.mn-net.com/media/pdf/5b/d0/d9/Instruction-NucleoSpin-Tissue.pdf.
137. Ben-David, U., et al., *Genetic and transcriptional evolution alters cancer cell line drug response.* Nature, 2018. **560**(7718): p. 325-330.
138. PerkinElmer Inc. *35S Methionine Labeling*. [cited 2023; Available from: https://www.perkinelmer.com/uk/lab-products-and-services/application-support-knowledgebase/radiometric/35s-methionine-

labeling.html#:~:text=services%20at%20PerkinElmer-,Overview,degradation%20of%20proteins%20in%20vivo.
139. Klein, E., et al., *Properties of the K562 cell line, derived from a patient with chronic myeloid leukemia.* Int J Cancer, 1976. **18**(4): p. 421-31.
140. Shimizu, Y. and R. DeMars, *Production of human cells expressing individual transferred HLA-A,-B,-C genes using an HLA-A,-B,-C null human cell line.* J Immunol, 1989. **142**(9): p. 3320-8.
141. Bryceson, Y.T., et al., *Activation, coactivation, and costimulation of resting human natural killer cells.* Immunol Rev, 2006. **214**: p. 73-91.
142. Laskowski, T.J., A. Biederstädt, and K. Rezvani, *Natural killer cells in antitumour adoptive cell immunotherapy.* Nature Reviews Cancer, 2022. **22**(10): p. 557-575.
143. Ponder, K.G. and L.H. Boise, *The prodomain of caspase-3 regulates its own removal and caspase activation.* Cell Death Discovery, 2019. **5**(1): p. 56.
144. Vogel, R., et al., *Mass Spectrometry Reveals Changes in MHC I Antigen Presentation After Lentivector Expression of a Gene Regulation System.* Molecular Therapy - Nucleic Acids, 2013. **2**: p. e75.
145. Sliker, B.H., et al., *HLA-B influences integrin beta-1 expression and pancreatic cancer cell migration.* Exp Cell Res, 2020. **390**(2): p. 111960.
146. Torikai, H., et al., *Toward eliminating HLA class I expression to generate universal cells from allogeneic donors.* Blood, 2013. **122**(8): p. 1341-9.
147. Zhu, K., et al., *HLA-A0201 positive pancreatic cell lines: new findings and discrepancies.* Cancer Immunology, Immunotherapy, 2007. **56**(5): p. 719-724.
148. Evanko, D., *Training GFP to fold.* Nature Methods, 2006. **3**(2): p. 76-76.
149. Cui, Y., et al., *Using Fluorescent Protein Fusions to Study Protein Subcellular Localization and Dynamics in Plant Cells.* Methods Mol Biol, 2016. **1474**: p. 113-23.
150. Goodman, S.R., *Chapter 1 - Tools of the Cell Biologist*, in *Medical Cell Biology (Third Edition)*, S.R. Goodman, Editor. 2008, Academic Press: San Diego. p. 1-26.
151. Surribas, A., et al., *Limitations using GFP as a protein expression reporter in Pichia pastoris.* Microbial Cell Factories, 2006. **5**(1): p. P56.
152. Saunders, M.J., et al., *Fluorogen activating proteins in flow cytometry for the study of surface molecules and receptors.* Methods, 2012. **57**(3): p. 308-17.
153. Kim, H.S., et al., *CReVIS-Seq: A highly accurate and multiplexable method for genome-wide mapping of lentiviral integration sites.* Molecular Therapy - Methods & Clinical Development, 2021. **20**: p. 792-800.
154. Waldmann, T., Y. Tagaya, and R. Bamford, *Interleukin-2, interleukin-15, and their receptors.* Int Rev Immunol, 1998. **16**(3-4): p. 205-26.
155. Rodella, L., et al., *Interleukin 2 and interleukin 15 differentially predispose natural killer cells to apoptosis mediated by endothelial and tumour cells.* Br J Haematol, 2001. **115**(2): p. 442-50.
156. Ring, A.M., et al., *Mechanistic and structural insight into the functional dichotomy between IL-2 and IL-15.* Nat Immunol, 2012. **13**(12): p. 1187-95.
157. Coffin, J.D., C. Homer-Bouthiette, and M.M. Hurley, *Fibroblast Growth Factor 2 and Its Receptors in Bone Biology and Disease.* J Endocr Soc, 2018. **2**(7): p. 657-671.
158. Hardikar, A.A., et al., *Human pancreatic precursor cells secrete FGF2 to stimulate clustering into hormone-expressing islet-like cell aggregates.* Proceedings of the National Academy of Sciences, 2003. **100**(12): p. 7117-7122.

159. Vavouri, T., et al., *Intrinsic protein disorder and interaction promiscuity are widely associated with dosage sensitivity.* Cell, 2009. **138**(1): p. 198-208.
160. Tang, Y.C. and A. Amon, *Gene copy-number alterations: a cost-benefit analysis.* Cell, 2013. **152**(3): p. 394-405.
161. Bolognesi, B. and B. Lehner, *Reaching the limit.* eLife, 2018. **7**: p. e39804.
162. Nguyen, O.T.P., et al., *An Immunocompetent Microphysiological System to Simultaneously Investigate Effects of Anti-Tumor Natural Killer Cells on Tumor and Cardiac Microtissues.* Front Immunol, 2021. **12**: p. 781337.
163. Ayuso, J.M., et al., *Evaluating natural killer cell cytotoxicity against solid tumors using a microfluidic model.* OncoImmunology, 2019. **8**(3): p. 1553477.
164. Marzagalli, M., et al., *A multi-organ-on-chip to recapitulate the infiltration and the cytotoxic activity of circulating NK cells in 3D matrix-based tumor model.* Front Bioeng Biotechnol, 2022. **10**: p. 945149.